To the Graduate Council:

I am submitting herewith a thesis written by Michael James Guthrie entitled "A Feasibility Study for an Eye Safe Raman Lidar Transmissometer." I recommend that it be accepted in partial fulfillment of the requirements for the degree of Master of Science, with a major in Physics.

R. H. Kohl, Major Professor

We have read this thesis
and recommend its acceptance:

Accepted for the Council:

Vice Chancellor
Graduate Studies and Research

A FEASIBILITY STUDY FOR AN EYE SAFE RAMAN LIDAR TRANSMISSOMETER

A Thesis

Presented for the

Master of Science

Degree

The University of Tennessee, Knoxville

Michael James Guthrie

June 1980

ACKNOWLEDGMENTS

The author is grateful for the support, advice and assistance rendered by his project and academic advisor, Dr. R. H. Kohl. Thanks are also extended to Drs. A. A. Mason, J. W. Lewis and K. C. Reddy for serving as members of the thesis committee and for their recommendations concerning the manuscript. Also, special thanks are given to Mr. David Sliney of the U. S. Department of the Army for his recommendations concerning the eye safety standards used in this study, and to Mr. Jim Hornkohl for his assistance in obtaining Franch-Condon factors for various molecules. Finally, the author is indebted to Mrs. June Jarrell for her invaluable help in the preparation and typing of the manuscript, and especially for her patience during some very long delays.

ABSTRACT

The feasibility of using an eye safe Raman lidar transmissometer for solving the Slant Visual Range (SVR) problem in aircraft landing approaches was investigated. The SVR problem and the inadequacy of lidar techniques utilizing scattering from atmospheric dispersions was reviewed. An eye safety study for near ultraviolet (UV) and near infrared (IR) lasers was conducted and the results were used as constraints on the lidar transmitter parameters.

Results of the investigation showed that the non-resonance Raman scattering cross sections of the major atmospheric gases considered, i.e., N_2 and O_2, are too low to achieve the desired backscattered return signals in transmittances as low as 10^{-5}. A slight enhancement of the Raman cross sections of N_2 and O_2 at incident wavelengths around 300 nm can be expected due to strong N_2 and O_2 absorption bands at shorter wavelengths. Values on the order of 10^{-28} cm^2/sr can be expected for the pure rotational Raman cross sections of N_2 and O_2 at 300 nm. With such cross sections it was determined that an eye safe Raman lidar transmissometer is physically feasible in transmittances as low as 10^{-3} in daylight (outside the solar Fraunhofer absorption lines) and 10^{-4} at night or

whenever the background noise is negligible with respect to the quantum fluctuation noise of the signal.

An investigation of the resonance Raman effect from major atmospheric gases was therefore conducted and an expression for the resonance Raman cross section in terms of the electronic oscillator strength, Franck-Condon factors and line strengths was derived. A search for absorption bands and lines of the major atmospheric gases in the near UV and near IR was conducted to determine the usefulness of the resonance Raman effect. It was found that oxygen has three weak bands in these regions but that these bands are too weak to give any noticeable resonance enhancement of the Raman cross section.

TABLE OF CONTENTS

LIST OF TABLES

LIST OF FIGURES

INTRODUCTION

The groundwork for Chapters I and II of this study is a forthcoming NASA report written by Dr. Ronald H. Kohl and this author. Chapters I and II discuss the foundations of the SVR problem and lidar transmissometer techniques respectively. Chapter III presents the results of the eye-safety study given in the above mentioned report. These chapters are essentially the introductory material vital to the main research of this study, which was determining the feasibility of using an eye safe Raman lidar transmissometer in solving the SVR problem. The results of this study are given in Chapters IV through VI.

CHAPTER I

LIDAR AND THE SLANT VISUAL RANGE PROBLEM

Slant Visual Range Problem (SVR) in Aircraft Landing Approaches

A pilot in making a final approach makes his descent down a 3 degree glide slope. Upon reaching a given point along this slope, the pilot must be able to observe sufficient visual cues on the ground if he is to continue the landing. The point at which this decision is made is called the decision point. It would be a great advantage, from both a safety standpoint and convenience to the pilot, if the control tower were able to inform the pilot, in advance, whether or not he had a chance of observing visual cues. Presently, this information is not available. Measurements of the visibility are usually made by estimating the illumination threshold and measuring the transmittance along a path a few meters above the ground which is parallel to and near a runway with a transmitter at one end and a receiver at the other. Such measurements are unable to give the actual transmittance along the pilot's line of sight. The basic problem, called the Slant Visual Range (SVR) problem, is illustrated in Figure 1.1. Obviously, any measurement made along the landing path of the aircraft would require

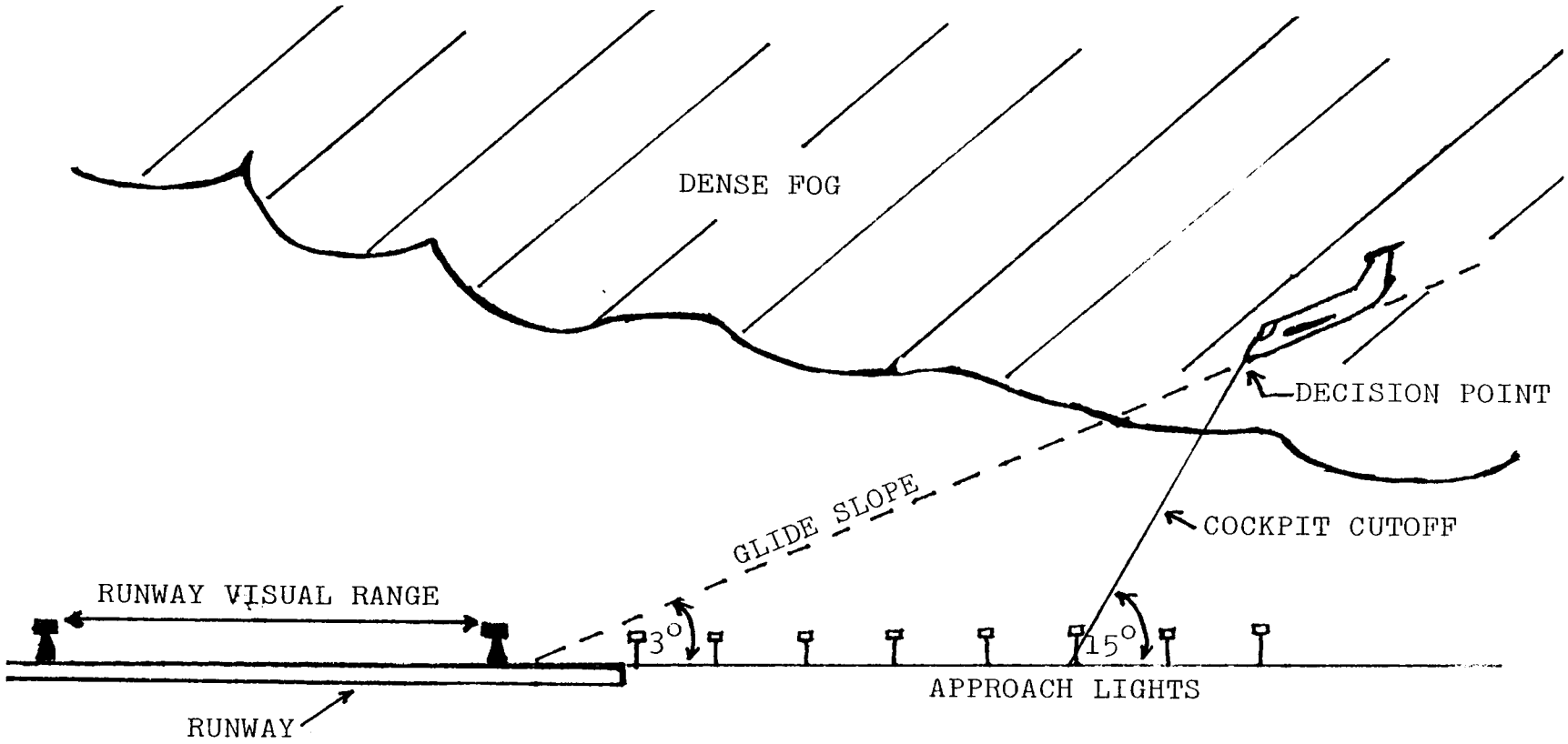

Figure 1.1. Slant Visual Range Problem on Aircraft Landing Approaches.

a single-ended device where receiver and transmitter are at the same location directed up along the visual path of interest.

The distances involved in the SVR problem are depicted in Figure 1.2. Points A and B are the Category I and II decision points respectively. The pilot is limited in his ability to see below the horizontal by the configuration of the cockpit. The standard angle taken for this limitation, called the cockpit cutoff, is 15 degrees and is also shown in Figure 1.2.

A defined sufficient visual cue for the pilot to continue with the landing has been made in terms of the approach lights, Reference [1]. If the pilot can see five or more approach lights from the cockpit cutoff forward, then he is observing sufficient visual cues for the continuation of the landing. Since the approach lights are spaced 30.5 meters apart, the pilot must essentially be able to observe a length of 152.4 meters on the ground from the decision point. This distance is depicted in Figure 1.2 for both Category I and II decision points.

Present regulations state that the runway environment must be in sight at the decision point. Some of the commercial airlines, however, require that the runway threshold lights be in sight at this point. The slant visual path from the Category II decision point (B) in

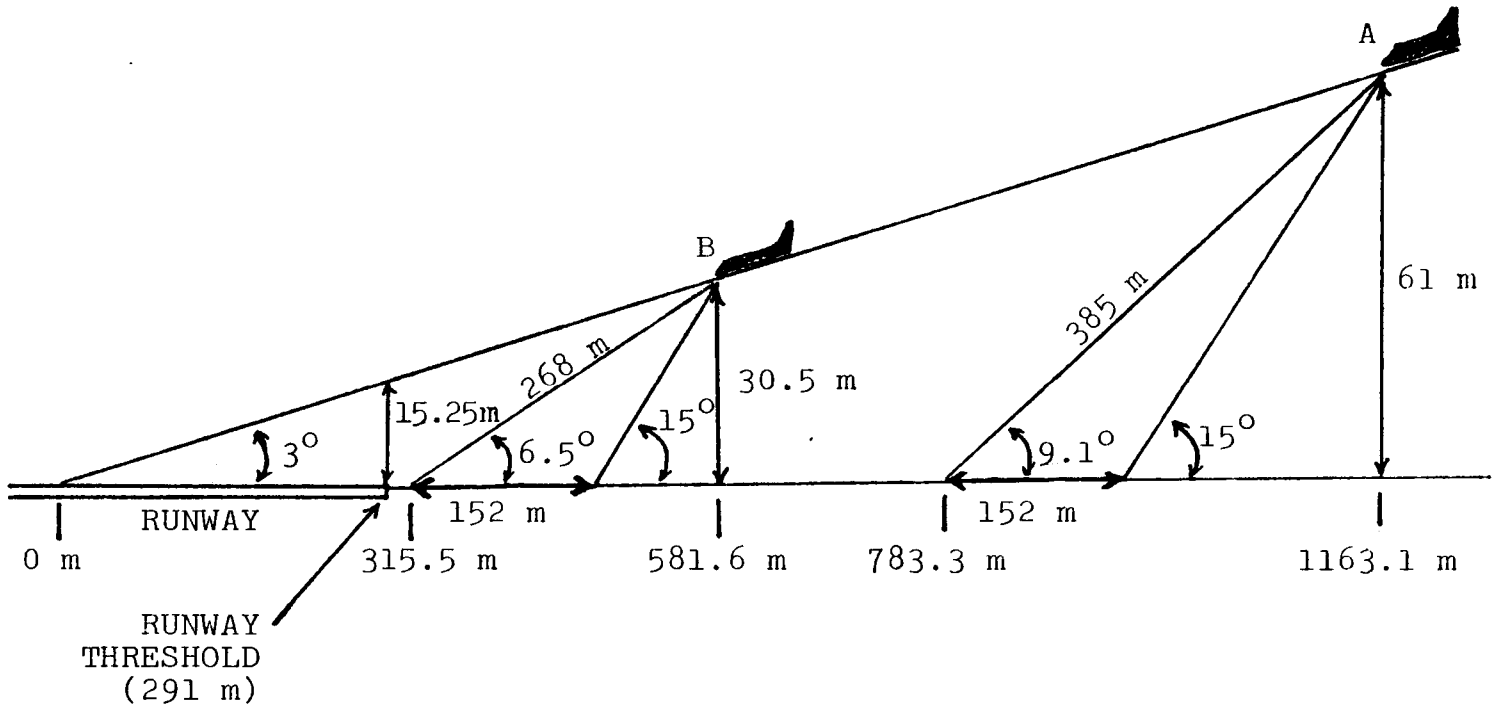

Figure 1.2. Distances Involved in the Slant Visual Range Problem.

Source: Kohl, R. H., and Guthrie, M. J. "A Feasibility Study of a Lidar Transmissometer Technique for the Slant Visual Range Problem in Aircraft Landing Approaches," NAS8-32635, National Aeronautics and Space Administration, Marshall Space Flight Center, Alabama (1978). (p. 81)

Figure 1.2 to the runway threshold differs little from the five-light criterion path from that decision point.

Principle and Advantage of the Lidar

Lidar is the acronym for Light Detection and Ranging. It is a single-ended technique which operates on principles similar to radar. As a single-ended technique it is worth investigating for possible use in measuring transmission in the SVR problem in aircraft landing approaches.

The lidar basically consists of a laser source, suitable transmitting and receiving optics, and a receiver. The laser generally transmits pulsed energy of short duration into the atmosphere. As the energy propagates it is scattered and absorbed by the particles and molecules in the air. This scattering and absorption decreases the intensity of the emitted beam and thus attenuates the beam. Part of this radiation is backscattered toward the receiver, where it is collected by optics and detected with a photodetector. If sufficient photons are observed and the photodetector is linear, the photodetector produces an electrical signal which is directly proportional to the power of the return signal at any given time. If most of the radiation scatters only once, then knowing the velocity of light, the range to the scattering volume

can be determined by the difference in time between transmission and reception. Figure 1.3 shows a typical lidar arrangement.

The amount of radiation backscattered from the atmosphere depends on the incident wavelength of the light and the properties of the particles, droplets, and molecules involved in the scattering process. Therefore, by analyzing the return signal in special cases it is often possible to derive range resolved information concerning atmospheric properties such as concentrations of pollutants, molecules or water vapor. Lidar techniques in monitoring the atmosphere have met with much success in recent years. Good reviews of such techniques are given in Reference [2].

There are basically three types of scattering utilized in the lidar technique. In Rayleigh and Mie scattering, the wavelength of the backscattered radiation is essentially the same as the wavelength of the incident radiation and therefore these processes are elastic scattering processes. The third type of scattering is an inelastic process where the wavelength of the scattered radiation is shifted from the wavelength of the incident radiation, by $\frac{\Delta E}{h}$ where ΔE is the separation of energy levels in the scatterer. This is called Raman scattering.

In Rayleigh scattering the incident light is scattered elastically from the molecules of the gas or

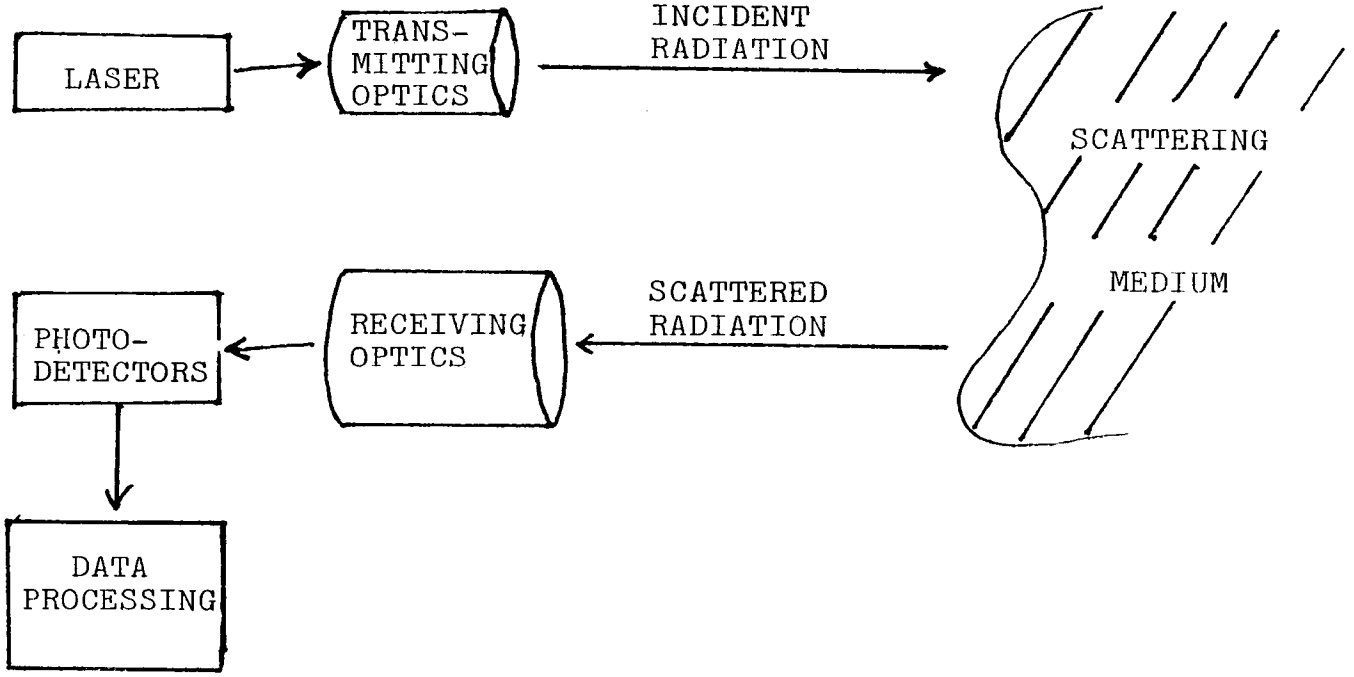

Figure 1.3. Typical Lidar System.

particles small compared to a wavelength. The interaction of the radiation field and the molecule leave the molecule in the same energy state as it was before the interaction. Mie scattering arises from scattering by particles or aerosols which are of the order of, or larger than, the wavelength, such as dust, water droplets, or other types of aerosols. Rayleigh and Mie scattered radiation compose the strongest atmospheric scattered radiation that a lidar receives.

Raman scattering involves interactions of the molecule and radiation field that leave the molecule in a different state than it was before the interaction. This type of interaction has certain advantages in that the wavelength of the scattered radiation is shifted by amounts determined uniquely by the molecule involved in the interaction. In the atmosphere Raman scattering returns are much weaker than the Rayleigh and Mie returns and this causes some limitations in its use in lidar systems.

It was desired to see if lidars could be used as transmissometers specifically for the SVR problem in aircraft landing approaches.

Lidar Operating Conditions in the SVR Problem

In discussing the operating conditions a lidar would have to perform under, it is necessary to explain

the concepts of visual range, spectral attenuation, and transmittance.

The visual range or simply visibility is defined as the distance at which one is able to see a large black object in daylight against the background of the sky. Table I.1 gives the International Visibility Code describing various conditions of visibility in the atmosphere.

The spectral attenuation coefficient, σ , is defined by

$$I = I_o \, e^{-\int_o^r \sigma(r')dr'} \quad , \tag{1-1}$$

where I and I_o are the intensities at wavelength, λ , entering and emerging unscattered respectively from a column of air length r . This attenuation coefficient is due to scattering and absorption by particles and molecules in the air. These processes are independent and σ may therefore be written as the sum of the attenuation due to each of these processes:

$$\sigma = \sigma_A + \sigma_B + \sigma_C \quad , \tag{1-2}$$

where σ_A is due to Rayleigh scattering by molecules,

σ_B is due to Mie scattering and particle absorption,

σ_C is due to absorption by the molecular gases.

TABLE I.1

INTERNATIONAL VISIBILITY CODE

Code No.	Description	Daylight Visual Range (metric) From	To	Exponential Attenuation Coefficient (km^{-1}) From	To
0	Dense fog		<50 m		>86
1	Thick fog	50 m	200 m	86	21
2	Moderate fog	200 m	500 m	21	8.5
3	Light fog	500 m	1 km	8.5	4.3
4	Thin fog	1 km	2 km	4.3	2.1
5	Haze	2 km	4 km	2.1	1.1
6	Light haze	4 km	10 km	1.1	0.43
7	Clear	10 km	20 km	0.43	0.21
8	Very clear	20 km	50 km	0.21	0.07
9	Exceptionally clear	>50 km		<0.07	

Source: Lawrence Dunkelman. "Horizontal Attenuation of Visible Light by the Lower Atmosphere," NRL Report 4031, September 10, 1952, p. 2.

The relation between visibility and the attenuation coefficient is given by [3]

$$V\bar{\sigma} = \ln(1/\eta) \quad , \tag{1-3}$$

where $\bar{\sigma}$ is the average attenuation of visible light and η is the value of the threshold brightness contrast of the eye. [Equation (1-3) is the result of uniform atmospheric conditions.] For daylight and large black objects η is usually taken to be .02 [3]. A value of η = .055 is used for transmissometer based calculations [4]. The difference between the values of .02 and .055 is due to several factors including the threshold criteria. The criterion used to obtain the .055 value was that the object be distinguishable in shape, whereas values of η lower than .055 were usually based on experiments where the criterion of visibility was any detection of a mark whose location was known. Thus, Equation (1-3) becomes

$$V\bar{\sigma} = 2.90 \ . \tag{1-4}$$

The ratio of the emerging unscattered intensity to the incident intensity is called the transmittance and is defined by

$$T(r) = I/I_o = e^{-\int_o^r \sigma(r')dr'} \ . \tag{1-5}$$

It has been shown [5] that transmittances as low as 10^{-5} along the pilot's visual path may be operational

at night. The distances involved for this transmittance are shown in Figure 1.2 (page 5) as r_A = .385 km and r_B = .268 km. A transmittance of 10^{-5} over these distances therefore corresponds to uniform attenuation coefficients of $\sigma(r_A)$ = 29.9 km^{-1} and $\sigma(r_B)$ = 43.0 km^{-1} . From Table I.1 it is seen that these attenuation coefficients correspond to thick fog conditions and are well below the daylight visual range required for a pilot to see daylight visual cues. It is therefore desirable to develop a lidar transmissometer that would be operational under a worst case transmittance of 10^{-5}. The maximum transmittance that the lidar must be capable of measuring well is the daylight visual cue threshold value of T = .055 .

CHAPTER II

THE LIDAR TRANSMISSOMETER

The Single Wavelength Lidar Equation

The basic expression for the return signal of a lidar system utilizing a single wavelength process is given by [5]

$$R(t) = K A_r \int_0^{\frac{ct}{2}} \frac{F(r)}{r^2} \beta(r) T^2(r) P(t - \frac{2r}{c}) dr \quad , \qquad (2\text{-}1)$$

where the constant K is the responsivity of the receiver when illuminated by a point source on the optic axis at infinity, A_r is the receiver aperture area, and r is the distance along the optic axis of the receiver.

The function $P(t - 2r/c)$ in Equation (2-1) is called the compressed pulse function. It is similar to the spatial power distribution of the output pulse $P(t - r/c)$ except that it travels at half the speed of light and is compressed along the optic axis by a factor of 2 . The emitted pulse is given by $P(t')$ with the pulse emission beginning at $t' = 0$.

$F(r)/r^2$ in Equation (2-1) is called the beam geometry factor and is given by

$$F(r) = \iint k(x,y,r)\ p(x,y,r)\ dxdy \quad , \qquad (2\text{-}2)$$

where the integral is over the x,y plane perpendicular to the optic axis at the distance r . The function k(x,y,r) is the ratio of the responsivity of the receiver to a point source at the position x,y,r to the responsivity K . p(x,y,r) is the transmitter beam power distribution in the x,y plane perpendicular to the optic axis at the distance r , and is normalized to one at each r . F(r) is therefore the overlap of the transmitter beam and the receiver field of view.

Equation (1-5) defines T(r) in Equation (2-2) and $\beta(r)$ is the fraction of the incident light radiation backscattered at the distance r per steradian per unit length of propagation in the atmosphere. It is assumed that all of the light detected is scattered through π radians. This assumption is good when the receiver and transmitter are placed sufficiently close to each other.

Methods of Measuring Transmittance Using the Single Wavelength Equation

Several laboratories have reported [1,6,7,8] experimental efforts to obtain $\sigma(r)$ directly from a short pulse single wavelength return without any additional information. These techniques neglect aspects of the single wavelength lidar equation, Equation (2-1), [9].

The common "ratio" method [1,6,7] of determining $\sigma(r)$ from the return signal utilizes the short pulse lidar equation

$$R(t) = K\, A_r\, E_p\, \frac{c}{2}\, \frac{F(r)}{r^2}\, H(r) \qquad (2\text{-}3)$$

where E_p is the energy in the output pulse,

$$H(r) = \beta(r)\, e^{-2\int_o^r \sigma(r')dr'} = \beta(r_1)\, e^{-2\int_{r_1}^r a(r')dr'} \qquad (2\text{-}4)$$

and

$$a(r') = -\frac{1}{2}\,\frac{1}{\beta(r')}\,\frac{d\beta(r')}{dr'} + \sigma(r') \quad . \qquad (2\text{-}5)$$

The value obtained for σ at $r = r_i$ using this method is

$$"\sigma(r_i)" = \frac{1}{2\Delta r_i} \ln\left[\frac{r_i^2\, R(t_i)\, F(r_{i+1})}{r_{i+1}^2\, R(t_{i+1})\, F(r_i)}\right] \quad , \qquad (2\text{-}6)$$

where $r_i = c\, t_i/2$, $r_{i+1} = r_k + \Delta r_i$ and Δr_i is ideally differentially small. Substituting Equations (2-3) and (2-4) in this expression indicates that what is obtained is

$$"\sigma(r_i)" = a(r_i) = -\frac{1}{2}\,\frac{1}{\beta(r_i)}\left[\frac{d\beta}{dr}\right]_{r_i} + \sigma(r_i) \quad , \qquad (2\text{-}7)$$

which gives the correct value for σ if the dispersion is homogeneous, and this often is not the case [9].

The common "slope" method [1,6,10] of determining the average $\sigma(r)$ from the return signal obtained using a short pulse lidar system uses an S function defined as

$$S(r) = \ln\left[\frac{r^2 R(t)}{F(r)}\right] \tag{2-8}$$

and seeks to obtain the average $\sigma(r)$ from $r = r_a$ to $r = r_b$ from

$$"\bar{\sigma}_{ab}" = -\frac{1}{2}\frac{\Delta S}{\Delta r} \quad . \tag{2-9}$$

It can be shown [9] that Equation (2-9) can be written as

$$"\bar{\sigma}_{ab}" = \frac{12}{(r_a - r_b)^3}\int_{r_3}^{r_b}\left[r - \frac{\bar{r}}{2}\right]\left[-\frac{1}{2}\ln\beta(r) + \tau(r)\right]dr \ , \tag{2-10}$$

where $\bar{r} = (r_b + r_a)/2$ and $\tau(r)$ is the optical depth to r .

This method also gives the correct result for homogeneous dispersions. The error in the measured σ can be attributed [9] to the first term in Equation (2-5).

Realizing the problems with the "ratio" and "slope" techniques, other methods [5,11,12] were sought which

would give the desired quantity of any transmittance measurement, $T(r)$.

The inversion of Equation (2-1) gives the product βT^2 . Therefore a relation must be found between β and T or equivalently between β and σ . Kohl [5] and Stewart [11,12] assume

$$\beta = \kappa\sigma \ , \tag{2-11}$$

where κ is constant in space over the region of the atmospheric dispersion contributing to the return radiation but may vary from lidar pulse to lidar pulse. Using Equations (1-5) and (2-11), one obtains

$$\beta(r)\ T^2(r)dr = \frac{\kappa}{2}\left[-\ dT^2(r)\right] \ , \tag{2-12}$$

where dT^2 is the differential change in T^2 with respect to r . Therefore Equation (2-1) may be written as

$$R(t) = K\ A_r\ \frac{\kappa}{2} \int_o^{\frac{ct}{2}} \frac{F(r)}{r^2}\ P(t - \frac{2r}{c}) \left[-\ dT^2(r)\right] \ . \tag{2-13}$$

If $F(r)/r^2$ and $P(t - 2r/c)$ can be held constant [5], the transmittance to the point $r = ct/2$ can be obtained directly from Equation (2-13). There are ways [5,11,12] that $F(r)/r^2$ can be made constant from a given $r = r_a > 0$ to some $r = r_b$ along the optic axis. The compressed pulse function $P(t - 2r/c)$ in Equation (2-13) must consist of a steep rise followed by a constant value.

This rise should take place over a distance that is short with respect to the allowable error in the distance interval to the decision point, r^* . Choosing r_a sufficiently short so that $T(r_a) \approx 1$, we may write Equation (2-13) as

$$R(t) = K A_r C \frac{\kappa}{2} \left[1 - T^2\left(\frac{ct}{2}\right)\right] \quad , \tag{2-14}$$

where $C = F(r)/r^2 \; P(t - 2r/c)$, and is constant over the interval $r_a \leq r = ct/2 \leq r_b$.

Stewart's approach [11,12] to the problem is essentially the same as the above except that he utilizes a short δ-function pulse in Equation (2-13) and integrates electronically.

Apparently if the atmospheric medium is optically thick from $r = 0$ to $r = r_b$ where $r^* < r_b$, so $T(r_b) << 1$, $T(r^*)$ can be obtained from Equation (2-14) as

$$T(r^*) = \left[1 - \frac{R(t^*)}{R(t_b)}\right]^{1/2} \quad . \tag{2-15}$$

If the atmospheric medium is not optically thick to $r = r_b$ the value of $T(r^*)$ obtained from Equation (2-15) will be too low. It has been shown in Reference [5] that the actual condition for Equation (2-15) to give a valid measurement is that the transmittance from r^* to r_b , $T(r^*,b)$, be not close to 1 .

There are problems encountered in the use of the above approach measurements. As mentioned above, there is the problem when $T(r^*,r_b)$ is not much less than one, giving a measured value of $T(r^*)$ lower than the actual value. Figure 2.1 illustrates hypothetical measurements where this problem arises. It can be seen from the figure that the measured transmittance $T'(r^*)$ stays close to the actual transmittance $T(r^*)$ until $T(R^*,r_b)$ gets very close to one. Thus one might expect this or similar [11,12] techniques to fail for low lying atmospheric dispersions such as ground fogs or blowing snow, etc.

Another problem is the requirement that the compressed pulse function attains a constant value after the initial rise of the pulse. The cross-sectional power distribution must also be uniform over the enlarged transmitter beam.

The problem of overcoming the ambiguity in the transmittance measurements has been studied in detail [5] and there appears to be no method of utilizing scattering from the atmospheric dispersion which is applicable to the SVR problem unless κ in Equation (2-3) is both constant and known.

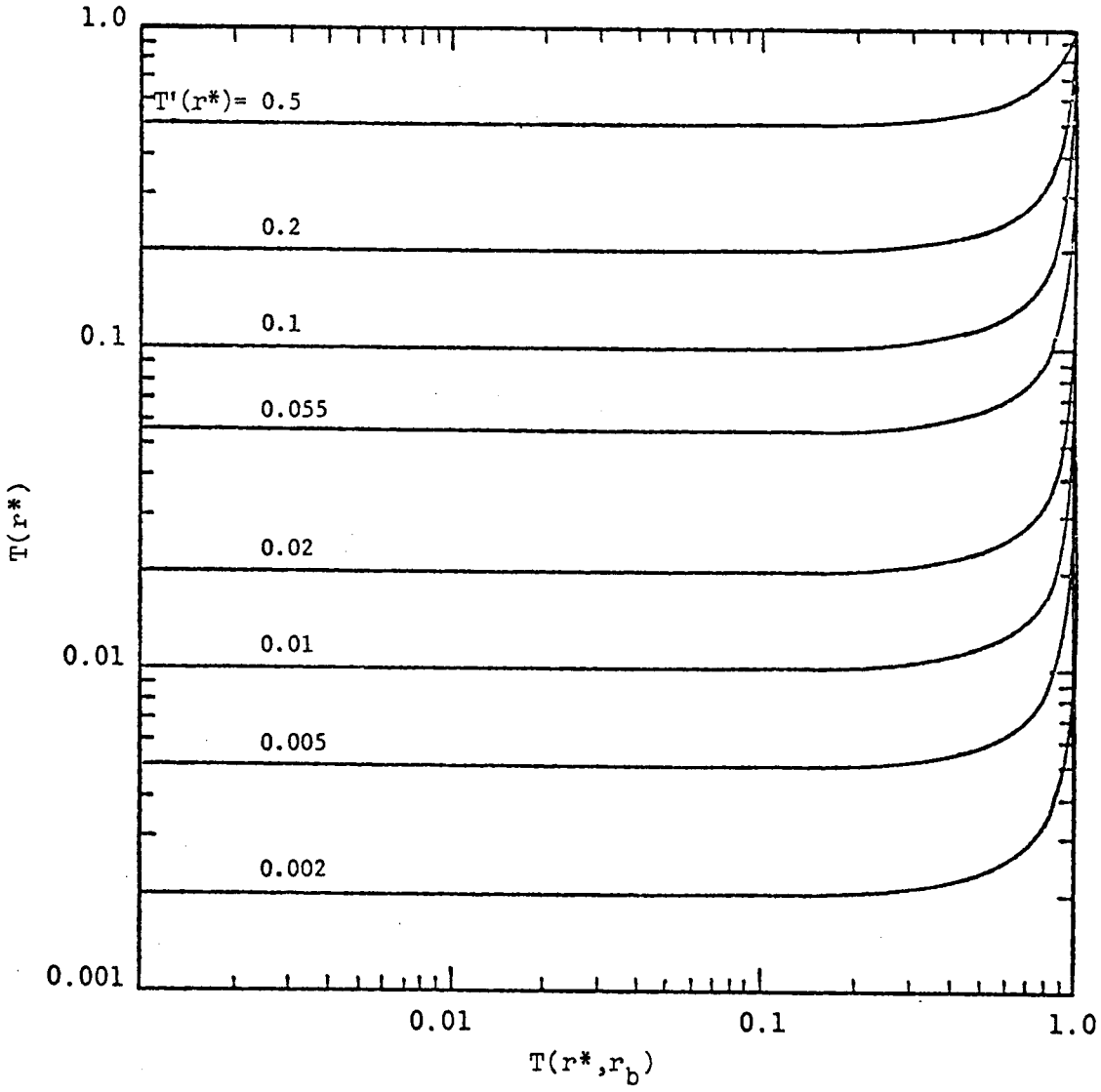

Figure 2.1. Actual Transmission T(r*) for Measured Transmission T'(r*) and $T(r^*,r_b)$.

Source: Kohl, R. H., and Guthrie, M. J. "A Feasibility Study of a Lidar Transmissometer Technique for the Slant Visual Range Problem in Aircraft Landing Approaches," NAS8-32635, National Aeronautics and Space Administration, Marshall Space Flight Center, Alabama (1978).

Method Utilizing Wavelength Shifted Scattering from the Atmospheric Gases

As the problems discussed above were realized, other means of utilizing lidar were sought. An unambiguous method of obtaining the transmittance utilizing wavelength shifted scattering from the gas was derived [5]. The lidar equation for such processes is again given by Equation (2-1) except that the backscatter coefficient $\beta(r)$ is replaced by $\beta_g(r)$, where $\beta_g(r)$ is the fraction of incident radiation of wavelength λ backscattered with wavelength λ' per steradian per unit length of propagation. $\beta_g(r)$ depends on the type of scattering from the gas being observed whereas σ depends on the atmospheric dispersions present.

If a short δ function, pulse of energy E_p , is emitted at $t = 0$, and assuming the transmittances of the incident and scattered wavelengths are approximately equal, we may write the wavelength shifted lidar equation as

$$R(t) = K A_r \frac{c}{2} E_p \frac{F(r)}{r^2} \beta_g(r) T^2(o,r) \quad , \qquad (2\text{-}16)$$

where $r = ct/2$ and $T(o,r)$ is defined by Equation (1-5).

Given the return signals at t_o and t^* , where $r_o = c\, t_o/2$ and $r^* = ct/2$, we obtain the ratio

$$\frac{R(t^*)}{R(t_o)} = \frac{F(r^*)/r^{*2}}{F(r_o)/r_o^2} \frac{\beta_g(r^*)}{\beta_g(r_o)} \left[\frac{T(0,r^*)}{T(0,r_o)}\right]^2 \quad . \qquad (2\text{-}17)$$

Choosing r_o sufficiently close to the lidar and such that $F(r_o) \neq 0$, the desired transmittance to the decision point is

$$T(r_o,r^*) = T(0,r^*) \; / \; T(0,r_o) \quad . \qquad (2\text{-}18)$$

Letting

$$\rho_f = \frac{F(r^*)/r^{*2}}{F(r_o)/r_o^2} \qquad (2\text{-}19)$$

and

$$\rho_g = \beta_b(r^*)/\beta_g(r_o) \quad , \qquad (2\text{-}20)$$

we have

$$T(r_o,r^*) = \left[\frac{R(t^*)/R(t_o)}{\rho_f \, \rho_g}\right]^{1/2} \quad . \qquad (2\text{-}21)$$

Therefore, knowing ρ_f and ρ_g , the transmittance to the decision point is known.

If an accumulation of the return signals from N pulses is obtained over a period of time for which T^2 does not vary significantly, Equation (2-16) becomes

$$\sum_{i=1}^{N} R_i(t) = \sum_{i=1}^{N} C_i \frac{F(r)}{r^2} \beta_g(r) \; T^2(o,r) \quad , \qquad (2\text{-}22)$$

where $C_i = K_i A_r E_{p_i} C/2$. Thus, Equation (2-21) becomes

$$T(r_o,r^*) = \left[\frac{\sum_{i=1}^{N} R_i(t^*) \quad \sum_{i=1}^{N} R_i(t_o)}{\rho_f \rho_g} \right]^{1/2} . \qquad (2\text{-}23)$$

$\beta_g(r)$ is proportional to the number density at r of the gas involved in the scattering process. The ratio $\rho_g = \beta(r^*)/\beta(r_o)$ for the distances involved in the SVR problem can therefore be taken as unity. It can be shown [5] that using $\rho_g = 1$ results in an error in the transmittance of about 0.5 percent.

The quantity ρ_f can be made constant in time by keeping F(r) constant at r^* and r_o , which is done by maintaining the alignment of the system.

One means of obtaining ρ_f [5] would be the measurement of σ in clear air over a long path in the vicinity of the operating lidar transmissometer under circumstances where one could be sure that the value of σ measured applied all along the measurement path and along the lidar beam from r_o to r^* . Under such conditions and with distances $r^* - r_o$, the value $2\sigma(r^* - r_o)$ would be less than 1. The contribution of the relative error in the measurement of σ to the relative error in ρ_f would be reduced by the factor $2\sigma(r^* - r_o)$. For example, if this factor were taken to be .02, a measurement in σ with a 10 percent error would determine ρ_f with a 2 percent error.

One means of obtaining wavelength shifted scattering from the atmospheric gas is via Raman scattering from a stable fraction of the gases of the atmosphere. The simplicity in principle of the method described above warranted the investigation into the use of Raman scattering, and the problem became one of obtaining suitable return signals.

Transmission Similarities in the Visible, Near UV and Near IR

A lidar designed for the purpose of solving the SVR problem would be directed along the pilot's line of sight in his approach for landing. For this reason it is desirable to design a system using invisible radiation in the near UV or near IR having the same or similar transmission properties in atmospheric dispersions as visible light.

An atmospheric attenuation model for the UV, visible, and IR wavelength regions has been developed by L. Elterman [13]. This model considered wavelengths from .27 μm to 4.0 μm . Calculation of attenuation at wavelengths shorter than .27 μm requires a detailed treatment of O_2 absorption band and at wavelengths longer than 4.0 μm the situation is complicated by the presence of the absorption bands of H_2O and CO_2 , and for this reason these regions were not included in the model.

Elterman's model starts with the molecular components of the atmospheric attenuation and then adds the components due to aerosols and ozone. Table II.1 lists the sea-level attenuation coefficients due to Rayleigh and Mie scattering and ozone absorption obtained from Elterman's model. Figure 2.2 shows spectral plots of each of these attenuation components and also the sum of these attenuation components given by

$$\sigma = \sigma_{RAYLEIGH} + \sigma_{AEROSOL} + \sigma_{OZONE} \quad . \qquad (2\text{-}24)$$

(It should be noted that the $\sigma_{AEROSOL}$ used by Elterman is much less than that encountered in transmission measurements.)

It can be seen from Figure 2.2 that the effects of ozone are negligible except in the region below .3 μm . At a wavelength of .28 μm the ozone effect would result in about a 15 percent error for a visible light transmission measurement at a transmittance of .055 over a distance of about .268 km . (The reader should note that the concentrations of ozone may vary from 0.0 to 0.05 PPM over a period of a month or more [14].)

It was necessary to consider the behavior of near UV and near IR radiation in passing through media whose predominant components are water particles or particles covered with an aqueous layer. For such cases it was necessary to insure that the complex indices of refraction

TABLE II.1

SEA LEVEL ATMOSPHERIC ATTENUATION COEFFICIENTS
FOR THE NEAR UV AND NEAR IR

σ (μm)	$\sigma_{RAYLEIGH}$ (km^{-1})	$\sigma_{AEROSOL}$ (km^{-1})	σ_{OZONE} (km^{-1})
.27	2.282×10^{-1}	2.90×10^{-1}	7.48×10^{-1}
.28	1.948×10^{-1}	2.70×10^{-1}	3.77×10^{-1}
.30	1.446×10^{-1}	2.60×10^{-1}	3.60×10^{-2}
.32	1.098×10^{-1}	2.50×10^{-1}	3.20×10^{-3}
.34	8.492×10^{-2}	2.40×10^{-1}	2.28×10^{-4}
.36	6.678×10^{-2}	2.40×10^{-1}	6.41×10^{-6}
.38	5.327×10^{-2}	2.30×10^{-1}	0.0
.40	4.303×10^{-2}	2.00×10^{-1}	0.0
.70	4.345×10^{-3}	1.35×10^{-1}	8.19×10^{-5}
.80	2.544×10^{-3}	1.27×10^{-1}	3.56×10^{-5}
.90	1.583×10^{-3}	1.20×10^{-1}	0.0
1.06	8.192×10^{-4}	1.13×10^{-1}	0.0
1.26	2.091×10^{-4}	1.08×10^{-1}	0.0
1.67	1.322×10^{-4}	9.80×10^{-2}	0.0
2.17	4.629×10^{-5}	8.50×10^{-2}	0.0
3.50	6.823×10^{-5}	7.00×10^{-2}	0.0
4.00	4.002×10^{-6}	6.80×10^{-2}	0.0

Source: Elterman, L. "UV, Visible, and IR Attenuation for Altitudes to 50 km, 1968," AF L68-0153 (AD671933), Air Force Cambridge Research Laboratories, Bedford, Massachusetts (1968), pp. 22-43.

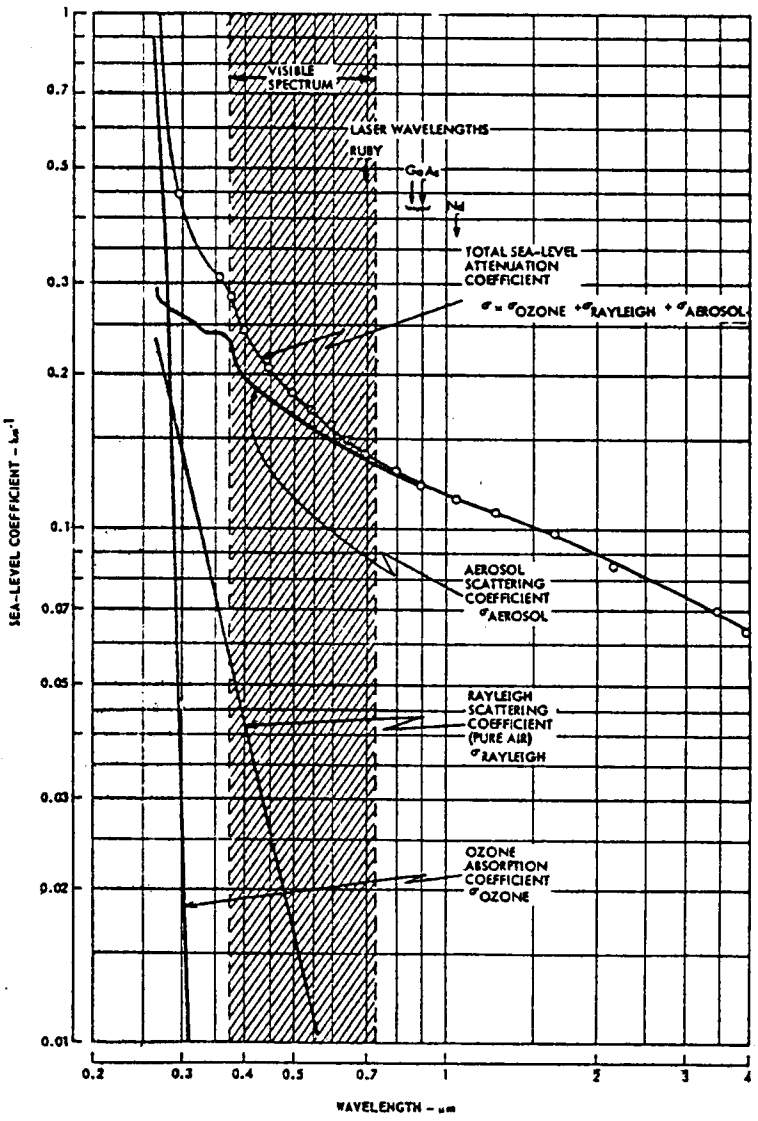

Figure 2.2. Sea Level Atmospheric Attenuation Coefficients in a Clear Standard Atmosphere.

Source: RCA Electro-Optics Handbook, Technical Series EOH-11, RCA, Harrison, New Jersey, 1974, p. 85.

did not vary significantly from those of the visible region of the spectrum. Table II.2 gives the values of the real part of the complex index of refraction, n, the imaginary part of the index of refraction, k , and the absorption coefficient χ for wavelengths from .2 μm to 2.21 μm , where index of refraction, $\bar{m}$, is defined by

$$\bar{m} = n + ik \quad . \tag{2-25}$$

It can be seen from the figure that k stays small compared to n in the near UV and n does not vary much from the visible from .4 μm to .25 μm . In the near IR, k rapidly gets larger as the wavelength increases and will play a role in the extinction properties if one goes too far. It should also be noted that the $(1/\lambda)^4$ dependence of Rayleigh and Raman scattering weighs heavily against the IR.

TABLE II.2

COMPLEX INDEX OF REFRACTION AND ABSORPTION COEFFICIENT OF WATER

λ_μ	n	k	$\varkappa$	λ_μ	n	k	$\varkappa$
0.20	1.424	8.0×10^{-2}	1.3×10^{-7}	1.20	1.323	1.020	9.74
0.25	1.377	3.0	6.0×10^{-8}	1.25	1.322	0.890	8.85
0.30	1.359	1.5	3.6	1.258	1.322	0.88	8.80
0.35	1.349	3.0×10^{-3}	8.0×10^{-9}	1.30	1.321	1.08	11.17
0.40	1.343	1.0	3.0	1.35	1.320	2.70	29.00
0.45	1.339	2.0×10^{-4}	7.0	1.40	1.320	13.00	14.48×10^{-5}
0.50	1.336	2.5	8.0	1.45	1.319	26.0	3.00×10^{-4}
0.55	1.334	3.5	1.5×10^{-9}	1.50	1.318	17.3	2.065
0.60	1.332	1.5×10^{-3}	7.0	1.55	1.317	9.6	1.184
0.65	1.331	2.5	1.3×10^{-6}	1.60	1.316	6.2	7.89×10^{-6}
0.70	1.330	6.0	3.3	1.65	1.316	5.1	6.70
0.75	1.329	2.5	1.49×10^{-7}	1.66	1.315	5.0	6.6×10^{-5}
0.76	1.329	2.6×10^{-2}	1.50	1.70	1.315	5.15	6.97
0.80	1.328	2.1	1.34	1.75	1.314	6.4	8.91
0.806	1.328	2.0	1.20	1.80	1.312	8.0	1.146×10^{-4}
0.85	1.327	4.1	2.77	1.85	1.311	9.5	1.399
0.90	1.328	6.7	4.80	1.90	1.309	80.5	1.217×10^{-3}
0.95	1.327	3.65×10^{-1}	2.76×10^{-6}	1.94	1.307	114.0	1.76
0.97	1.327	4.3	3.55	1.95	1.307	110.0	1.707
1.00	1.326	3.55	2.82	2.00	1.304	68.0	1.082
1.05	1.325	1.31	1.10	2.05	1.302	41.0	6.689×10^{-4}
1.06	1.325	1.28	1.07	2.10	1.300	26.0	4.345
1.10	1.324	1.90	1.66	2.15	1.296	19.0	3.25
1.15	1.3235	8.00	7.32	2.20	1.293	16.0	2.8
1.19	1.323	1.05×10^{0}	9.90	2.21	1.292	15.5	2.72

Source: K. Ya. Kondrat 'ev. "Radiation Characteristics of the Atmosphere and the Earth's Surface," NASA TTF-678 (1973), p. 92.

CHAPTER III

EYE SAFETY LIMITATIONS FOR NEAR IR AND NEAR UV LASERS

Safety Standards Used

Since there is the possibility that a pilot will look into the lidar beam, it was required that eye safety be incorporated in the development of a lidar for the SVR problem. The basis for this eye safety investigation [5] was the ANSI Standard Z136.1-1976 [15].

The results and discussion of this chapter are essentially those included in a forthcoming NASA report [5] written by Ronald H. Kohl and this author. The results of this chapter are used in the following chapters as a condition under which the feasibility of an operational eye-safe Raman lidar transmissometer was investigated. It was discovered that this standard had some shortcomings and in these cases Mr. David Sliney of the U. S. Department of the Army was consulted. Mr. Sliney is a member of the Z136 Committee on Laser Safety. His recommendations were referred to as the Sliney Patch and are given in Appendix I.

Range of Pulse Lengths Considered

The distances involved in the SVR problem are from Figure 1.2 (page 5), .268 km and .385 km . An error of about 30.5 meters was considered the maximum allowable for these distances. This put an upper limit of about 200 nsec on the output pulse length of the lidar. The lowest pulse length considered in ANSI Z136.1-1976 was 1.0 nsec; therefore, this study considered pulse lengths in the range of 1.0 nsec to 200 nsec.

Possible Total Exposure Times

According to the Sliney Patch (Appendix I), the total exposure time used in the eye safety calculations should be the total time one is exposed to the laser beam in a given 24-hour period. This time can be restricted to the times someone in an aircraft would be exposed to the beam as access to the beam from the ground would be prevented. This could be accomplished by placing a fence around the lidar site with properly marked warning signs.

To estimate the time a person in a landing aircraft would be exposed to the beam, a low ground speed of 26.8 m/sec (60 miles per hour) was assumed. If the aircraft travels down the 3 degree glide slope and the beam diameter is 1 m , then for a beam elevated at 6.5 degrees the exposure time is slightly less than 1 sec.

An estimate of an upper limit on the exposure time was obtained by assuming the aircraft remained in the beam from a point at twice the altitude of the 3 degree glide slope to the lidar site. This condition yields exposure times of 136 sec and 56 sec for the beams elevated at 6.5 degrees and 9.1 degrees respectively. It was therefore reasonable to take 100 sec as the upper limit to the exposure times considered.

Optimum Pulse Repetition Frequencies

A minimum pulse repetition frequency (PRF) of 1 Hz was assumed for an operational lidar transmissometer. It was found that for wavelengths above .31 μm , and for the pulse lengths and exposure times considered, the eye safe output energy for a single pulse will usually give an output energy that is less than the eye-safe output energy allowed for the total exposure time when a PRF of 1 Hz is used. Therefore, the PRF may be increased until the output energy in a given total exposure time reaches the allowed value for eye safety. This PRF is referred to as the optimum PRF. If the PRF is increased above the optimum value, the energy per pulse must correspondingly be reduced in order to keep the output energy in the total exposure time eye safe.

Increasing the PRF allows the return signal to be summed over a number of pulses in a second and this

increases the signal-to-noise ratio (SNR). In an eye-safe system this increase will only take place up to the optimum PRF because the return per second is fixed for all PRF above the optimum. Thus, the SNR value will decrease for PRF's above the optimum in an eye-safe system.

The optimum PRF results based on the ANSI Z136.1-1976 and the Sliney Patch are as follows:

Dependence on pulse length and total exposure time. For the near UV range of .31 μm to .4 μm , total exposure times between 10^{-2} sec to 10^{3} sec, and pulse lengths between 10^{-9} sec to 10 sec, it was found that the optimum PRF is inversely proportional to the pulse length raised to the 1/4 power. In addition, it is also inversely proportional to the total exposure time for total exposure times greater than 10 sec, and for the wavelength range .315 μm to .4 μm it is inversely proportional to the 3/4 power of the total exposure time for total exposure times less than 10 sec.

In the near IR wavelength range from .7 μm to 1.4 μm with pulse lengths between 1 nsec and 10 μsec and total exposure times between 10^{-4} sec and 10^{3} sec, the optimum PRF is independent of the pulse length. If the optimum PRF in the near IR is greater than 10^{3} Hz, it is inversely proportional to the total exposure time raised to the 1/4 power.

Figure 3.1 shows the optimum PRF for the near IR and near UV plotted as a function of wavelength for various exposure times and pulse lengths. In the near UV the optimum PRF is pulse length dependent and the solid curve represents a 200 nsec pulse while the dashed curve represents a 20 nsec pulse.

Discrete pulse effect. The maximum number of pulses in a given total exposure time (TTE) is approximated by the product of the PRF and TTE. This approximation is good until the maximum number of pulses in the TTE drops below 10. This occurs in Figure 3.1 in the interval between .304 μm and .311 μm . An expanded plot of this region is shown in Figure 3.2. The dashed portion of the curve indicates 10 or less pulses in the TTE. In the wavelength interval where these discrete pulse effects occur it often is not possible to have each pulse at its maximum energy and attain the maximum allowed average output energy in a second. For example, consider a short pulse with a maximum allowed output energy that is 2/3 the maximum output energy allowed during the TTE. If the PRF is such that only one pulse occurs in the TTE, then the average output energy in a second is below the maximum. By increasing the PRF, the average output energy in a second increases. When two

Figure 3.1. Optimum Pulse Repetition Frequency (Optimum PRF) as a Function of Wavelength in the Near Ultraviolet (NUV) and Near Infrared (NIR) for Various Total Exposure Times and Pulse Lengths.

The optimum PRF is the pulse repetition frequency at which the signal-to-noise ratio is an optimum in eye-safe lidars where the returns from successive pulses do not interfere with one another. Note the large relative shift in the NUV and NIR ordinates. The curves are labeled with the applicable total exposure times. In the NUV wavelengths the curves of 200 nsec pulse length are solid, the curves of 20 nsec pulse length are dotted. In the NIR wavelengths the curves are pulse length independent.

Source: Kohl, R. H., and Guthrie, M. J. "A Feasibility Study of a Lidar Transmissometer Technique for the Slant Visual Range Problem in Aircraft Landing Approaches," NAS8-32635, National Aeronautics and Space Administration, Marshall Space Flight Center, Alabama (1978), p. 53.

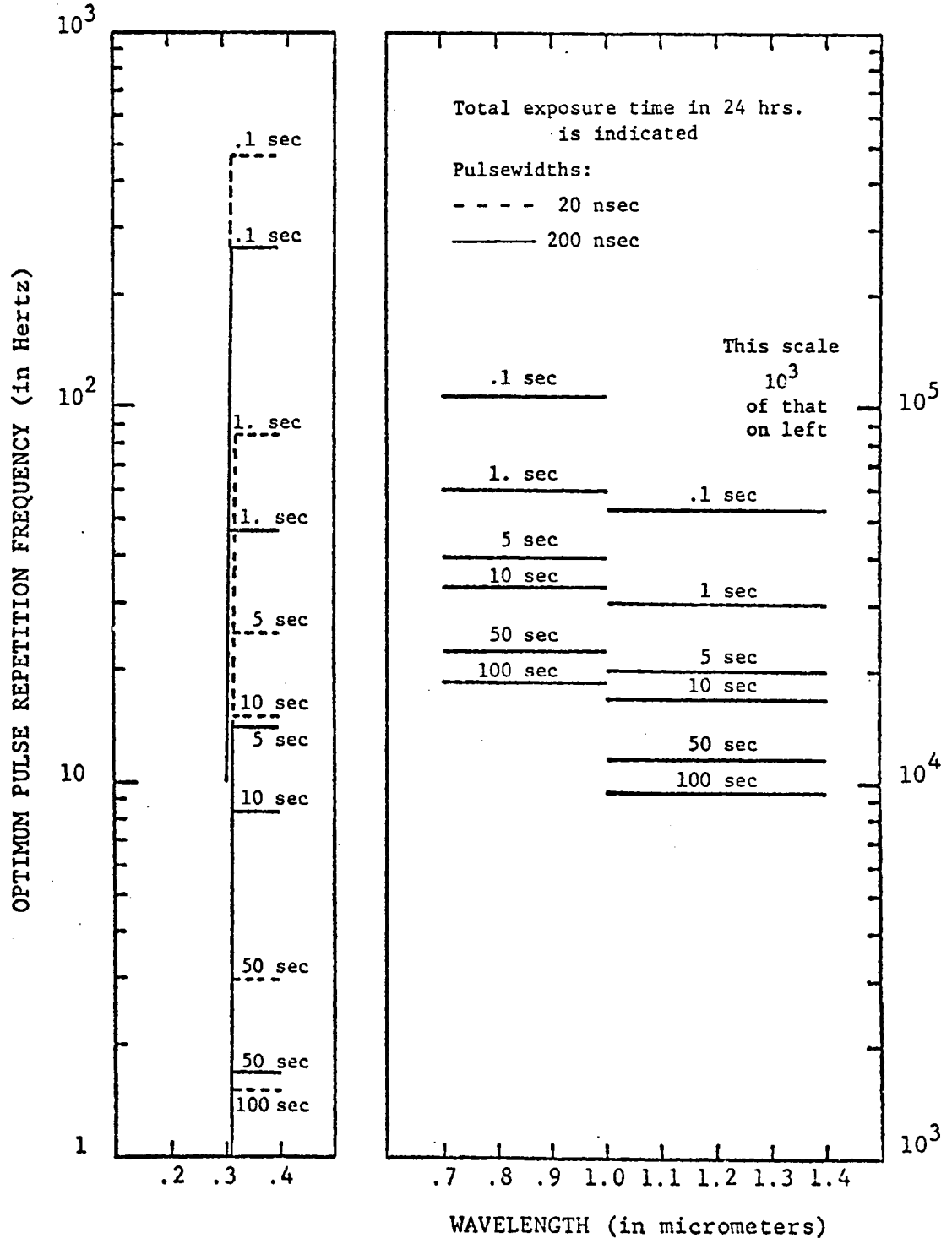
OPTIMUM PULSE REPETITION FREQUENCY (in Hertz)
10^3
10^2
10
1
.1 sec
.1 sec
1. sec
1. sec
5 sec
10 sec
5 sec
10 sec
50 sec
50 sec
100 sec
.2 .3 .4
Total exposure time in 24 hrs. is indicated
Pulsewidths:
- - - - 20 nsec
——— 200 nsec
This scale 10^3 of that on left
.1 sec
1. sec
5 sec
10 sec
50 sec
100 sec
.1 sec
1 sec
5 sec
10 sec
50 sec
100 sec
10^5
10^4
10^3
.7 .8 .9 1.0 1.1 1.2 1.3 1.4
WAVELENGTH (in micrometers)

Figure 3.1.

Figure 3.2. Optimum Pulse Repetition Frequencies in the Transition Region in the Near Ultraviolet Where Discrete Pulse Effects May Be Important.

Each curve is labeled with the total exposure time and pulse width (in parentheses). Segments of 10 and less pulses in the total exposure time interval are indicated in dashes. Actual values in these segments may be system dependent.

Source: Kohl, R. H., and Guthrie, M. J. "A Feasibility Study of a Lidar Transmissometer Technique for the Slant Visual Range Problem in Aircraft Landing Approaches," NAS8-32635, National Aeronautics and Space Administration, Marshall Space Flight Center, Alabama (1978), p. 56.

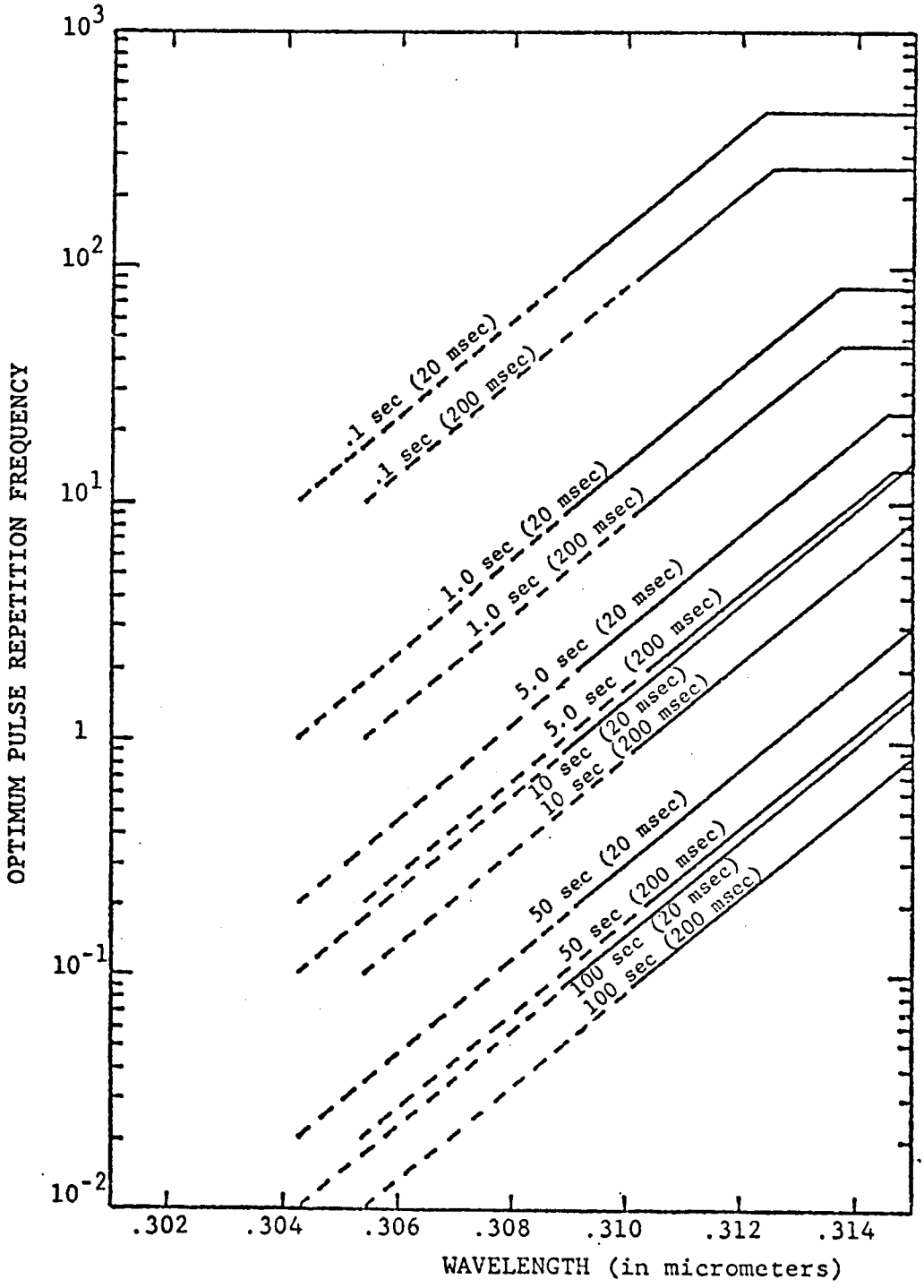
OPTIMUM PULSE REPETITION FREQUENCY
10^3
10^2
10^1
1
10^{-1}
10^{-2}
.1 sec (20 msec)
.1 sec (200 msec)
1.0 sec (20 msec)
1.0 sec (200 msec)
5.0 sec (20 msec)
5.0 sec (200 msec)
10 sec (20 msec)
10 sec (200 msec)
50 sec (20 msec)
50 sec (200 msec)
100 sec (20 msec)
100 sec (200 msec)
.302
.304
.306
.308
.310
.312
.314
WAVELENGTH (in micrometers)

Figure 3.2.

pulses occur in the TTE the maximum allowed energy per pulse must then be decreased, otherwise the maximum allowed value for the TTE would be exceeded by 1/3. Thus, at the PRF where two pulses just fit into the TTE, the energy per pulse must be decreased. The PRF can again be increased until a third pulse is just short of entering the TTE. It is this PRF that gives the maximum allowed average output energy in a second for the example. If the PRF is increased above this value, the third pulse enters the TTE and a reduction in the energy per pulse is again necessary. This effect is illustrated in Figure 3.3.

If the number of pulses in the TTE is greater than 10 at the optimum PRF, the discrete pulse effect makes a difference of less than 10 percent and the effect is considered negligible.

Wavelengths shorter than .304 μm and optimum PRF's less than 1 Hz. For wavelengths below .304 μm there is no optimum PRF because a single pulse in the TTE at its maximum allowed energy will always give the maximum allowed energy for the TTE. In this wavelength region and in the case where the optimum PRF is less than the operational minimum of 1 Hz, the PRF is set to 1 Hz and the individual pulses are reduced in energy until the maximum allowed energy

Figure 3.3. Discrete Pulse Effects at 0.306 μm at a Total Exposure Time of 0.5 Seconds.

A plot of the allowed output energy per pulse as a percentage of the maximum allowed output energy per pulse (solid line) and the averaged allowed output energy in one second as a percentage of the maximum average allowed output energy in a second (dashed line), both as functions of pulse repetition frequency (PRF). The discontinuities occur with increasing PRF when it is possible for one more pulse to appear inside a time interval equal to the total exposure time. The 2 possible optimum operating points are just under 2 and just under 4 Hertz.

Source: Kohl, R. H., and Guthrie, M. J. "A Feasibility Study of a Lidar Transmissometer Technique for the Slant Visual Range Problem in Aircraft Landing Approaches," NAS8-32635, National Aeronautics and Space Administration, Marshall Space Flight Center, Alabama (1978), p. 59.

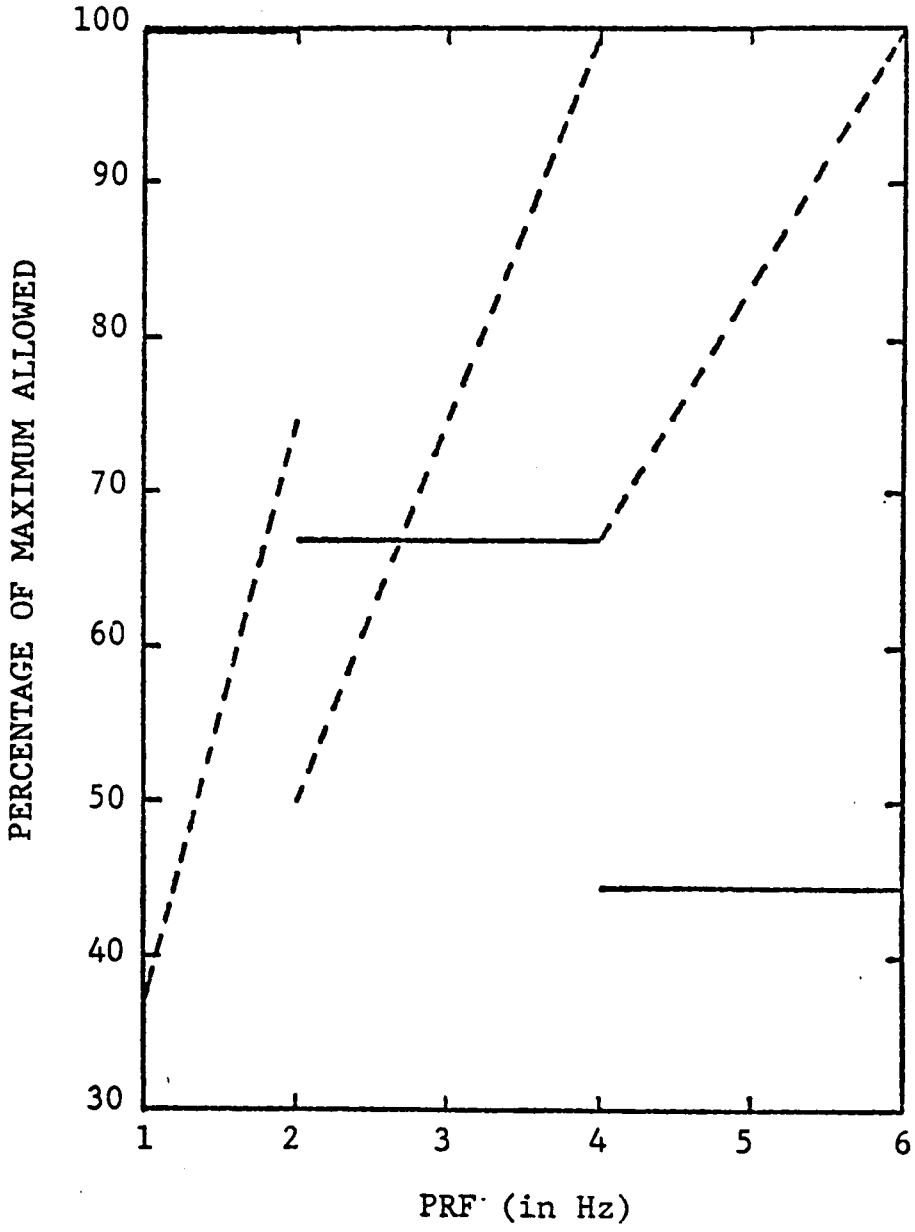
100
90
80
70
60
50
40
30
PERCENTAGE OF MAXIMUM ALLOWED
1
2
3
4
5
6
PRF (in Hz)

Figure 3.3.

for the TTE is attained. The PRF can then be increased to the value that just prevents one more pulse from entering the TTE. This PRF is the optimum under the condition of meeting the operational minimum PRF (MPRF), and is just less than the largest integer of the product (TTE)(MPRF) divided by the TTE. The distinction between this optimum PRF and the MPRF is significant only when the number of pulses in the TTE, (MPRF)(TTE) is small.

Maximum Allowed Output Energy

Using ANSI Z136.1-1976 and the Sliney Patch, the eye-safe allowed output energy per unit area per pulse (AOEPP) and the average allowed output energy per unit area per second (AAOE) were determined. The AAOE is obtained by simply multiplying the AOEPP by the PRF. These values were obtained for the wavelengths, TTE's, PRF's, and pulse lengths in the regions discussed above. The AOEPP is at a maximum for PRF's at the optimum and below, and the AAOE is at its maximum for PRF's at the optimum and above. Thus, at the optimum PRF both will be a maximum.

Figure 3.4 shows the maximum AOEPP obtained by using an MPRF of 1 Hz. The choice of an MPRF of 1 Hz affects the values for all TTE's in the wavelength region from about .3 μm to .2 μm , and in the wavelength region .314 μm to .4 μm when the pulselength is 200 nsec and the TTE is

Figure 3.4. Maximum Allowed Output Energy Per Pulse for An Eye Safe Lidar (Bare Eye) With an Operational Minimum Frequency of 1 Hz.

The specific choice of 1 Hz affects the values for all total exposure times in the wavelength interval from about 0.3 micrometers to 0.2 micrometers, and for total exposure times of greater than 82 seconds at 200 nanoseconds pulsewidth from 0.315 to 0.4 micrometers. The values from 0.2 to about 0.3 micrometers and in the infrared are here pulsewidth independent.

Source: Kohl, R. H., and Guthrie, M. J. "A Feasibility Study of a Lidar Transmissometer Technique for the Slant Visual Range Problem in Aircraft Landing Approaches," NAS8-32635, National Aeronautics and Space Administration, Marshall Space Flight Center, Alabama (1978), p. 63.

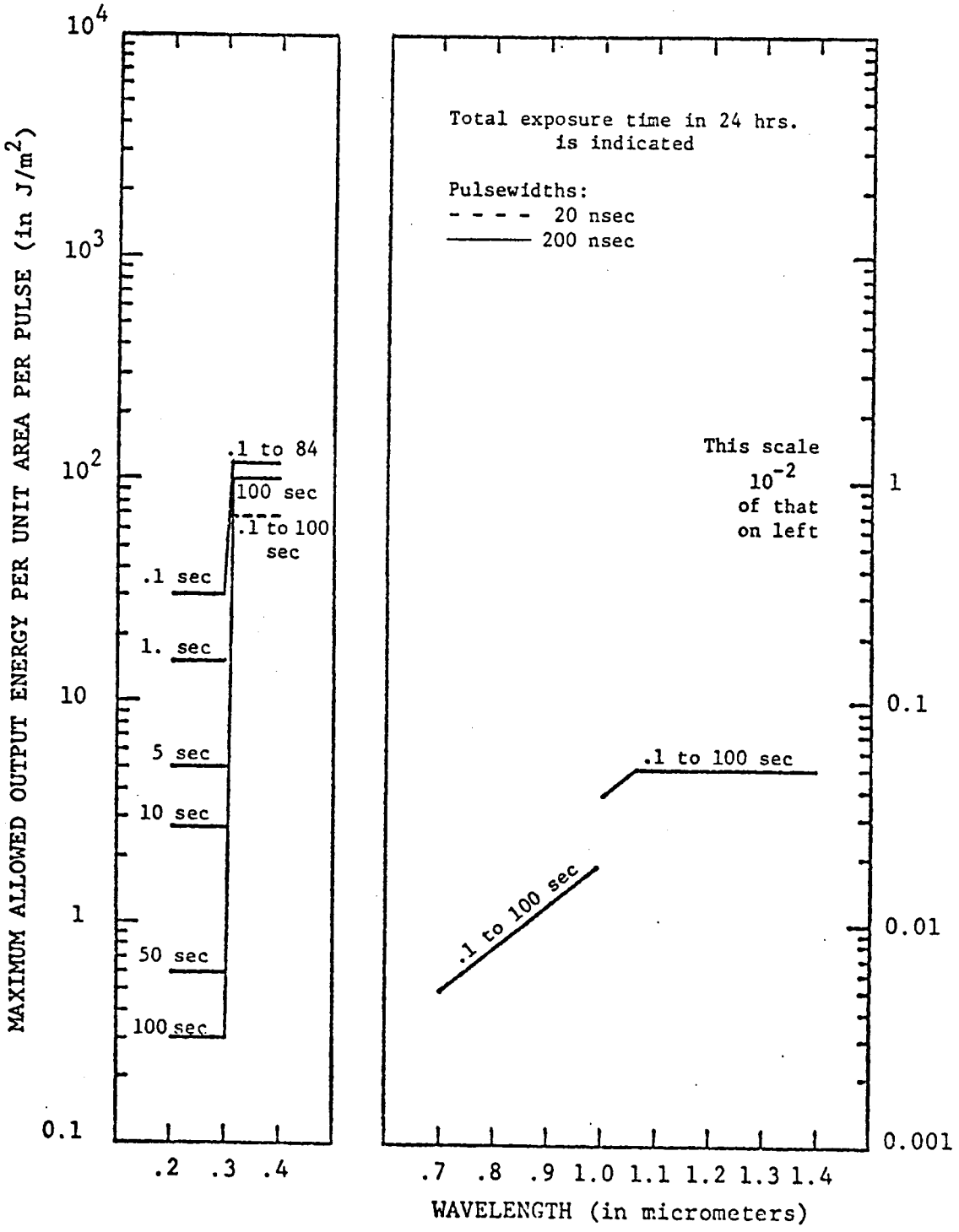
MAXIMUM ALLOWED OUTPUT ENERGY PER UNIT AREA PER PULSE (in J/m²)
10⁴
10³
10²
10
1
0.1
.1 to 84
100 sec
.1 to 100 sec
.1 sec
1. sec
5 sec
10 sec
50 sec
100 sec
.2 .3 .4
Total exposure time in 24 hrs. is indicated
Pulsewidths:
- - - - 20 nsec
——— 200 nsec
This scale 10⁻² of that on left
1
0.1
0.01
0.001
.1 to 100 sec
.1 to 100 sec
.7 .8 .9 1.0 1.1 1.2 1.3 1.4
WAVELENGTH (in micrometers)

Figure 3.4.

greater than 84 sec. The values of the AOEPP are independent of the pulselength in the near IR and from .2 μm to .3 μm in the near UV.

Figure 3.5 shows the maximum AAOE values obtained by using the optimum PRF's given in Figure 3.1, page 36. It can be seen that the maximum AAOE is independent of the pulselength. In the wavelength region from .315 μm to .4 μm the maximum AAOE is inversely proportional to $(TTE)^{3/4}$, and in the near IR region from .7 μm to 1.4 μm it is inversely proportional to $(TTE)^{1/4}$.

Figures 3.6 and 3.7 show the maximum AOEPP and maximum AAOE weighted by $(1/\lambda)^4$, since Rayleigh and Raman scattering cross-sections are proportional to $(1/\lambda)^4$.

Figures 3.8 through 3.11 give the same results obtained above but these have been put in terms of photon numbers rather than energy.

Figure 3.5. Maximum Allowed Average Output Energy in a Second for an Eye Safe Lidar (Bare Eye).

The total exposure times are indicated. Note that there is no dependence on pulsewidth.

Source: Kohl, R. H., and Guthrie, M. J. "A Feasibility Study of a Lidar Transmissometer Technique for the Slant Visual Range Problem in Aircraft Landing Approaches," NAS8-32635, National Aeronautics and Space Administration, Marshall Space Flight Center, Alabama (1978), p. 65.

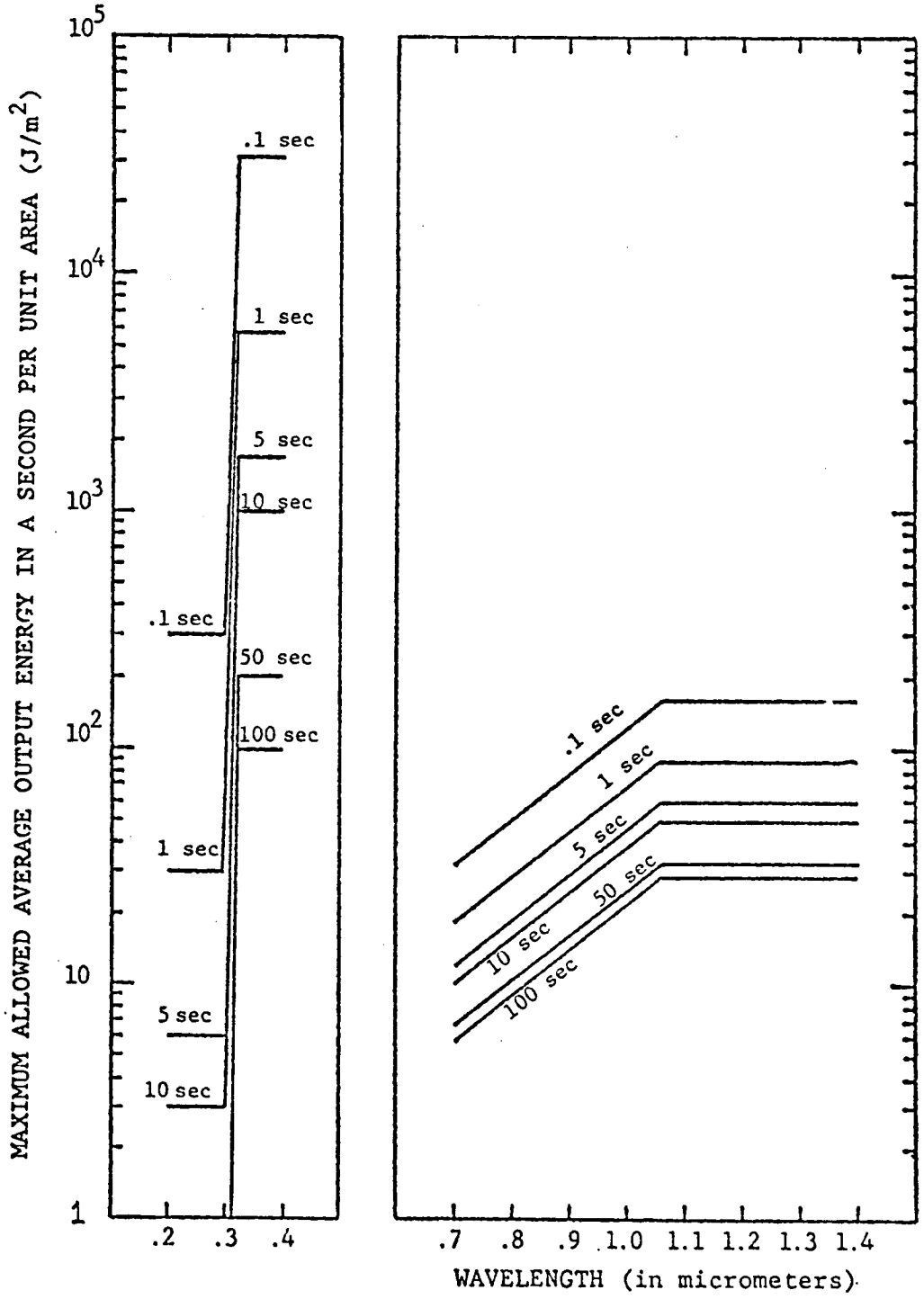
MAXIMUM ALLOWED AVERAGE OUTPUT ENERGY IN A SECOND PER UNIT AREA (J/m²)
10⁵
10⁴
10³
10²
10
1
.1 sec
1 sec
5 sec
10 sec
.1 sec
50 sec
100 sec
1 sec
5 sec
10 sec
.2
.3
.4
.1 sec
1 sec
5 sec
10 sec
50 sec
100 sec
.7
.8
.9
1.0
1.1
1.2
1.3
1.4
WAVELENGTH (in micrometers)

Figure 3.5.

Figure 3.6. Scattering Efficiency Weighted Maximum Allowed Output Energy per Pulse.

From 0.2 micrometers to about 0.3 micrometers and in the near infrared the values shown are pulse length independent. The weighting used is the inverse of wavelength to the fourth power, appropriate for Rayleigh and non-resonant Raman scattering.

Source: Kohl, R. H., and Guthrie, M. J. "A Feasibility Study of a Lidar Transmissometer Technique for the Slant Visual Range Problem in Aircraft Landing Approaches," NAS8-32635, National Aeronautics and Space Administration, Marshall Space Flight Center, Alabama (1978), p. 67.

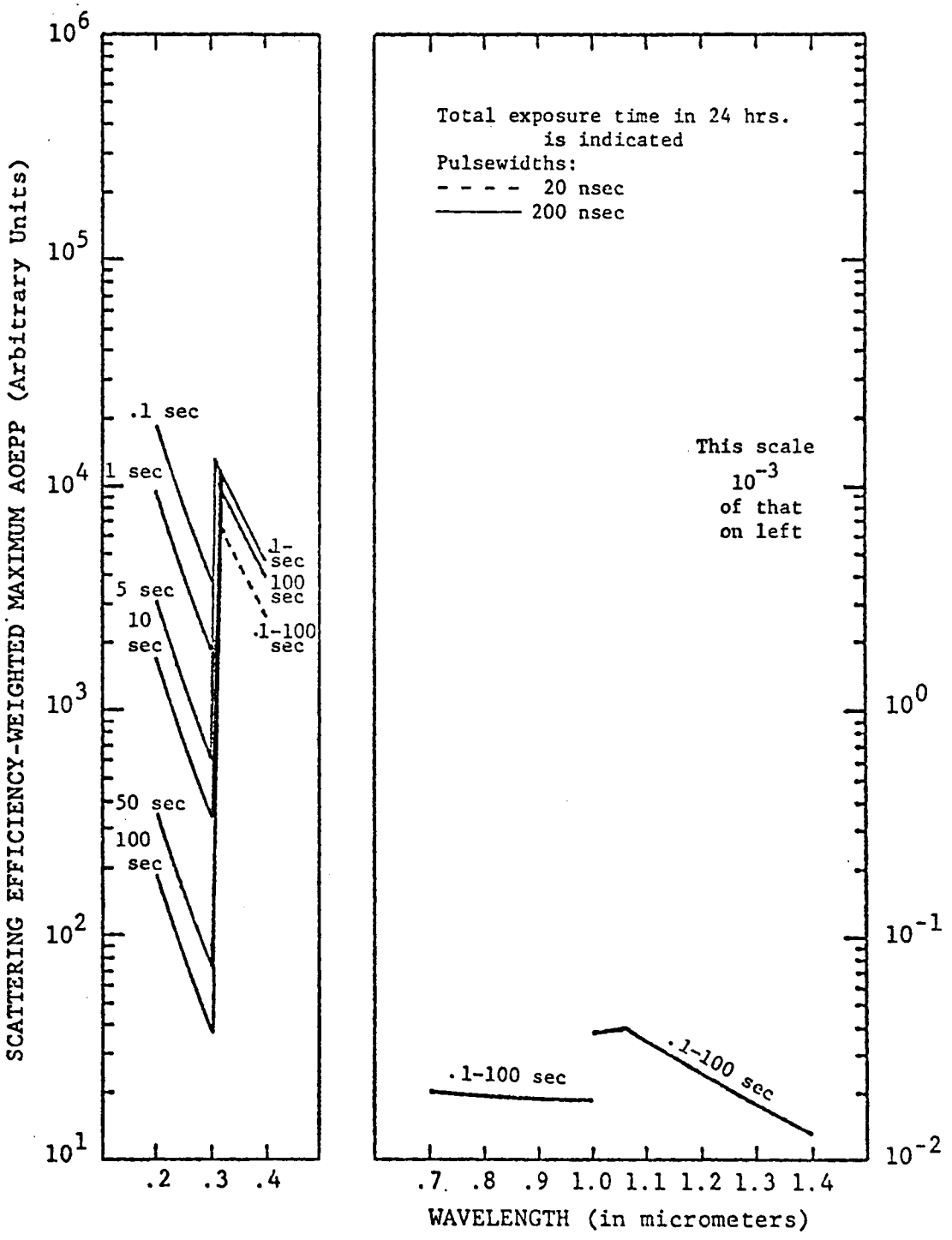
SCATTERING EFFICIENCY-WEIGHTED MAXIMUM AOEPP (Arbitrary Units)
10^6
10^5
10^4
10^3
10^2
10^1
.1 sec
1 sec
5 sec
10 sec
50 sec
100 sec
.1-sec
100 sec
.1-100 sec
.2 .3 .4
Total exposure time in 24 hrs. is indicated
Pulsewidths:
- - - - 20 nsec
——— 200 nsec
This scale 10^{-3} of that on left
10^0
10^{-1}
10^{-2}
.1-100 sec
.1-100 sec
.7 .8 .9 1.0 1.1 1.2 1.3 1.4
WAVELENGTH (in micrometers)

Figure 3.6.

Figure 3.7. Scattering Efficiency Weighted Maximum Allowed Average Output Energy in a Second.

Total exposure times are indicated. Note that there is no dependence on pulsewidth. The weighting is as in Figure 3.6.

Source: Kohl, R. H., and Guthrie, J. J. "A Feasibility Study of a Lidar Transmissometer Technique for the Slant Visual Range Problem in Aircraft Landing Approaches," NAS8-32635, National Aeronautics and Space Administration, Marshall Space Flight Center, Alabama (1978), p. 69.

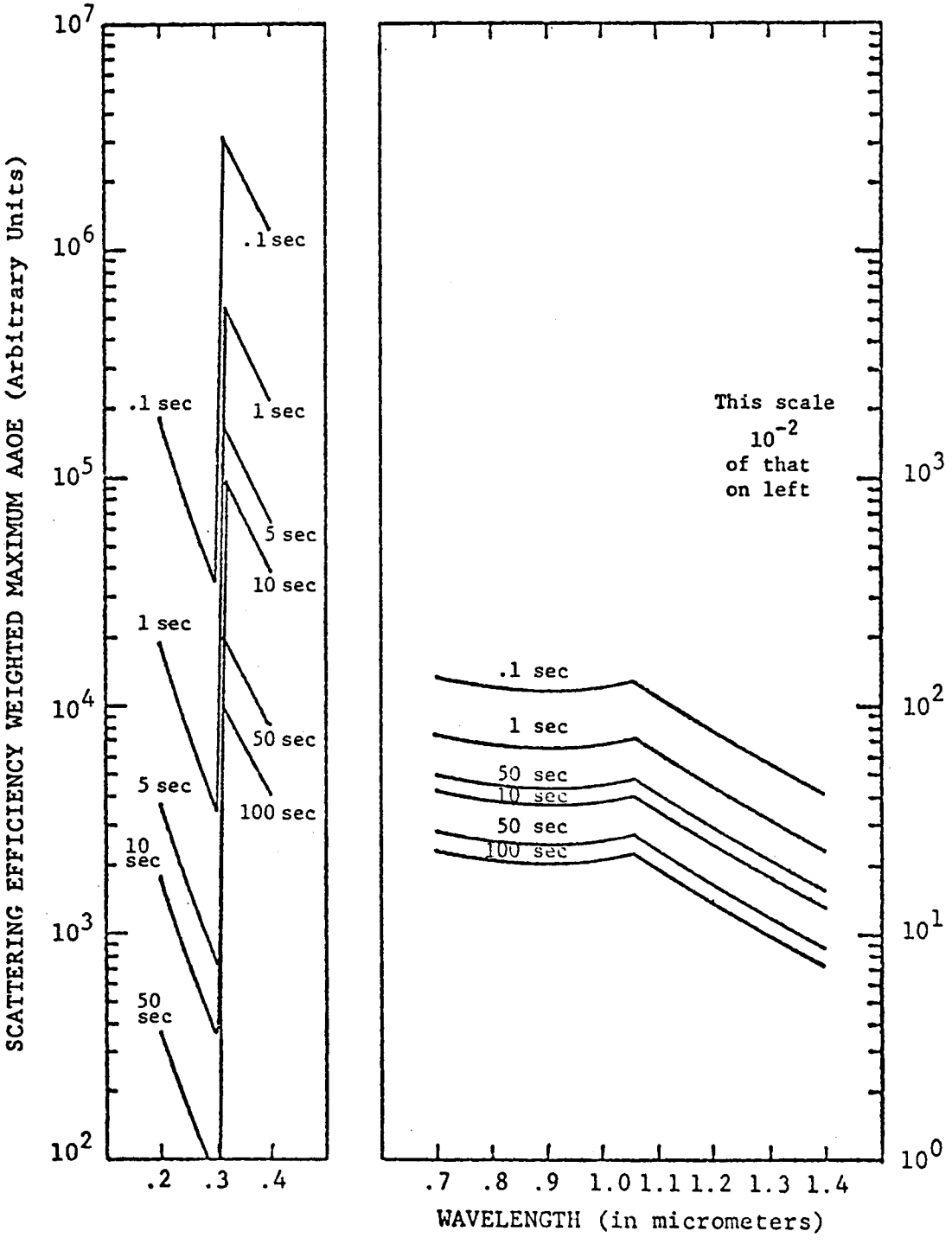
SCATTERING EFFICIENCY WEIGHTED MAXIMUM AAOE (Arbitrary Units)
10^7
10^6
10^5
10^4
10^3
10^2
.1 sec
1 sec
5 sec
10 sec
50 sec
100 sec
.2
.3
.4
This scale
10^{-2}
of that
on left
10^3
10^2
10^1
10^0
.7
.8
.9
1.0
1.1
1.2
1.3
1.4
WAVELENGTH (in micrometers)

Figure 3.7.

Figure 3.8. Maximum Allowed Output Photons Per Pulse Per Unit Area for an Eye Safe Lidar (Bare Eye) With an Operational Minimum Pulse Frequency of 1 Hz.

The values from 0.2 to about 0.3 micrometers and in the near infrared are here pulsewidth independent. See caption on Figure 3.4, page 44.

Source: Kohl, R. H., and Guthrie, M. J. "A Feasibility Study of a Lidar Transmissometer Technique for the Slant Visual Range Problem in Aircraft Landing Approaches," NAS8-32635, National Aeronautics and Space Administration, Marshall Space Flight Center, Alabama (1978), p. 72.

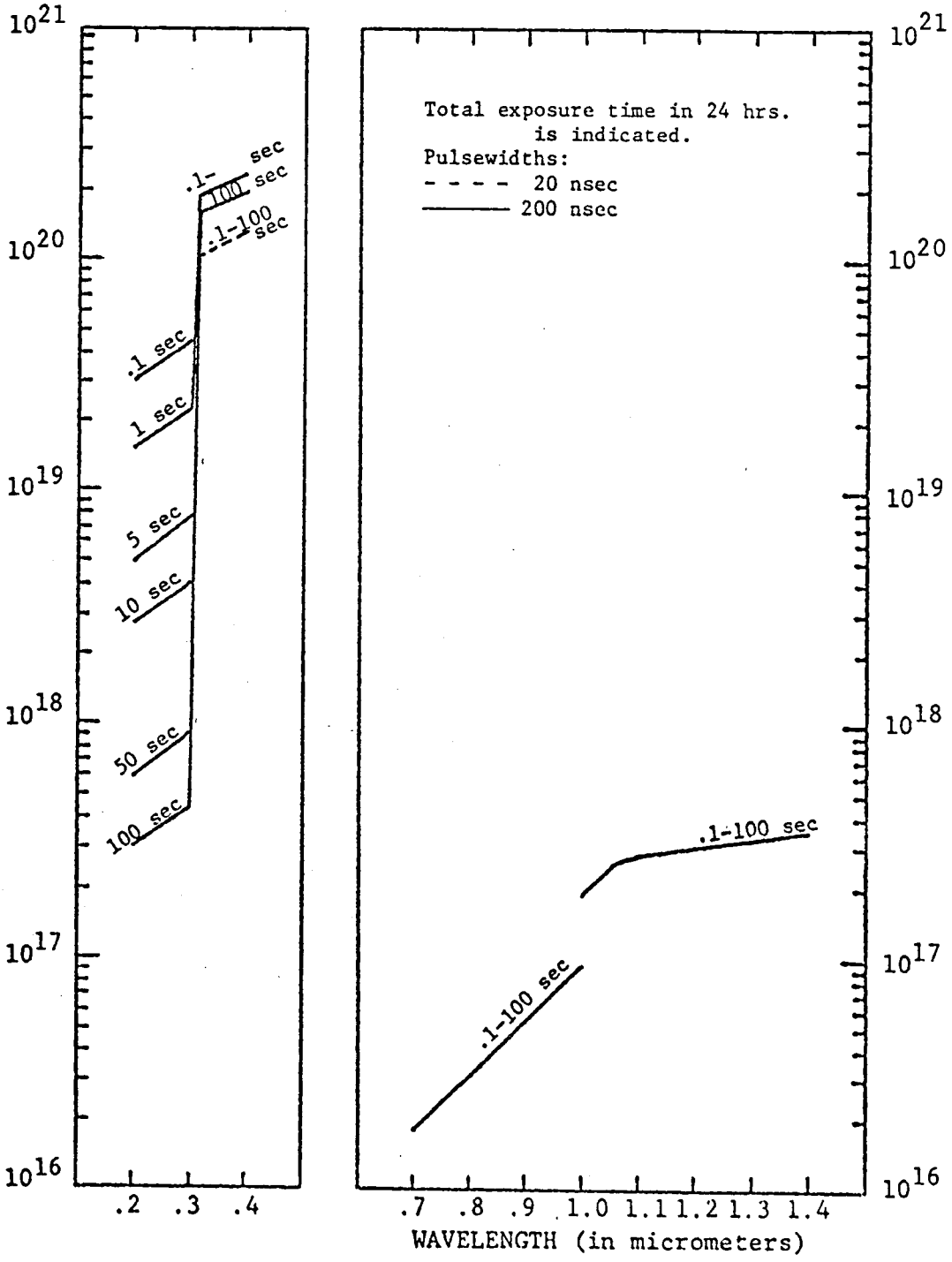
10^{21}
10^{20}
10^{19}
10^{18}
10^{17}
10^{16}
.1- sec
.1-100 sec
.1 sec
1 sec
5 sec
10 sec
50 sec
100 sec
.2 .3 .4
Total exposure time in 24 hrs. is indicated.
Pulsewidths:
- - - - 20 nsec
——— 200 nsec
.1-100 sec
.1-100 sec
.7 .8 .9 1.0 1.1 1.2 1.3 1.4
WAVELENGTH (in micrometers)

Figure 3.8.

Figure 3.9. Maximum Allowed Average Output Photons in a Second for an Eye Safe Lidar (Bare Eye).

The total exposure times are indicated. Note that there is no dependence on pulsewidth.

Source: Kohl, R. H., and Guthrie, M. J. "A Feasibility Study of a Lidar Transmissometer Technique for the Slant Visual Range Problem in Aircraft Landing Approaches," NAS8-32635, National Aeronautics and Space Administration, Marshall Space Flight Center, Alabama (1978), p. 74.

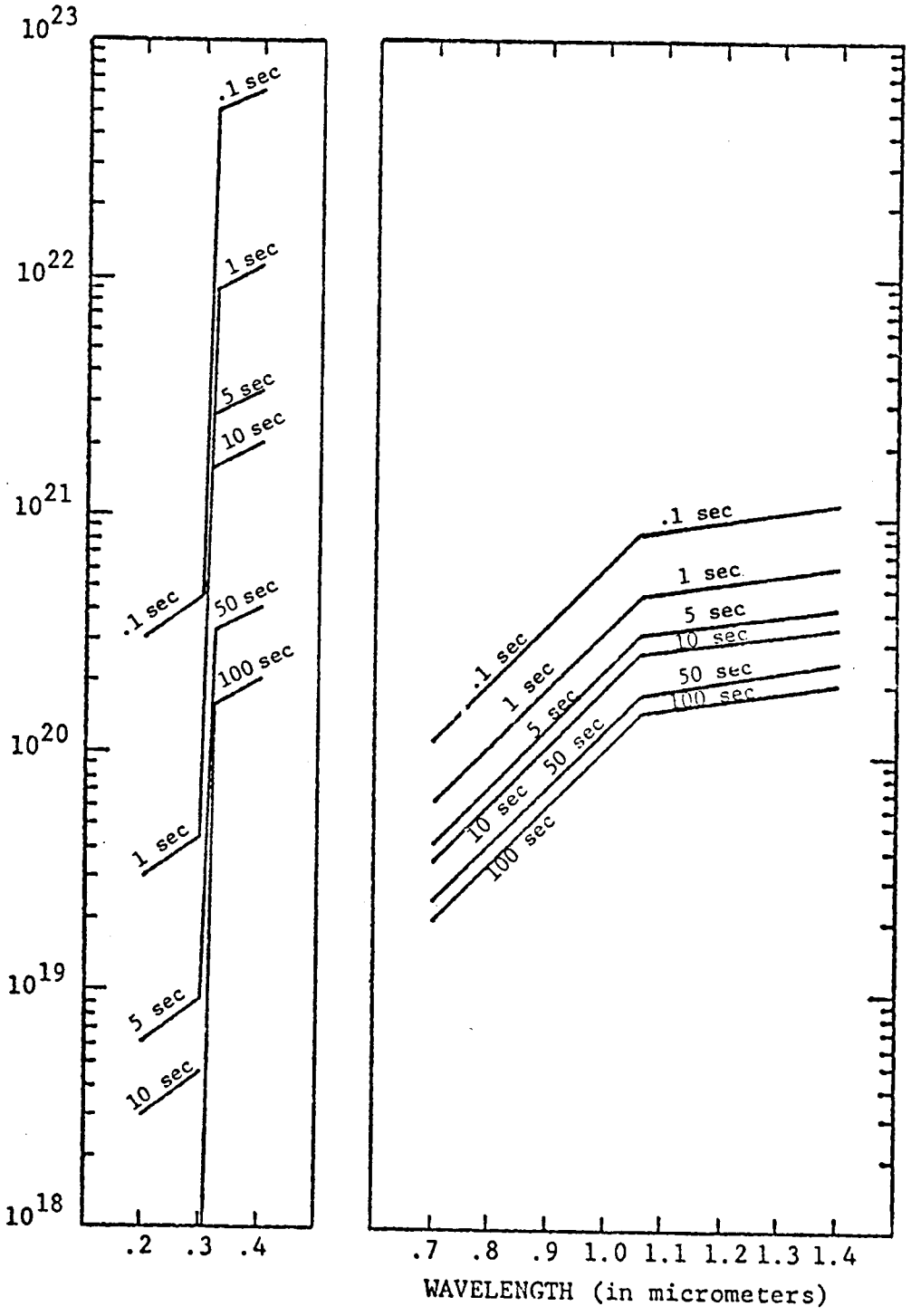
10^{23}
10^{22}
10^{21}
10^{20}
10^{19}
10^{18}
.1 sec
1 sec
5 sec
10 sec
50 sec
100 sec
.2
.3
.4
.7
.8
.9
1.0
1.1
1.2
1.3
1.4
WAVELENGTH (in micrometers)

Figure 3.9.

Figure 3.10. Scattering Efficiency Weighted Maximum Allowed Output Photons per Pulse.

From 0.2 micrometers to about 0.3 micrometers and in the near infrared the values shown are pulse length independent. The weighting used is the inverse of wavelength to the fourth power, appropriate for Rayleigh and non-resonant Raman scattering.

Source: Kohl, R. H., and Guthrie, M. J. "A Feasibility Study of a Lidar Transmissometer Technique for the Slant Visual Range Problem in Aircraft Landing Approaches," NAS8-32635, National Aeronautics and Space Administration, Marshall Space Flight Center, Alabama (1978), p. 76.

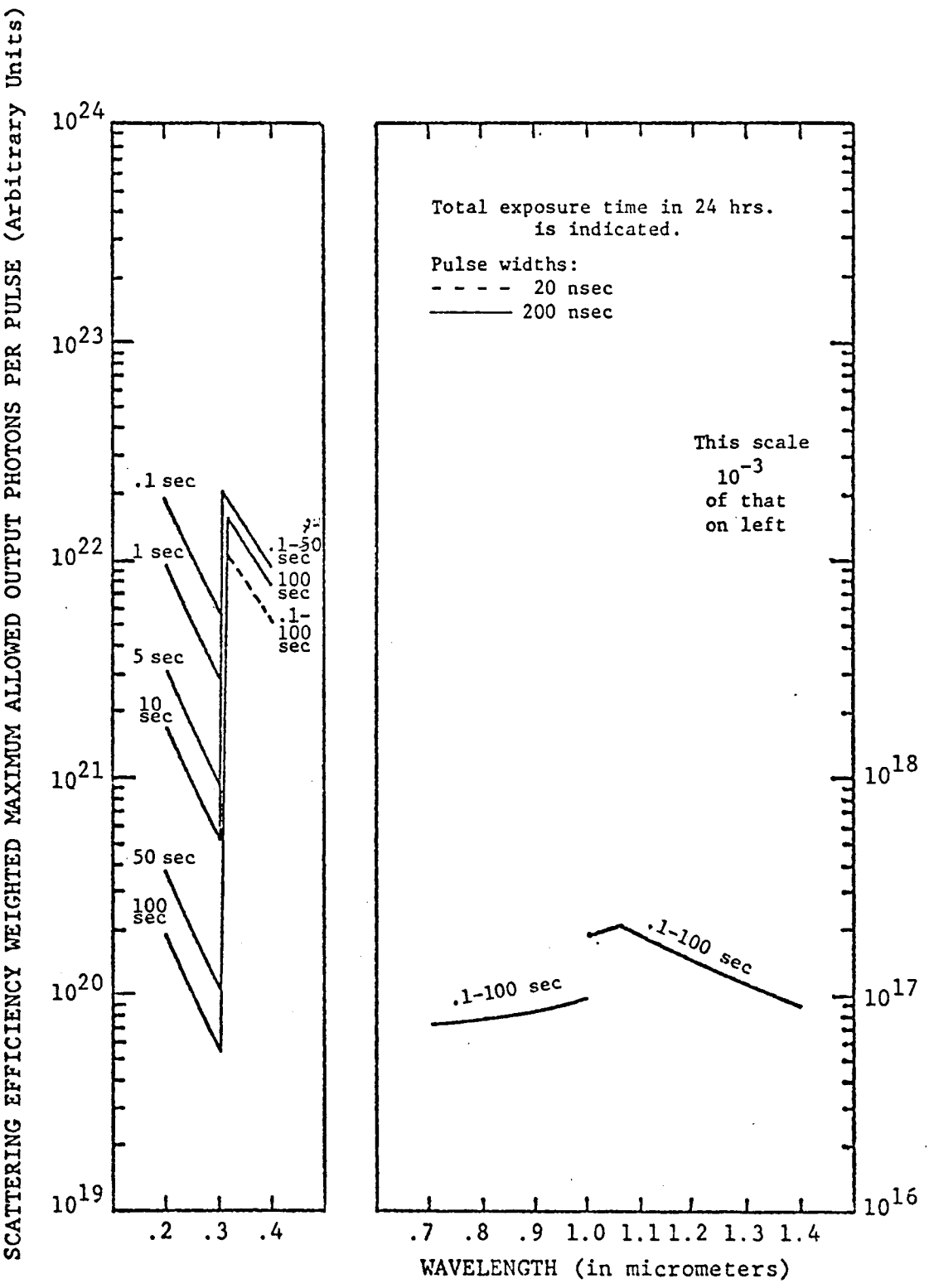
SCATTERING EFFICIENCY WEIGHTED MAXIMUM ALLOWED OUTPUT PHOTONS PER PULSE (Arbitrary Units)
10^{24}
10^{23}
10^{22}
10^{21}
10^{20}
10^{19}
.1 sec
1 sec
5 sec
10 sec
50 sec
100 sec
.1-50 sec
100 sec
.1-100 sec
.2 .3 .4
Total exposure time in 24 hrs. is indicated.
Pulse widths:
- - - - 20 nsec
——— 200 nsec
This scale 10^{-3} of that on left
10^{18}
10^{17}
10^{16}
.1-100 sec
.1-100 sec
.7 .8 .9 1.0 1.1 1.2 1.3 1.4
WAVELENGTH (in micrometers)

Figure 3.10.

Figure 3.11. Scattering Efficiency Weighted Maximum Allowed Average Output Photons in a Second.

The weighting is as in Figure 3.10.

Source: Kohl, R. H., and Guthrie, M. J. "A Feasibility Study of a Lidar Transmissometer Technique for the Slant Visual Range Problem in Aircraft Landing Approaches," NAS8-32635, National Aeronautics and Space Administration, Marshall Space Flight Center, Alabama (1978), p. 78.

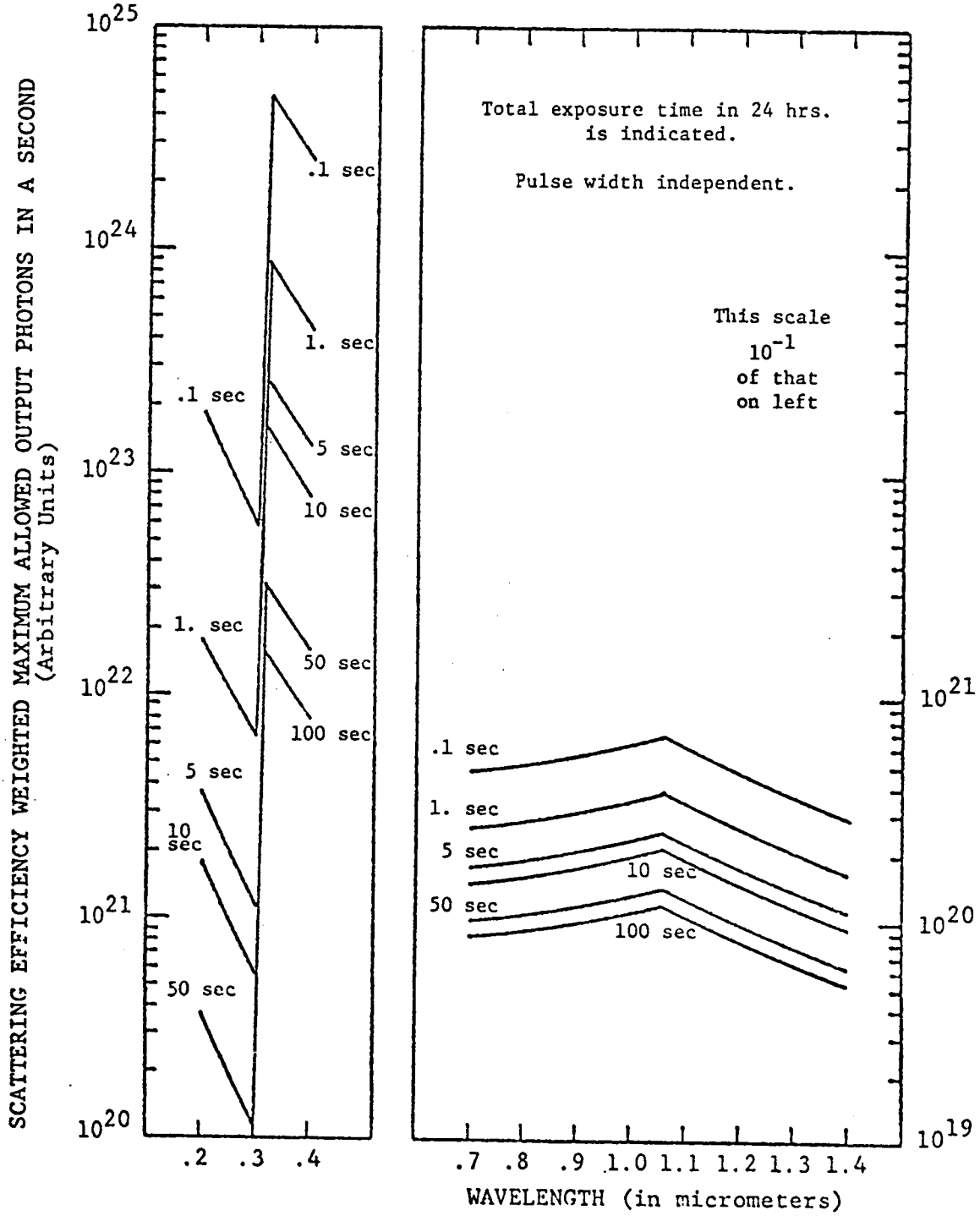
SCATTERING EFFICIENCY WEIGHTED MAXIMUM ALLOWED OUTPUT PHOTONS IN A SECOND
(Arbitrary Units)
10^{25}
10^{24}
10^{23}
10^{22}
10^{21}
10^{20}
.1 sec
1. sec
5 sec
10 sec
50 sec
100 sec
Total exposure time in 24 hrs.
is indicated.
Pulse width independent.
This scale
10^{-1}
of that
on left
10^{21}
10^{20}
10^{19}
.2 .3 .4
.7 .8 .9 1.0 1.1 1.2 1.3 1.4
WAVELENGTH (in micrometers)

Figure 3.11.

CHAPTER IV

RAMAN SCATTERING LIDAR SYSTEMS AND THE RAMAN SCATTERING CROSS SECTION

Introduction to Raman Lidar

A spectral analysis of light scattered from molecules in gases reveals sideband frequencies ν_R that are shifted up and down in frequency from the incident frequency ν_o . These shifts are equal to the vibrational-rotational frequencies, ν_{vr} , of the molecules. Thus, ν_r is given by

$$\nu_R = \nu_o \pm \nu_{vr} \cdot \qquad (4\text{-}1)$$

The sideband frequencies that are below ν_o are called Stokes lines, while those above ν_o are called anti-Stokes lines. Each molecule has unique values of ν_{vr} and therefore the Raman scattered frequencies give a direct indication of the molecular species present [16,17,18,19,20].

Figure 4.1 shows a schematic of a lidar system that utilizes Raman scattering. The system is essentially the same as that shown in Figure 1.3 (page 8) except that it has the specific capability of looking at the return radiation at wavelengths other than that transmitted.

As discussed in Chapter I, the spectrum of the back-scattered radiation consists of the Rayleigh and Mie

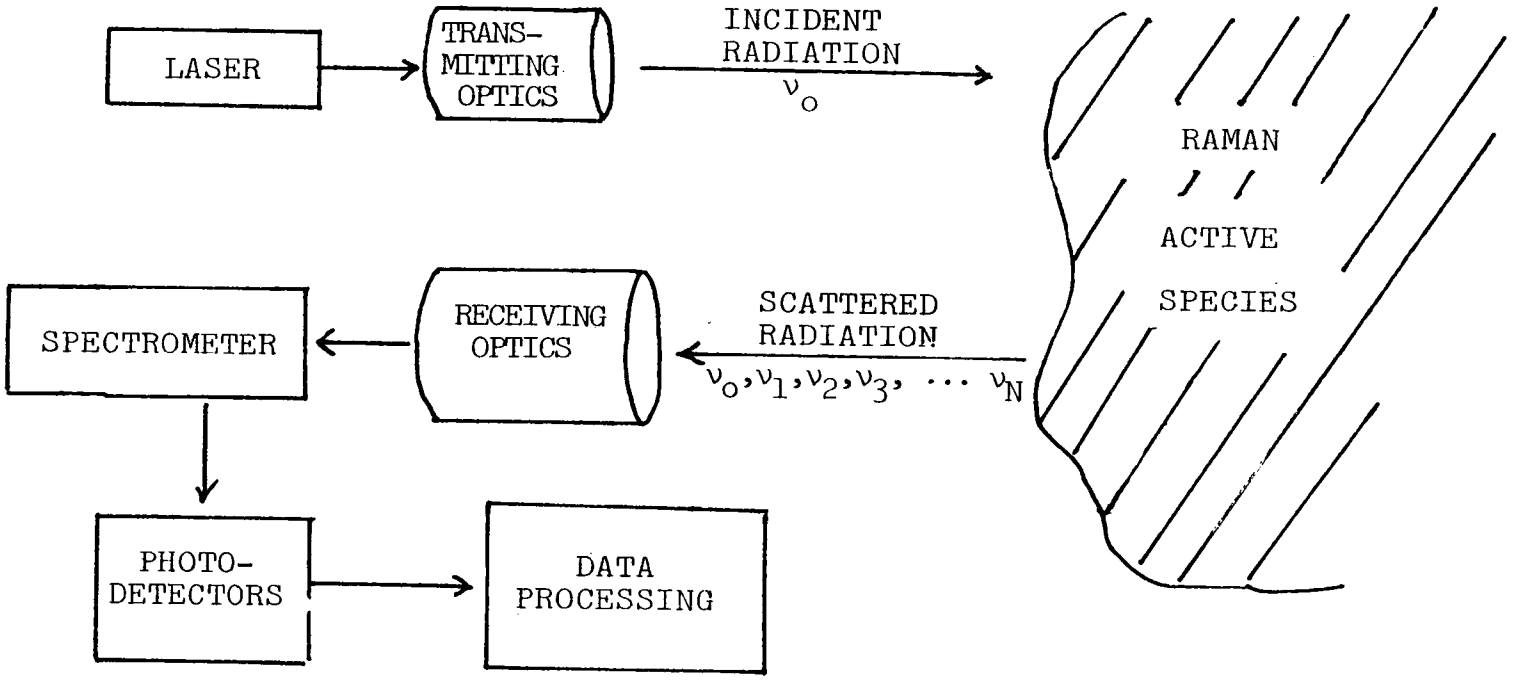

Figure 4.1. Arrangement of a Raman Lidar System.

scattered components at essentially the same frequency as the transmitted laser frequency, ν_o , and the Raman shifted frequencies ν_1 , ν_2 , ν_3 , ... ν_n due to the Raman active molecules in the atmosphere. These spectral components may be detected and analyzed for such information as the molecular species, concentrations, and location in the atmosphere. Figure 4.2 shows some of the frequency shifts of the vibrational-rotational Raman spectra of molecules found in the atmosphere.

Experimental Raman Lidar Systems

Raman lidar systems have been used for the study of major components of the atmosphere since 1967, when Leonard [21] first detected Raman scattering from atmospheric O_2 and N_2 using a pulsed N_2 laser. Since then Raman scattering has been used in various applications such as monitoring pollutants, temperature profiles, and water vapor profiles [2,22]. Cooney [23] has measured the Raman intensity from N_2 molecules as a function of range up to 3 km, employing a Q-switched ruby laser with 250 MW peak output at 694.3 nm. Melfi, et al. [24], have observed Raman backscatter from atmospheric N_2, O_2, and H_2O at night. Their system employed a frequency doubled ruby laser with an output power of .04 Joules at 3471.5Å and a 40 cm diameter receiving telescope. They were able

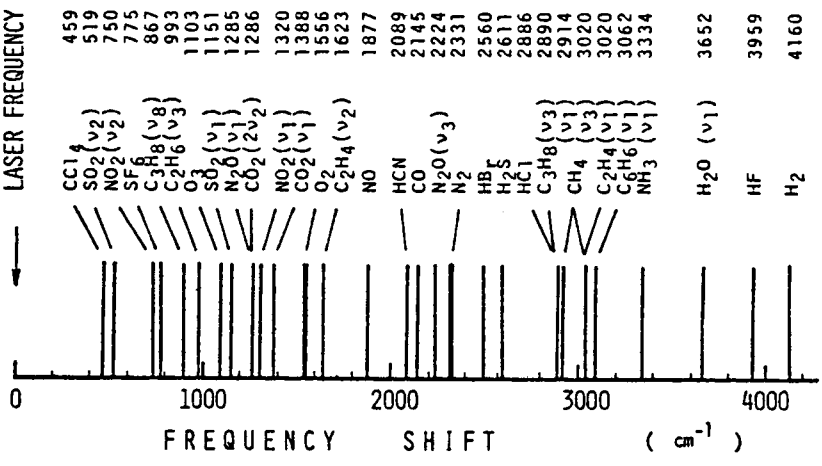

Figure 4.2. Q-Branch of Vibrational-Rotational Raman Spectra of Molecules Found in the Atmosphere.

Source: H. Inaba, T. Kobayasi, Opto-Electronics 4 (1972), pp. 101-123.

to obtain water vapor mixing ratios up to around 2.5 km by observing the ratio of H_2O to N_2 Raman backscattered intensities. The Raman scattered wavelengths were observed using both a double monochromator and interference filters.

Hirschfeld, et al. [25], have reported the remote detection of H_2O, SO_2, CO_2 and kerosene vapor under controlled conditions with a range resolution of 10 m in daylight operation. This system consisted of an 8 percent efficient frequency doubled ruby laser with a 2 J output and a pulse repetition frequency of 2 Hz. The receiver consisted of a 90 cm aperture telescope and a Czerny Turner polychromator with a bandwidth of 5Å. The estimated detection ability was about 30 PPM of SO_2 and 1.7 PPM of kerosene at a distance of 200 m. Figure 4.3 shows N_2 returns obtained by this system in terms of counts per minute over a distance of up to 700 m under thin fog conditions.

The measurement of transmission utilizing Raman scattering has been demonstrated by Leonard and Caputo [26]. They have conducted experiments over distances of a quarter-mile and produced consistent results when compared to measurements using a double-ended device. The measurements were performed using a pulsed N_2 laser operating at a peak power of 100 KW, a pulse duration of 10 nsec, and

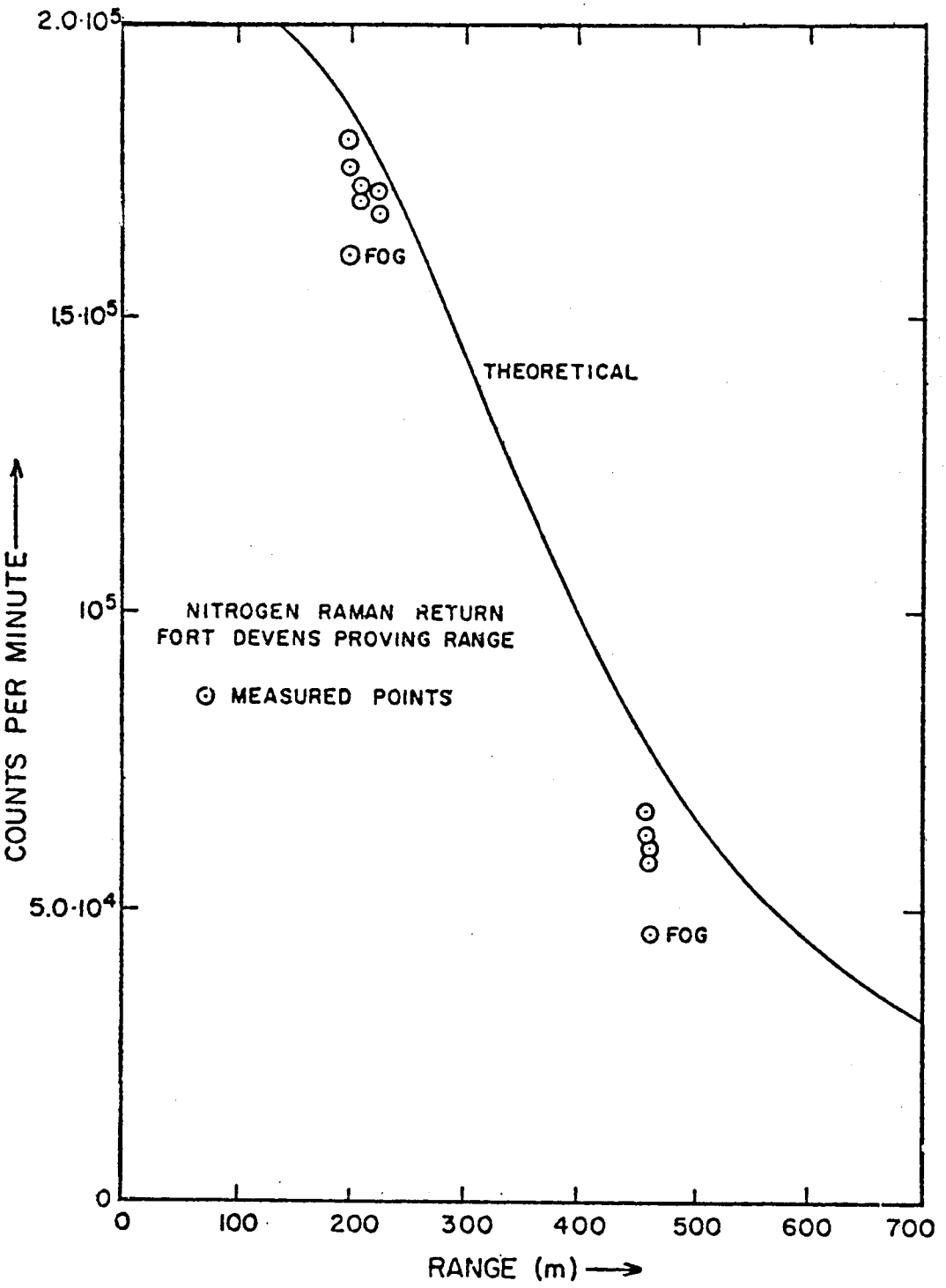

Figure 4.3. N_2 Raman Returns.

Source: Hirschfeld, T., Sshildkraut, E. R., Tannenbaum, Harvey, and Tannenbaum, David. "Remote Spectroscopic Analysis of PPM-Level Air Pollutants by Raman Spectroscopy," Appl. Physics Lett., Vol. 22, No. 1, 1973.

a pulse repetition frequency of 500 Hz. Their receiving system consisted of a 25 cm Newtonian telescope and a SPEX Model 1702 scanning spectrometer. They utilized non-resonant Raman scattering from N_2 with before and after comparison to obtain the transmittance.

An analysis of a lidar system utilizing resonance Raman scattering has been reported by Rosen, et al. [27]. This analysis has been primarily performed in the interest of detecting pollutants in the atmosphere. Their results are based on an expression for strong resonance Raman scattering cross sections obtained from using an approximation similar to that described later in this chapter. They assumed a tunable laser matched to the electronic transition resonance of the molecules with an output energy of .05 mJ and a pulse repetition frequency of 100 Hz. These values were assumed to prevent potential eye-safety hazards. For the detector parameters they used a collector area of 1 m^2, total detection efficiency of .1, a detector field of view of 10^{-5} sr, and a detector bandwidth of .1 nm. Under these conditions and a range resolution of 10 m, they predicted that SO_2 and NO concentrations greater than 10 PPM could be detected in daylight over distances of a few hundred meters. This sensitivity is about 10 times the sensitivity of the system reported by Hirschfeld, et al., using ordinary Raman scattering, and is achieved at lower

laser output energy which is desired in the interest of eye safety.

The Raman-Scattering Cross Section

For the Raman scattering process, the value of $\beta_g(r)$ in Equation (2-16) is given by the product

$$\beta_g(r) = N(r) \frac{d\sigma}{d\Omega_R} \qquad (4-2)$$

where $N(r)$ is the number density of the Raman scattering species at the distance r, and $d\sigma/d\Omega_R$ is the Raman scattering cross section per molecule of the species.

The Raman scattering cross section, $d\sigma/d\Omega_R$, is the basic quantity required to calculate the return signal observed by a lidar from a given molecular species.

Non-Resonant Raman Cross Sections

Equation (A-34) in Appendix II gives the general quantum mechanical expression for the differential transition probability for light scattering. With the assumption that the incident frequency, ν_o, is much less than any electronic transition of the molecule, i.e., the off resonance condition, Melfi [28] has evaluated this expression for the pure rotational and vibrational-rotational cross sections using Placzek's polarizability theory [29]. If α, β and α', β' are the isotropic and

anisotropic part of the polarizability in the molecular and laboratory coordinate systems respectively, he obtained for homonuclear molecules:

(1) Rayleigh and pure rotational Raman cross sections

$$\left(\frac{d\sigma}{d\Omega}\right)_{\parallel} = \frac{\omega_o^4}{c^4}\left(\alpha^2 + \frac{1}{45}\beta^2\right) \qquad \text{for } \Delta J = 0 , \qquad (4\text{-}3)$$

$$\left(\frac{d\sigma}{d\Omega}\right)_{\parallel} = \frac{\omega_o^4}{c^4}\frac{3}{45}\beta^2 \qquad \text{for all transitions } \Delta J = \pm 2 , \qquad (4\text{-}4)$$

$$\left(\frac{d\sigma}{d\Omega}\right)_{\perp} = \frac{\omega_o^4}{c^4}\left(\frac{3}{180}\beta^2\right) \qquad \text{for } \Delta J = 0 , \qquad (4\text{-}5)$$

and $$\left(\frac{d\sigma}{d\Omega}\right)_{\perp} = \frac{\omega_o^4}{c^4}\left(\frac{9}{180}\beta^2\right) \qquad \text{for all transitions } \Delta J = \pm 2 , \qquad (4\text{-}6)$$

where $\omega_o = 2\pi\nu_o$, J is the change in rotational quantum number from the initial to final state, and the symbols $\parallel$ and $\perp$ indicate the polarization of the scattered light parallel and perpendicular to the incident light polarization, respectively.

(2) Vibrational-rotational Raman cross sections

$$\left(\frac{d\sigma}{d\Omega}\right)_{\parallel} = \frac{\omega_R^4}{c^4}\frac{\hbar}{2m\omega_{vr}}\left(\frac{\alpha'^2 + \frac{1}{45}\beta'^2}{1 - e^{-\hbar\omega_{vr}/KT}}\right) \qquad \text{for } \Delta J = 0 \quad \Delta v = +1 , \qquad (4\text{-}7)$$

$$\left(\frac{d\sigma}{d\Omega}\right)_{\parallel} = \frac{\omega_R^4}{c^4}\frac{\hbar}{2m\omega_{vr}}\frac{\frac{3}{45}\beta'^2}{1 - e^{-\hbar\omega_{vr}/KT}} \qquad \text{for all transitions } \Delta J \pm 2\Delta v = +1 , \qquad (4\text{-}8)$$

$$\left(\frac{d\sigma}{d\Omega}\right)_{\perp} = \frac{\omega_R^4}{c^4} \frac{\hbar}{2m\omega_{vr}} \frac{\frac{3}{180}\beta'^2}{1 - e^{-\hbar\omega_{vr}/KT}} \quad \text{for } \Delta J = 0,\ \Delta v = +1, \tag{4-9}$$

$$\left(\frac{d\sigma}{d\Omega}\right)_{\perp} = \frac{\omega_R^4}{c^4} \frac{\hbar}{2m\omega_{vr}} \frac{\frac{9}{180}\beta'^2}{1 - e^{-\hbar\omega_{vr}/KT}} \quad \text{for all transitions } \Delta J = 2,\ \Delta v = +1, \tag{4-10}$$

where v is the vibrational quantum number of the state, $\omega_{vr} = 2\pi\nu_{vr}$ and $\omega_R = \omega_o - \omega_{vr}$. Transitions involving $\Delta v = -1$ were not considered since the effect is negligible in the temperature range of interest in this study.

Table IV.1 gives molecular constants used by Melfi to calculate Raman scattering cross sections for N_2 and O_2. Results of these calculations for incident light at 3471.5Å are summarized in Tables IV.2 and IV.3.

Resonant-Raman Scattering Cross Sections

Equation (A-34) in Appendix II could be written approximately as

$$\frac{d\omega}{dr} = \frac{e^4\omega^4}{c^4\hbar^2} \left| \sum_m \frac{\langle n|\vec{R}\cdot\vec{\lambda}'^*|m\rangle\langle m|\vec{R}\cdot\vec{\lambda}|0\rangle}{\omega_{mo} - \omega_o + i\,\gamma_m} + \sum_m \frac{\langle n|\vec{R}\cdot\vec{\lambda}|m\rangle\langle m|\vec{R}\cdot\vec{\lambda}'^*|0\rangle}{\omega_{mn} + \omega_o + i\,\gamma_m} \right|^2 \tag{4-11}$$

where γ_m is the half width of the state m .

Sufficiently near a resonance, one or a few terms in Equation (4-11) will predominate, and unless the

TABLE IV.1

MOLECULAR CONSTANTS OF N_2 AND O_2

	$\alpha \times 10^{24}$ (cm^3)	$\beta \times 10^{24}$ (cm^3)	$\alpha' \times 10^{16}$ (cm^2)	$\beta' \times 10^{16}$ (cm^2)	ν_j $v = 0 \rightarrow 1$	B_e (cm^{-1})	α_e
N_2	1.79	0.95	1.6	2.2	2330.7	2.010	0.0187
O_2	1.63	1.2	1.4	2.3	2554.7	1.44566	0.01579

Source: S. H. Melfi. "Raman Backscatter of Laser Radiation in the Earth's Atmosphere," Ph.D. Dissertation, College of William and Mary, Williamsburg, Virginia (1970), p. 30.

TABLE IV.2

CROSS SECTIONS OF N_2 AND O_2 FOR RAYLEIGH BACKSCATTER AND THE SUM OF THE PURE ROTATIONAL RAMAN BACKSCATTER WITH λ_o = 3471 Å

	$\frac{d\sigma}{d\Omega}(\omega_o)$ $\Delta J = 0$ ($cm^2 ster^{-1}$)	$\frac{d\sigma}{d\Omega}(\omega_o)$ All Transitions $\Delta J = \pm 2$ ($cm^2 ster^{-1}$)	$\frac{d\sigma}{d\Omega}(\omega_o)$ $\Delta J = 0$ ($cm^2 ster^{-1}$)	$\frac{d\sigma}{d\Omega}(\omega_o)$ All Transitions $\Delta J = \pm 2$ ($cm^2 ster^{-1}$)
N_2	3.5×10^{-27}	6.5×10^{-29}	1.6×10^{-29}	3.2×10^{-29}
O_2	2.9×10^{-27}	1.0×10^{-28}	2.6×10^{-29}	5.1×10^{-29}

Source: S. H. Melfi. "Raman Backscatter of Laser Radiation in the Earth's Atmosphere," Ph.D. Dissertation, College of William and Mary, Williamsburg, Virginia (1970), p. 30.

TABLE IV.3

BACKSCATTER CROSS SECTIONS OF N_2 AND O_2 FOR $v = 0 \rightarrow 1$, $\Delta J = 0$ VIBRATIONAL TRANSITION (Q-BRANCH), AND THE SUM OF THE VIBRATION-ROTATION TRANSITIONS (O-BRANCH PLUS S-BRANCH); $\lambda_{N_2} = 3777$ Å, $\lambda_{O_2} = 3669$ Å

	$\frac{d\sigma}{d\Omega}(\omega_o)$ $\Delta J = 0$ ($cm^2 ster^{-1}$)	$\frac{d\sigma}{d\Omega}(\omega_o)$ All Transitions $\Delta J = \pm 2$ ($cm^2 ster^{-1}$)	$\frac{d\sigma}{d\Omega}(\omega_o)$ $\Delta J = 0$ ($cm^2 ster^{-1}$)	$\frac{d\sigma}{d\Omega}(\omega_o)$ All Transitions $\Delta J = \pm 2$ ($cm^2 ster^{-1}$)
N_2	2.1×10^{-30}	2.5×10^{-31}	6.4×10^{-32}	1.3×10^{-31}
O_2	2.4×10^{-30}	4.1×10^{-31}	1.0×10^{-31}	2.0×10^{-31}

Source: S. H. Melfi. "Raman Backscatter of Laser Radiation in the Earth's Atmosphere," Ph.D. Dissertation, College of William and Mary, Williamsburg, Virginia (1970), p. 31.

molecule is highly excited, only the first term in the sum will contribute [30]. Thus, Equation (4-11) becomes

$$\frac{d\omega}{d\Omega} \cong \frac{e^4 \omega_R^4}{c^4 \hbar^2} \left| \sum_m \frac{\langle n|\vec{R} \cdot \vec{\lambda}'^*|m\rangle\langle m|\vec{R} \cdot \vec{\lambda}|0\rangle}{\omega_{mo} - \omega_o + i\,\gamma_m} \right|^2 . \qquad (4\text{-}12)$$

In the case where one intermediate state is involved in the resonance, we have

$$\frac{d\omega}{d\Omega} = \frac{e^4 \omega_R^4}{c^4 \hbar^2} \frac{\left|\langle n|\vec{R} \cdot \vec{\lambda}'^*|m\rangle\right|^2 \left|\langle m|\vec{R} \cdot \vec{\lambda}|0\rangle\right|^2}{(\omega_{mo} - \omega_o)^2 + \gamma_m^2} . \qquad (4\text{-}13)$$

Let $\hat{\phi}$ be the operator that transforms the molecular-fixed coordinates into the space-fixed coordinates. Equation (4-13) may then be written as

$$\frac{d\omega}{d\Omega} = \frac{e^4 \omega_R^4}{c^4 \hbar^2} \frac{\left|\langle n|\hat{\phi}(\vec{R} \cdot \vec{\lambda}'^*)|m\rangle\right|^2 \left|\langle m|\hat{\phi}(\vec{R} \cdot \vec{\lambda})|0\rangle\right|^2}{(\omega_{mo} - \omega_o)^2 + \gamma_m^2} . \qquad (4\text{-}14)$$

The state vectors may be written explicitly in terms of the electronic, vibrational, and rotational states; thus we have

$$\frac{d\omega}{d\Omega} = \frac{e^4 \omega_R^4}{c^4 \hbar^2} \frac{\left|\langle \varepsilon_n v_n J_n|\hat{\phi}(\vec{R} \cdot \vec{\lambda}'^*)|J_m v_m \varepsilon_m\rangle\right|^2}{(\omega_{mo} - \omega_o)^2 + \gamma_m^2} \cdot \left|\langle \varepsilon_m v_m J_m|\hat{\phi}(\vec{R} \cdot \vec{\lambda})|J_o v_o \varepsilon_o\rangle\right|^2 . \qquad (4\text{-}15)$$

The rotational part of the states depend on $\hat{\phi}$ whereas the electronic and vibrational parts of the state vector are independent of $\hat{\phi}$ and we may write Equation (4-15) as

$$\frac{d\omega}{d\Omega} = \frac{e^4 \omega_R^4}{c^4 \hbar^2} \frac{\left|\langle n|\vec{R}\cdot\vec{\chi}'^*|m\rangle\right|^2 \left|\langle m|\vec{R}\cdot\vec{\chi}|0\rangle\right|^2 \left|\langle J_n|\hat{\phi}|J_m\rangle\right|^2}{(\omega_{mo} - \omega_o)^2 + \gamma_m^2}$$

$$\cdot \left|\langle J_m|\hat{\phi}|J_o\rangle\right|^2 , \qquad (4\text{-}16)$$

where we have suppressed the electronic and vibrational quantum numbers in the notation, and $\left|\langle J_n|\hat{\phi}|J_m\rangle\right|^2$ and $\left|\langle J_m|\hat{\phi}|J_o\rangle\right|^2$ are respectively the line strengths S_{nm} and S_{mo} for the given transition.

The band absorption oscillator strength for the transition $0 \rightarrow m$ is defined by [16]

$$f_{mo} = \frac{2m\,\omega_{mo}}{3\hbar} \sum_{\lambda} \left|\langle m|\vec{R}\cdot\vec{\chi}|0\rangle\right|^2 \qquad (4\text{-}17)$$

and for the transition $m \rightarrow n$

$$f_{nm} = \frac{2m\,\omega_{nm}}{e\hbar} \sum_{\lambda'} \left|\langle n|\vec{R}\cdot\vec{\chi}'^*|m\rangle\right|^2 . \qquad (4\text{-}18)$$

Therefore, Equation (4-13) summed over all polarizations can be written in terms of the oscillator strengths and line strengths as

$$\frac{d\omega}{d\Omega} \cong \frac{\omega_R^4}{\omega_{mo}\,\omega_{nm}} \left(\frac{e}{mc^2}\right)^2 \frac{f_{mo}\, f_{nm}}{(\omega_{mo} - \omega_o)^2 + \gamma_m^2} S_{nm}\, S_{mo} \cdot \tag{4-19}$$

The Franck-Condon factor for a transition $i \rightarrow m$ is defined as

$$q_{mi} = \left|\langle m|i\rangle\right|^2 \tag{4-20}$$

and it is normalized such that

$$\sum_m q_{mi} + \int q_{m'i}\, dm' = 1 \tag{4-21}$$

where m and m' index the vibrational states of the specific intermediate electronic state involved in the resonance, and the integral is over the continuum states m' .

The electronic absorption oscillator strength, $f_{e\ell}$ for the specific electronic transition involved, is related to the absorption oscillator strength, f_{mi} , by [31]

$$f_{e\ell} = \frac{f_{mi}\, \bar{\omega}}{q_{mi}\, \omega_{mi}} \quad , \tag{4-22}$$

where

$$\bar{\omega} = \sum_m (\omega_{mi}\, q_{mi}) + \int (\omega_{m'i}\, q_{m'i})\, dm' \quad . \tag{4-23}$$

Equation (4-23) gives the Franck-Condon factor weighted average frequency of the transition. The integral over m' represents those transitions that are disassociative.

In general, $\bar{\omega}$ is of the same order as ω_{ki} and we may approximate $f_{e\ell}$ by

$$f_{e\ell} \cong \frac{f_{mi}}{q_{mi}} \quad . \tag{4-24}$$

Assuming the initial and final electronic states are the same and using this expression for $f_{e\ell}$, we may write the resonant-Raman cross section in terms of the Franck-Condon factors, the electronic oscillator strength, and the line strengths

$$\frac{d\sigma}{d\Omega} \cong \frac{\omega_R^4}{4\ \omega_{mo}\ \omega_{nm}} \left[\frac{e^2}{mc^2}\right]^2 \frac{q_{mo}\ q_{nm}\ f_{e\ell}^2}{(\omega_{mo} - \omega_o)^2 + \gamma_m^2}\ \rho_o\ S_{nm}\ S_{mo}\ , \tag{4-25}$$

where ρ_o is the relative thermal population of the initial state.

It should be noted that the above expression for the resonant-Raman cross sections are approximate values and that the degeneracies of the states were not considered. This treatment is, however, sufficient for the purposes of this study, since an order of magnitude value for the cross section would give a good indication

of the Raman scattered return signal in an operational lidar system.

If the incident frequency ω_o is sufficiently close to the resonance frequency, ω_{mo} , we have $\omega_{mo} \cong \omega_o$ and $\omega_R \cong \omega_{nm}$. Thus, Equation (4-25) in the near resonance approximation becomes

$$\frac{d\sigma}{d\Omega} \cong \frac{\omega_R^3}{4\,\omega_o} \left[\frac{e^2}{mc^2}\right]^2 \frac{q_{mo}\, q_{nm}\, f_{e\ell}^2}{(\omega_o - \omega_{mo})^2 + \gamma_m^2}\, \rho_o\, S_{nm}\, S_{mo} \,. \tag{4-26}$$

Near Resonance to Molecular Absorption Bands

The above approximations have been shown to work well for cases where the oscillator strengths are large and where the absorption lines are distinct and well separated [27,30]. It may not always be possible to obtain this condition with molecules, and in this case it is necessary to consider near resonance to molecular bands. Penny [30] has noted that, in the case of resonance with absorption bands, interference effects can occur in the sum over the intermediate states m within the absolute square in Equation (4-11). He has shown that these effects may be neglected if the separation from resonance is large compared to the width of the nearest band of centerline angular frequency ω^* , but small in comparison

to the separation between bands. Assuming that the initial and final electronic states are the same, and neglecting rotational structure, Penny [30] obtains an expression of the form

$$\frac{d\sigma}{d\Omega} \cong \frac{\omega_R^3}{4\,\omega_o}\left(\frac{e^2}{mc^2}\right)\frac{f_{e\ell}^{\,2}}{(\omega_o-\omega^*)^2}\sum_{om} P_o\, q_{mo}\, q_{nm} \quad , \qquad (4\text{-}27)$$

where P_o is the fractional population of the initial vibrational state O, and the summation includes the integral over the continuum states. $P_o = 1$ for N_2 and O_2 at the atmospheric temperatures and pressures considered in this study.

An indication of the resonance enhancement from an absorption band can be obtained from Equation (4-27) by summing over all of the final states and using the normalization condition given by Equation (4-27). This results in an estimate of the differential cross section for the Rayleigh plus vibrational-rotational Raman scattering,

$$\left(\frac{d\sigma}{d\Omega}\right)_{\substack{\text{Rayleigh}\\ \text{vib-rot Raman}}} \cong \frac{\omega^3}{4\,\omega_o}\left(\frac{e^2}{mc^2}\right)^2\frac{f_{e\ell}^{\,2}}{(\omega_o-\omega_{mn}^*)^2} \quad . \qquad (4\text{-}28)$$

Estimate of Desirable Raman Cross Sections for Use in the SVR Problem

Equation (2-16) may be written in terms of the number of signal photons detected per unit time. With

only photons returning from a range increment L being observed, time integration yields the signal photons observed per pulse and multiplication by the pulse repetition frequency gives the average number of signal photons detected per second as

$$S = 2.69 \times 10^5 \eta (PRF) \frac{E_p}{\hbar \omega_o} \frac{A_r L}{r^2} \beta'_g(r) T^2(o,r) \tag{4-29}$$

where ω_o is the laser frequency, L is the range increment in meters, η is the total detection efficiency, and PRF is the pulse repetition frequency. A_r in this expression is in cm^2, E_p is in joules, and r is in km. Here $\beta'_b(r)$ is given by

$$\beta'_g(r) = \beta'_g = N' \frac{d\sigma}{d\Omega} \tag{4-30}$$

where N' is the PPM concentration of the atmospheric gas at sea level.

The number of background counts detected from skylight in a second is given by Rosen [27]

$$B = \eta(PRF) \frac{W(\omega_R)\Delta\lambda}{\hbar \omega_R} A_r \phi \frac{2L}{c} \tag{4-31}$$

where $W(\omega_R)$ = the background radiance at the scattered wavelength (W/cm^2 - Sr - Å);

$\Delta\lambda$ = the detector bandwidth (Å);

ϕ = detector field of view (Sr);

$\frac{2L}{c}$ = gate time for the range increment (sec).

A general estimate of the sensitivity of a lidar system can be obtained from the signal-to-noise ratio (SNR). For the pulse-gated photon counting scheme, the SNR is given by [32,27]

$$SNR = \frac{S}{\sqrt{B}} \tag{4-32}$$

where we have assumed that the noise is predominantly due to the background radiance.

Using Equations (4-29), (4-30), (4-31), and (4-32), we may write

$$SNR = 2.69 \times 10^5 \frac{E_p N'}{\omega_o r^2} T^2 \sqrt{\frac{\eta C A_r L \omega_R (PRF)}{2\pi W(\omega_R) \Delta\lambda\phi}} \frac{d\sigma}{d\Omega} \tag{4-33}$$

which is an expression relating the SNR to the Raman cross sections under various operational parameters.

To obtain information concerning the order of magnitude of $d\sigma/d\Omega_R$ necessary for useful returns under the visibility conditions described in Chapter I, we may define

$$\alpha = \frac{d\sigma}{d\Omega_R}^{NEEDED} = 3.72 \times 10^{-6} (SNR) \frac{\omega_o r^2}{E_p N'} \sqrt{\frac{2\pi \Delta\lambda\phi W(\omega_R)}{\eta C A_r L \omega_R (PRF)}} \frac{1}{T^2} . \tag{4-34}$$

By assuming the maximum range of r we may obtain values for α given various transmittances T using Equation (4-34) provided we know the operational parameters on the right side of the equation.

One of these parameters is $W(\omega_R)$, the background radiance at the scattered wavelength. Figure 4.4 shows a spectral plot of the irradiance of direct solar and global radiation at sea level on the earth. This plot shows the irradiance for various air masses, m , defined as the secant of the zenith angle of the sun. We may obtain a worst case background radiance by considering direct sunlight incident on a cloud or fog bank in the receiver field of view. Figure 4.5 illustrates the worst case configuration.

The irradiance, $\tilde{h}$, and the radiance $W(\omega)$ are related by [15]

$$W(\omega) = \frac{\tilde{h}\ \rho_\lambda}{\pi} \quad , \tag{4-35}$$

where ρ_λ is the albedo of a diffuse object at wavelength λ . The mean value of the albedo of a cloud of water vapor has been found to be about 85 percent in the near UV and visible, and about 78 percent to 45 percent in the near IR [33]. Values for the background radiance $W(\omega)$ in Equation (4-34) can therefore be calculated for the worst case condition using Equation (4-35). Using

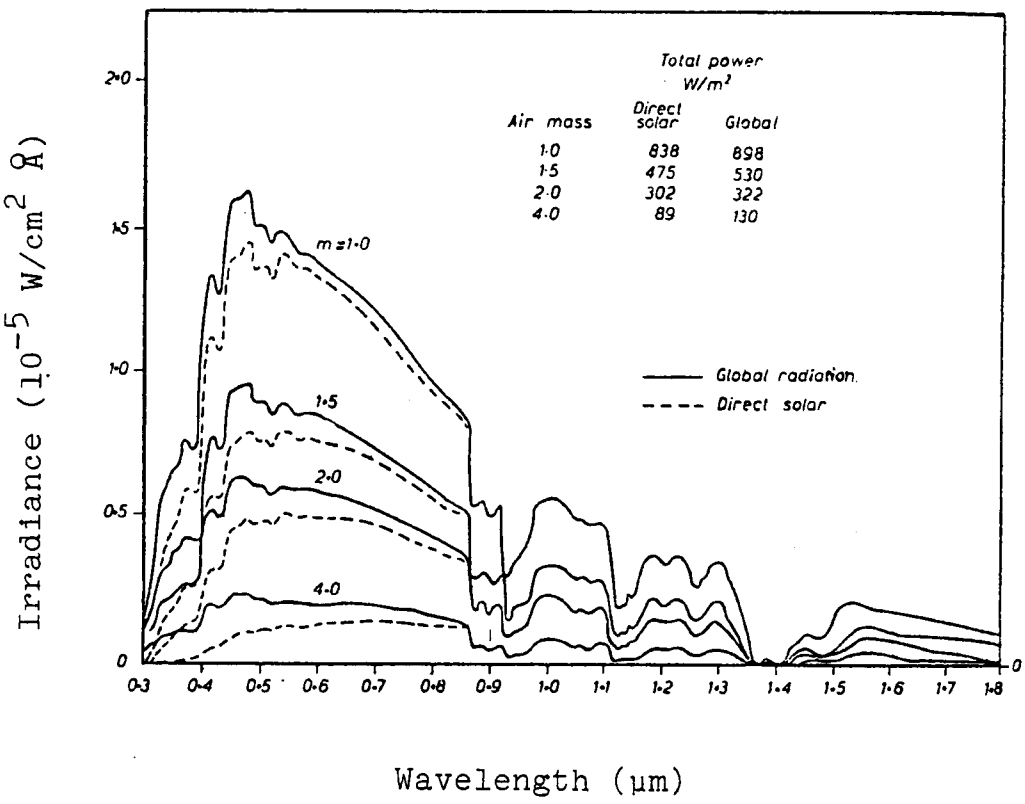

Figure 4.4. Spectral Power Distribution of Direct Solar and Global Radiation Incident on Horizontal Surface at Sea Level.

Source: S. T. Henderson, Daylight and Its Spectrum, John Wiley & Sons, New York, 1977, p. 192.

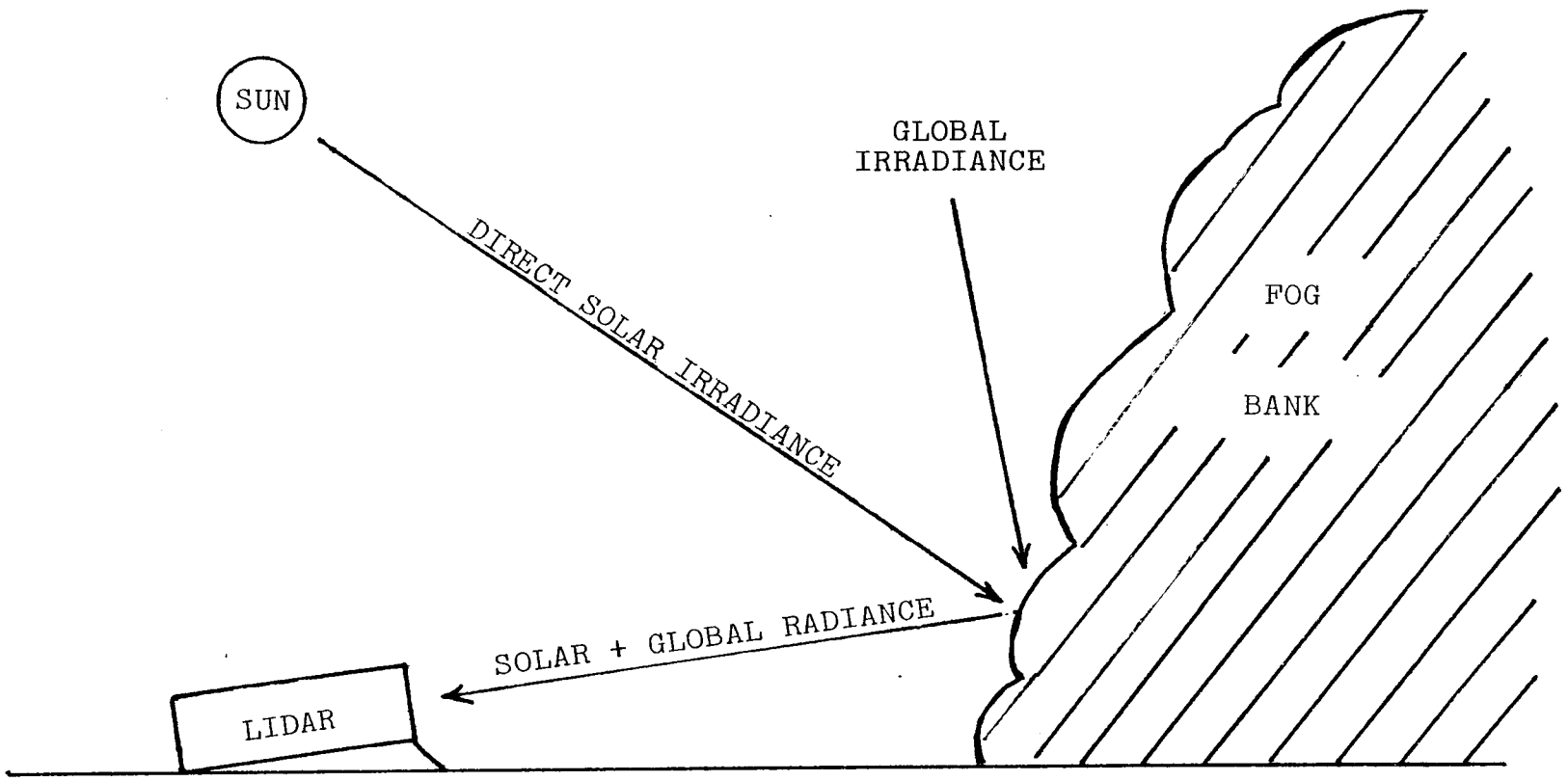

Figure 4.5. Worst Case Background Radiance.

transmitted wavelengths of .35 μm and .75 μm to represent the near UV and near IR and assuming non-resonant Raman scattering from O_2 and N_2 the following values for the background radiance $W(\omega_R)$ were calculated using Equation (4-35) and the irradiance plot in Figure 4.4 for an air mass, m = 1 :

$$W_{O2}(3702\text{Å}) = 2.03 \times 10^{-6} \frac{W}{cm^2\ sr\ \text{Å}} ,$$

$$W_{N_2}(3811\text{Å}) = 2.03 \times 10^{-6} \frac{W}{cm^2\ sr\ \text{Å}} ,$$

$$W_{O2}(8491\text{Å}) = 1.67 \times 10^{-6} \frac{W}{cm^2\ sr\ \text{Å}} ,$$

$$W_{N_2}(9089\text{Å}) = 1.04 \times 10^{-6} \frac{W}{cm^2\ sr\ \text{Å}} .$$

The values for $\Delta\lambda$, ϕ , and η were taken to be those used by Rosen [27] since these were based on present technological capabilities.

Again using wavelengths of .35 μm and .75 μm to represent the near UV and near IR, the other lidar parameters in Equation (4-34) were obtained using the maximum values allowed by eye safety restrictions for an exposure time of 50 sec described in Chapter III and the SVR geometry given in Chapter II. These are the ultimate restrictions on an eye-safe lidar, and the corresponding parameters are listed in Table IV.4.

TABLE IV.4

OPERATIONAL EYE SAFE RAMAN LIDAR PARAMETERS

Lidar Parameters	λ = .35 μm	λ = .75 μm	Remarks
ω_o	5.39×10^{15} rad/sec	2.51×10^{15} rad/sec	
$\omega_R(N_2)$	4.95×10^{15} rad/sec	2.07×10^{15} rad/sec	ν_{vr} = 2331 cm^{-1}
$\omega_R(O_2)$	5.09×10^{15} rad/sec	2.22×10^{15} rad/sec	ν_{vr} = 1556 cm^{-1}
r*	.385 km	.385 km	Figure 1.2 Category I decision point
A_r	1.0×10^4 cm^2	1.0×10^4 cm^2	
E_p	70 J	1.2×10^{-2} J	Figure 3.4
L	30.5 m	30.5 m	
PRF	3 Hz	2.2×10^4 Hz	Figure 3.1

An estimate of minimum SNR value needed for a maximum error of 10 percent in the transmission is obtained from an error analysis of Equation (2-23), page 24. This analysis gives a minimum SNR value of 5. Using this SNR, α can be calculated for various transmittances using the lidar parameters given above.

Figures 4.6 and 4.7 show plots of α versus T for the near UV and near IR using incident wavelengths of .35 μm and .75 μm . These plots were obtained using Equation (4-34). Comparison of these α values with estimates for the actual non-resonance Raman cross sections at these wavelengths were obtained by weighting the results in Table IV.2, page 72, by $(1/\lambda)^4$. The pure rotational Raman cross sections were used because these are about 2 orders of magnitude larger than the vibrational-rotational Raman cross sections (see Tables IV.2 and IV.3, pages 72 and 73). Thus, for N_2 the pure rotational Raman cross sections are 9.4×10^{-29} cm^2/sr and 2.9×10^{-30} cm^2/sr . for incident wavelengths of .35 μm and .75 μm respectively, and for O_2 the corresponding cross sections are 1.46×10^{-28} cm^2/sr and 5.27×10^{-30} cm^2/sr . It can be seen from Figures 4.6 and 4.7 that these cross sections in the near UV are about 4 orders smaller than the α value needed for the worst case SVR transmittance measurement of $T = 10^{-5}$, and in the near IR the cross sections are about 7 orders

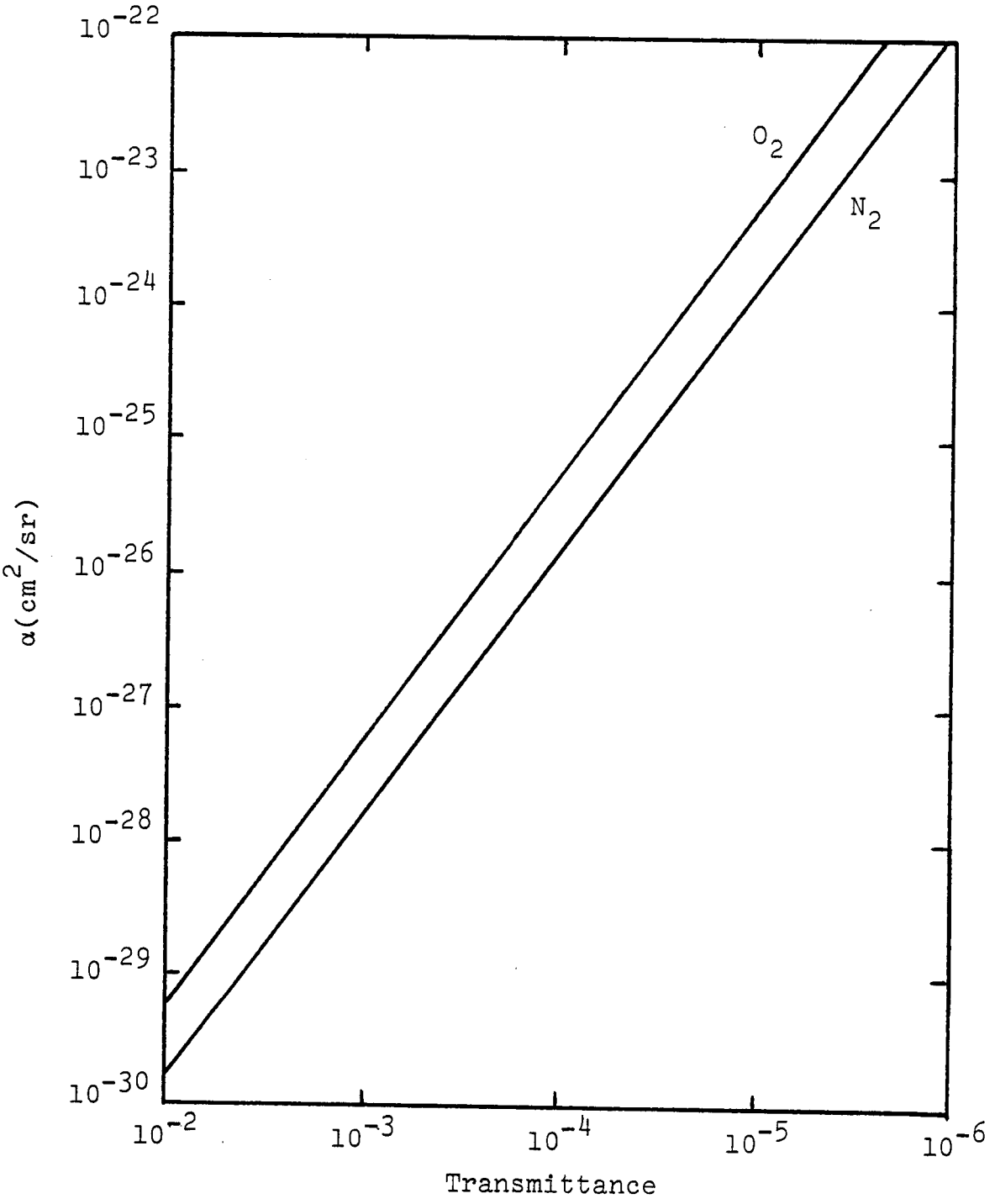

Figure 4.6. Raman Cross Sections of N_2 and O_2 Required to Make Worst Case Eye-Safe SVR Transmittance Measurement Using SNR = 5 and Incident Wavelength of 0.35 μm.

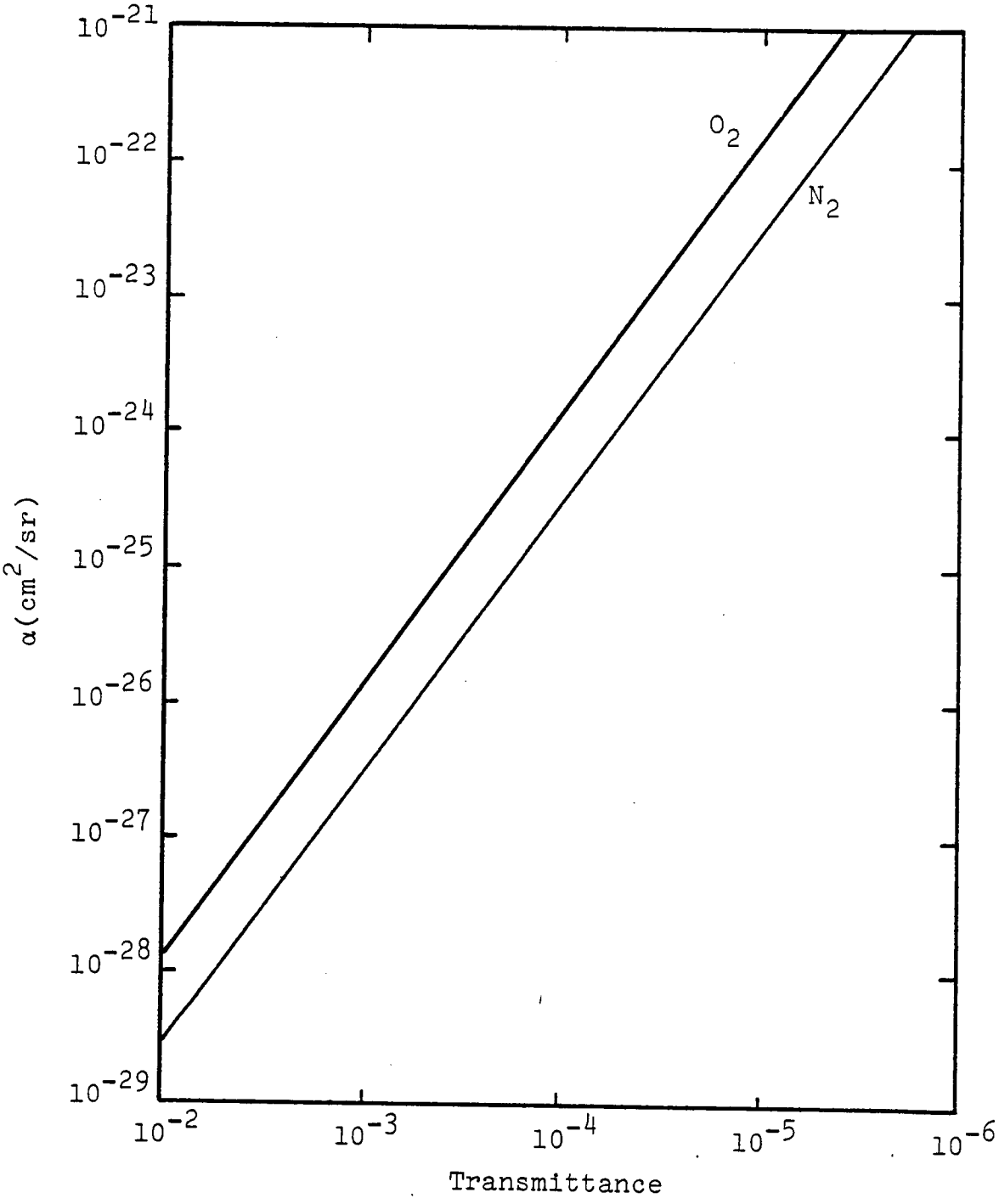

Figure 4.7. Raman Cross Sections of N_2 and O_2 Required to Make Worst Case Eye-Safe SVR Transmittance Measurement Using SNR = 5 and Incident Wavelength of 0.75 μm.

of magnitude smaller than the needed α value for the same worst case transmittance.

Slight Enhancements of the Non-Resonant Cross Sections in the UV

There is evidence that a slight enhancement of the non-resonance Raman cross section in N_2 and O_2 occurs in the near UV due to stronger absorption bands of N_2 and O_2 further down in the UV [30]. Penny, et al. [30], calculated the Rayleigh cross section of N_2 at STP for incident light at 300 nm . He obtained a $\sigma_{Rayleigh}(N_2) = 6.60 \times 10^{-27}$ cm^2/sr . $\sigma_{Raman}/\sigma_{Rayleigh}$ ratios were also measured and values of 1.50×10^{-3} and 1.44×10^{-3} were obtained. An average of these results yielded

$$\sigma_{Raman}(N_2) = 9.7 \times 10^{-30} \text{ cm}^2/\text{sr} \pm 25\%$$

for the Q-branch vibrational-rotational Raman cross section from N_2 summed over all scattered light polarizations. It is interesting to note that the $(1/\lambda)^4$ extrapolation of the cross sections measured in the visible region yields about 4.63×10^{-30} cm^2/sr . The measured value is about 2.1 times larger. Penny believes that this enhancement is due to the proximity to the strong UV resonances of N_2 , which begin near 140 nm .

The ratio of O_2 to N_2 Q-branch vibrational-rotational cross sections for incident light at 300 nm was also measured by Penny, et al. This yielded 1.59 ± 20% for the ratio which was larger than the 1.24 value obtained at 514.5 nm . Thus the O_2 cross section increases faster than the N_2 cross section and this was considered reasonable since the strong O_2 UV resonances begin at longer wavelengths than the N_2 UV resonances.

T. A. Coney and J. A. Salzman [34] have developed a theoretical model for the Raman rotational spectrum of air and have checked their results with experiment. These results show that the ratio $\sigma_{rot\text{-}Raman}(O_2)/\sigma_{rot\text{-}Raman}(N_2)$ of 1.59 obtained from Melfi's calculations at 3471.5Å was lower than the actual value of 2.14 ± .36 . Since Melfi assumed that there were no resonance effects in his calculations, this increase appears also to be due to the proximity of the O_2 UV resonance.

Assuming the ratio of the pure rotational Raman cross section to the Rayleigh cross section of N_2 remains constant over the wavelength region of the near UV, we can obtain an approximate value for the pure rotational cross sections of N_2 and O_2 . According to Melfi's calculations the ratio of the total pure rotational cross section (both $\parallel$ and $\perp$ components) $\sigma_{total\ rot}(N_2/\sigma_{Rayleigh}(N_2)$ is 2.77×10^{-2} . Using Penny's value for the Rayleigh cross section for incident light at 300 nm

a pure rotational cross section of 1.38×10^{-28} cm^2/sr was obtained for N_2 . Thus, the $\sigma_{rot}(O_2)/\sigma_{rot}(N_2)$ obtained by Coney and Salzman gives a pure rotational cross section for O_2 of 3.98×10^{-28} cm^2/sr . This value for the O_2 rotational cross section may be lower than the actual value since it is expected that the ratio $\sigma_{ROT}(O_2)/\sigma_{ROT}(N_2)$ will have increased further with an incident wavelength of 3000Å rather than 3471.5Å since 3000Å is still closer to the O_2 strong UV resonances beginning around 2400Å .

The slight enhancement of the non-resonant cross sections discussed here do not alter the conclusions of the last subsection; it was therefore necessary to investigate the possibility of obtaining a resonance enhancement of the Raman cross sections due to absorption lines and bands of N_2 and O_2 in the near IR and near UV wavelength regions of interest. This investigation is discussed in the next chapter.

CHAPTER V

RESONANCE RAMAN SCATTERING FROM ATMOSPHERIC GASES

Principal Gases Considered

The three principal gases--nitrogen, oxygen and argon--represent 99.6 percent of the atmosphere, and are always present in the same concentrations. Table V.1 represents a summary of the gases present in the dry atmosphere. It can be seen that there are various trace gas components with variable concentrations present.

In choosing the scattering gas to be used in the Raman lidar transmissometer technique, one must insure that the concentration be constant at all times, and unless one anticipates largely enhanced Raman cross sections the concentration must be high. Since the ground state of argon does not permit electronic Raman scattering in the wavelength regions of interest [35], nitrogen and oxygen are the natural choice for use in a Raman lidar transmissometer.

Search for Resonant Raman Transitions in N_2 and O_2 in the Near IR and Near UV

It was shown in Chapter IV that the non-resonance pure rotational Raman cross sections for N_2 and O_2 in the wavelength regions of interest were less than the

TABLE V.1

SUMMARY OF THE GAS COMPOSITION OF DRY (WATER VAPOR-FREE) ATMOSPHERIC AIR IN THE TROPOSPHERE

Type of Gas	Chemical Symbol	Concentration ppm	Concentration $\mu g/m^3$	Residence Time
Principal gases				
Nitrogen	N_2	780000	$976 \cdot 10^6$	Continuous
Oxygen	O_2	209400	$298 \cdot 10^6$	Continuous
Argon	Ar	9300	$16.6 \cdot 10^6$	Continuous
Trace gases (constant)				
Helium	He	5.2	920	About $2 \cdot 10^6$ years
Neon	Ne	18	$1.6 \cdot 10^4$	Continuous
Krypton	Kr	1.1	4100	Continuous
Xenon	Xe	0.086	500	Continuous
Trace gases (variable)				
Carbon dioxide	CO_2	200-400	$(4-8) \cdot 10^5$	4 years
Carbon monoxide	CO	0.01-0.2	10-200	About 0.3 years
Methane	CH_4	1.2-1.5	850-1100	About 100 years
Formaldehyde	CH_2O	0-0.1	0-16	?
Nitrogen oxides	N_2O	0.25-0.6	500-1200	About 4 years
	NO_2	$(1-4.5) \cdot 10^{-3}$	2-8	A few days
Ammonia	NH_3	0.002-0.02	2-20	?
Hydrogen sulfide	H_2S	$(2-20) \cdot 10^{-3}$	3-30	About 40 days
Sulfur dioxide	SO_2	0-0.02	0-50	About 5 days
Chlorine	Cl_2	$(3-15) \cdot 10^{-4}$	1-5	A few days
Iodine	J_2	$(0.4-4) \cdot 10^{-5}$	0.05-0.5	?

TABLE V.1 (CONTINUED)

Type of Gas	Chemical Symbol	Concentration ppm	Concentration $\mu g/m^3$	Residence Time
Hydrogen fluoride	HF	$(0.8\text{-}18) \cdot 10^{-3}$	0.7-16	?
Hydrogen	H_2	0.4-1.0	36-90	?
Ozone	O_3	0-0.05	0-100	About 60 days

Source: Israel, H., and Israel, G. W. Trace Elements in the Atmosphere, Ann Arbor: Ann Arbor Science, 1974, p. 6.

α values necessary for the minimum detection SNR of 5 for the worst case transmittance. For this reason a search was conducted over the wavelength intervals .27 μm to .4 μm and .7 μm to 1.4 μm for absorption bands and lines of N_2 and O_2 . These wavelength intervals were chosen so as to reasonably comply with the visible light transmission similarity requirements. References [36], [37], and [38] were used to obtain the absorption band systems and molecular constants of N_2 and O_2 .

The results of this investigation showed that, for standard atmospheric temperatures and pressures [39], N_2 has no absorption band systems in the wavelength intervals of interest. Oxygen on the other hand has three weak absorption band systems in these regions. These are the Herzberg I and II systems in the near UV and the Atmospheric system in the near IR.

Order of magnitude estimates of the resonance Raman cross section due to an absorption line in one of these bands can be obtained by assuming $\omega_R \cong \omega_o \cong \omega_{mo}$ in Equation (4-26), page 78; thus we have

$$\frac{d\sigma}{d\Omega}_{LINE} \cong \frac{\omega_R^2}{4} \left(\frac{e^2}{mc^2}\right)^2 \frac{q_{mo}\, q_{nm}\, f_{e\ell}^2}{\gamma_m^2} \rho_o\, S_{nm}\, S_{mo} \quad . \quad (5\text{-}1)$$

For standard atmospheric temperatures and pressures γ_m is essentially equal to the pressure broadened line

width [27]. We may use the Lorentz formula [40] to obtain the magnitude of γ_m ,

$$\gamma_{m_1} \cong 2\, Q_1\, \bar{N}_2 \sqrt{\frac{8\ kT(M_1^{-1} + M_2^{-1})}{\pi}} \quad , \qquad (5\text{-}2)$$

where Q_1 is the collision cross section for the gas of type 1, $\bar{N}_2$ is the concentration of gas of type 2, k is the Boltzman constant, T is the gas kinetic temperature, and M_1 and M_2 are the molecular masses of the molecules of types 1 and 2.

Using Equation (5-2), we find the pressure broadened line width of O_2 due to N_2 is $\gamma_o \cong 10^8$ rad/sec .

Tables V.2, V.3, and V.4 give the band origins of the O_2 band systems considered. Figure 5.1 shows a microphotometer tracing obtained by Baum and Dunkelman [41] in measuring UV attenuation coefficients. The Herzberg I , O_2 bands are clearly visible and labeled with wavelengths in the figure. The Herzberg II bands are much weaker and cannot be resolved.

Because of the weakness of the Herzberg II system (there is also a lack of information concerning its electronic oscillator strength), this system was abandoned as a potential source for resonance Raman scattering.

TABLE V.2

$C^1\Sigma_u^-$ - $X^3\Sigma_g^-$ HERZBERG II SYSTEM BAND ORIGINS OBSERVED IN ABSORPTION λ(Å)

v" \ v'	6	7	8	9	10
0	2714.5	2672.3	2634.0	2599.2	2568.0

Source: Suchard, S. N., and Melzer, J. E., Editors. Spectroscopic Data, Vol. 2. New York: IFI/Plenum Data Company, 1976.

TABLE V.3

$A^3\Sigma_u^+$ - $X^3\Sigma_g^-$ HERZBERG I SYSTEM BAND ORIGINS OBSERVED IN ABSORPTION

v',v"	λ(Å)	v',v"	λ(Å)	v',v"	λ(Å)
0,0	2857	2,0	2738	4,0	2638
1,0	2795	3,0	2686	5,0	2594
6,0	2555	8,0	2490	10,0	2444
7,0	2520	9,0	2464	11,0	2430

Source: Rosen, B., Editor. Spectroscopic Data Relative to Diatomic Molecules. New York: Pergamon Press, 1970.

TABLE V.4

$b^1\Sigma_g^+ - X^3\Sigma_g^-$ ATMOSPHERIC SYSTEM
BAND ORIGINS λ(Å)

v" \ v'	0	1	2	3	4
0	7619.33	6882.47	6286.61	5795.13	5383.49

Source: Krupenie, Paul H. "The Spectrum of Molecular Oxygen," J. Phys. Chem. Reference Data, Vol. 1, No. 2, pp. 423-534, 1972.

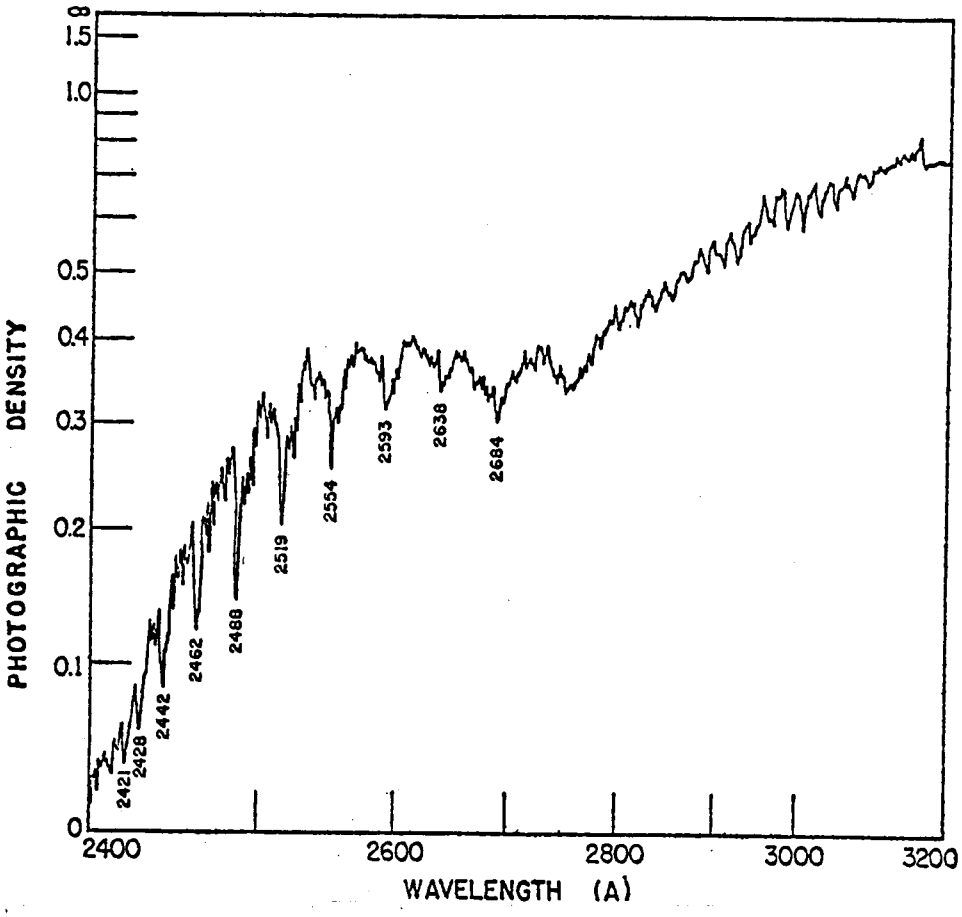

Figure 5.1. Microphotometer Tracing Showing the Herzberg I Oxygen Bands. The bands are labeled along the figure.

Source: Baum, William A., and Dunkelman, Lawrence. "Horizontal Attenuation of Ultraviolet Light by the Lower Atmosphere," J. Opt. Soc. of America, Vol. 45, No. 3, p. 166, 1955.

Oscillator strengths for the Herzberg I and Atmospheric systems were found to be very small, $f_{e\ell} = 2 \times 10^{-7}$ [38] and $f_{e\ell} = 2.47 \times 10^{-10}$ [36], respectively.

The Franck-Condon factors for the Herzberg I and Atmospheric systems are given in Tables V.5 and V.6. Using the Franck-Condon factors, oscillator strengths, and line strengths [42] for the 2737Å band of the Herzberg I system and the 7708Å and 7619Å bands of the Atmospheric system Equation (5-1) gives results several orders of magnitude lower than the non-resonance Raman cross sections at the same wavelengths obtained using $(1/\lambda)^4$ weighting. This indicates that no resonance enhancement occurs from the lines due to the weakness of the systems, i.e., small oscillator strengths.

TABLE V.5

FRANCK-CONDON FACTORS O_2 $A^3\Sigma_u^+ - X^3\Sigma_g^-$
HERZBERG I SYSTEM

v'' / v'	0	1	2	3	4	5	6	7	8	9	10
0	1.809-6	3.339-5	2.916-4	1.605-3	6.248-3	1.840-2	4.260-2	7.935-2	1.214-1	1.546-1	1.654-1
1	1.488-5	2.383-4	1.765-3	8.012-3	2.479-2	5.519-2	8.985-2	1.052-1	8.298-2	3.500-2	1.510-3
2	6.300-5	8.761-4	5.494-3	2.041-2	4.924-2	7.924-2	8.158-2	4.457-2	4.492-3	1.049-2	5.486-2
3	1.836-4	2.222-3	1.179-2	3.553-2	6.516-2	7.053-2	3.593-2	1.434-3	1.700-2	5.478-2	4.681-2
4	4.201-4	4.439-3	1.989-2	4.816-2	6.469-2	4.103-2	3.900-3	1.162-2	4.595-2	3.559-2	1.700-3
5	7.975-4	7.382-3	2.794-2	5.368-2	4.998-2	1.343-2	2.713-3	3.372-2	3.537-2	3.171-3	1.414-2
6	1.307-3	1.066-2	3.412-2	5.134-2	3.040-2	8.570-4	1.669-2	3.605-2	1.034-2	4.851-3	3.357-2
7	1.874-3	1.354-2	3.679-2	4.277-2	1.386-2	1.724-3	2.668-2	2.223-2	3.734-5	2.013-2	2.515-2
8	2.375-3	1.536-2	3.570-2	3.168-2	4.153-3	7.860-3	2.642-2	8.092-3	4.344-3	2.454-2	8.205-3
9	2.624-3	1.539-2	3.097-2	2.090-2	4.588-4	1.232-2	1.946-2	1.184-3	1.068-2	1.771-2	4.555-4
10	2.462-3	1.332-2	2.370-2	1.231-2	4.947-5	1.249-2	1.152-2	2.020-5	1.203-2	9.046-3	6.301-4
11	1.715-3	8.762-3	1.426-2	6.011-3	3.515-4	8.568-3	5.372-3	4.550-4	8.314-3	3.434-3	1.676-3

Source: Krupenie, Paul H. "The Spectrum of Molecular Oxygen," J. Phys. Chem. Reference Data, Vol. 1, No. 2, pp. 423-534, 1972.

TABLE V.6

$O_2 b^1\Sigma_g^+ - X^3\Sigma_g^-$ ATMOSPHERIC SYSTEM

v' \ v"	0	1	2	3
0	9.308×10^{-1}	6.660×10^{-1}	2.523×10^{-3}	5.648×10^{-5}
1	6.647×10^{-2}	7.928×10^{-1}	1.322×10^{-1}	8.284×10^{-3}
2	2.639×10^{-3}	1.315×10^{-1}	6.527×10^{-1}	1.943×10^{-1}
3	6.911×10^{-5}	8.753×10^{-3}	1.924×10^{-1}	5.144×10^{-1}

Source: Krupenie, Paul H. "The Spectrum of Molecular Oxygen," J. Phys. Chem. Reference Data, Vol. 1, No. 2, pp. 423-534, 1972.

CHAPTER VI

CONCLUSIONS

In Chapter IV it was shown that the non-resonance pure-rotational and vibrational-rotational Raman scattering cross sections in the near IR were too small to measure an operational transmittance of 10^{-2} in daylight. These results indicate that the use of near IR wavelengths in the Raman lidar transmissometer technique is restricted to transmittances above 10^{-2}. This fact is mainly due to the $(1/\lambda)^4$ dependence of the Raman scattering cross section and the eye safety limitations for the near IR.

The use of near UV wavelengths is more favorable than that of the near IR. Non-resonance pure-rotational Raman cross sections in the near UV are on the order of 10^{-28} cm^2/sr , which indicates that the near UV wavelengths are able to meet the minimum operational requirements for transmittances down to 10^{-3} in daylight.

It was shown that a slight enhancement of the N_2 and O_2 Raman scattering cross sections in the near UV can be expected due to the strong absorption bands of these molecules further down in the UV. The slightly enhanced pure-rotational Raman scattering cross sections of the N_2 and O_2 molecules were estimated to be about 1.5 times larger than the respective cross sections obtained by using $(1/\lambda)^4$ weighting for an incident wavelength of 300 nm .

These cross sections are, however, still on the order of 10^{-28} cm^2/sr and therefore do not change the conclusions drawn from the non-resonance UV discussion above.

It should be emphasized that the values plotted in Figures 4.6, page 88, and 4.7, page 89, were obtained under the assumption that the noise was dominated by background noise. In cases where the background noise is negligible in comparison with the noise due to statistical fluctuations in the signal, and assuming other sources of noise may be neglected, the signal-to-noise ratio becomes $\sqrt{S}$.

In Chapter IV the minimum signal-to-noise ratio for an operational eye safe Raman lidar transmissometer was shown to be 5. Assuming that the noise is dominated by the statistical fluctuations in the signal and given this minimum SNR of 5, we obtain a theoretical limit on the number of signal photons detected per second, i.e., 25. This result indicates that on this basis an eye safe Raman lidar transmissometer utilizing pure-rotational Raman scattering from N_2 and O_2 is physically feasible for transmittances as low as 10^{-4} during nighttime operation and other cases where the background noise may be neglected.

Daylight operation at transmittances lower than 10^{-3} may also be possible if the background noise can be significantly reduced. One means of doing this would be

to utilize the Fraunhofer absorption lines of the solar spectrum, as done by Shipley, et al. [43], and others. For a Raman lidar the output wavelength would be chosen so that the returning Raman shifted wavelength falls on a Fraunhofer absorption line. This technique, however, needs further investigation to determine which of the Fraunhofer lines in the UV would be most favorable for reducing the background counts.

In addition, there is the problem of multiply-scattered radiation in the return signal. This effect has been neglected in this study; however, rough estimates indicate that the effect may be significant in transmittances of 10^{-4} and lower for the lidar and SVR geometries used in this study. Cohen, et al. [44], have recently performed theoretical calculations in agreement with experiment that demonstrate that the Raman multiple scattering effect is not negligible. Further studies of the use of an eye safe Raman lidar transmissometer for the purpose of solving the SVR problem should therefore be directed toward determining the magnitude of this effect in the return signal and possible means of overcoming it.

LIST OF REFERENCES

LIST OF REFERENCES

1. Lifsitz, J. R. "Lidar Systems for Measuring Visibility: A Technical Assessment," FAA-RD-74-149, Federal Aviation Administration, Washington, D.C. (1974).

2. Hinkley, E. D., Editor. "Laser Monitoring of the Atmosphere," Topics in Applied Physics, Vol. 14. New York: Springer-Verlag, 1976.

3. Middleton, W. E. Knowles. Vision Through the Atmosphere. Toronto: University of Toronto Press, 1968.

4. Douglas, C. A., and Booker, R. L. "Visual Range: Concepts, Instrumental Determination, and Aviation Applications," FAA-RD-77-8, Federal Aviation Administration, Washington, D.C. (1977).

5. Kohl, R. H., and Guthrie, M. J. "A Feasibility Study of a Lidar Transmissometer Technique for the Slant Visual Range Problem in Aircraft Landing Approaches," NAS8-32635, National Aeronautics and Space Administration, Marshall Space Flight Center, Alabama (1978).

6. Lifsitz, J. R. "The Measurement of Atmospheric Visibility with Lidar: TSC Field Test Results," FAA-RD-74-29, Federal Aviation Administration, Washington, D.C. (1974).

7. Brown, R. T., Jr. "A New Lidar for Meteorological Application," J. Appl. Meteor. 12, 698-708.

8. Ruger, J. F. "Using Lidar for Measuring Visibility," Optical Propagation in the Atmosphere, AGARD-CP-183, Paper 44 (1976).

9. Kohl, R. H. "Discussion of the Interpretation Problem Encountered in Single Wavelength Lidar Transmissometers," Manuscript CS-195A, The University of Tennessee Space Institute, Tullahoma, Tennessee (1978).

10. Viezee, W., Oblanas, J., and Collis, R.T.H. "Evaluation of the Lidar Technique of Determining Slant Range Visibility for Aircraft Landing Operations," AFCRL-TR-73-0708 (AD 776054), Air Force Cambridge Research Laboratories, Bedford, Mass. (1973).

11. Stewart, H. S., Brouwer, W., Shuler, M. "Design Principles of a Slant Range Transmissometer for Airport Use in Atmospheric Aerosols: Their Optical Properties and Effects," NASA CP-2004, Paper TuC6 (1976).

12. Stewart, H. S., Suler, M. P. Jr., Brouwer, W. "Single Ended Transmissometer Using the Analog Zone Principle," Presented at the Workshop on Remote Sensing of the Marine Boundary Layer, Vail C O, H.S.S. Incl, Bedford, Mass. (1976).

13. Elterman, L. "UV, Visible, and IR Attenuation for Altitudes to 50 km, 1968," AF L 68-0153 (AD 671 933), Air Force Cambridge Research Laboratories, Bedford, Mass. (1968).

14. Israel, H., Israel, G. W. Trace Elements in the Atmosphere. Ann Arbor: Ann Arbor Science Publishers Inc., 1974.

15. American National Standard for the Safe Use of Lasers (ANSI Z136.1-1976). New York: American National Standards Institute Inc., 1976.

16. Herzberg, Gerhard. Molecular Spectra and Molecular Structure, Second Edition. New York: Van Nostrand Reinhold Company, 1950.

17. Szymanski, H. A., Editor. Raman Spectroscopy, Theory and Practice, Vol. 1. New York: Plenum Press, 1967.

18. Louisell, William H. Quantum Statistical Properties of Radiation. New York: John Wiley & Sons, 1973.

19. Long, D. A. Raman Spectroscopy. New York: McGraw-Hill, 1977.

20. Baym, Gordon. Lectures on Quantum Mechanics. Reading: W. A. Benjamin Inc., 1977.

21. Leonard, D. A. "Observation of Raman Scattering from the Atmosphere Using a Pulsed Nitrogen Laser," Nature 216, p. 142 (1967).

22. 8th International Laser Radar Conference June 6th through 9th, 1977. Conference Abstracts, Drexel University, Philadelphia, 1977.

23. Cooney, J. A. "Measurement on the Raman Component of Laser Atmospheric Backscattering," Appl. Physics Lett., Vol. 12, p. 40 (1968).

24. Melfi, S. H. "Remote Measurements of the Atmosphere Using Raman Scattering," Appl. Optics, Vol. 11, p. 1605 (1972).

25. Hirschfeld, T., Sshildkraut, E. R., Tannenbaum, Harvey, and Tannenbaum, David. "Remote Spectroscopic Analysis of PPM-Level Air Pollutants by Raman Spectroscopy," Appl. Physics Lett., Vol. 22, No. 1, 1973.

26. Leonard, Donald A., and Caputo, Bernard. "Single-Ended Atmospheric Transmissometer," Optical Engineering, Vol. 13, No. 1, p. 10 (1974).

27. Rosen, H., Robrish, P., and Chamblain. "Remote Detection of Pollutants Using Resonance Raman Scattering," Appl. Optics, Vol. 14, No. 11, p. 2703 (1975).

28. Melfi, S. H. "Raman Backscatter of Laser Radiation in the Earth's Atmosphere," Ph.D. Dissertation, College of William and Mary, Williamsburg, Virginia (1970).

29. Placzek, G. "Rayleigh-Streuung und Raman-Effekt," Handbuch der Radiologie, Vol. VI, 2, pp. 205-374. Leipzig: Akademische Verlag, 1934.

30. Penney, C. M., Morey, W. W., St. Peters, R. L., Silverstein, S. D., Lapp, M., and White, D. R. "Study of Resonance Light Scattering for Remote Optical Probing," NASA CR-132 363, Langley Research Center, 1973.

31. Bethke, W. "Oscillator Strengths in the Far Ultraviolet. I. Nitric Oxide," J. Chem. Phys., Vol. 31, No. 3, 1959.

32. Inaba, H., and Kobayosi, T. "Laser Raman Radar--Laser Raman Scattering Methods for Remote Detection and Analysis of Atmospheric Pollution," Opto-Electronics 4, pp. 101-123 (1972).

33. Kondrat 'ev. Radiation Characteristics of the Atmosphere and the Earth's Surface, NASA TTF-678.

34. Coney, Thom A., and Salzman, Jack A. "Determination of the Temperature of Gas Mixtures by Using Laser Raman Scattering," NASA TN-D7126, Lewis Research Center, Ohio, 1973.

35. Wiese, W. L., Smith, M. W., and Miles, B. M. Atomic Transition Probabilities, Vol. II, Sodium Through Calcium, U. S. Department of Commerce, NSRDS-NBS22, 1969.

36. Suchard, S. N., and Melzer, J. E., Editors. Spectroscopic Data, Vol. 2. New York: IFI/Plenum Data Company, 1976.

37. Rosen, B., Editor. Spectroscopic Data Relative to Diatomic Molecules. New York: Pergamon Press, 1970.

38. Krupenie, Paul H. "The Spectrum of Molecular Oxygen," J. Phys. Chem. Reference Data, Vol. 1, No. 2, pp. 423-534, 1972.

39. Weast, Robert C., Editor. CRC Handbook of Chemistry and Physics, 59th Ed. West Palm Beach: CRC Press Inc., 1978-1979.

40. Mitchell, Allen C., and Zenansky, Mark W. Resonance Radiation and Excited Atoms, 4:155. Cambridge: Cambridge University Press, 1961.

41. Baum, William A., and Dunkelman, Lawrence. "Horizontal Attenuation of Ultraviolet Light by the Lower Atmosphere," J. Opt. Soc. of America, Vol. 45, No. 3, p. 166, 1955.

42. Allen, Harry C., and Cross, Paul C. Molecular Vib-Rotors. New York: John Wiley and Sons Inc., 1963.

43. Shipley, S. T., Eloranta, E. W., et al. "The Evaluation of a Shuttle Borne Lidar Experiment to Measure the Global Distribution of Aerosols and Their Effect on the Atmospheric Heat Budget," Final Report on NASA Grant NSG 1057, April 1975. Dept. of Meteorology, Univ. of Wisconsin, Madison, Wisconsin 53706.

44. Cohen, A., Leiman, M., and Cooney, J. "Lidar Measurements of Rotational Raman and Double Scattering," Applied Optics, Vol. 17, No. 12, p. 1905 (1978).

APPENDICES

APPENDIX I

THE SLINEY PATCH

In cases where the ANSI Z136.1-1978 laser eye safety standard lacked guidelines or was ambiguous, assistance was obtained from Mr. David Sliney of the U. S. Department of the Army. Mr. Sliney is a laser safety expert and a member of the Z136 committee. His recommendations are referred to as the Sliney Patch and consist of the following [5].

1. The use of the thermal effects Maximum Permissible Exposure (MPE) criteria at wavelengths less than .315 μm in addition to the ANSI MPE criteria based on the UV photo-chemical interaction. (The more conservative MPE results of the two are used.) The additional MPE in this wavelength region was taken to be $.56\ t^{1/4}\ J/cm^2$, for exposure durations t between 10^{-9} and 10 seconds, and $1\ J/cm^2$ for exposure durations between 10 and 10^3 seconds from .315 μm to .4 μm, which is more conservative than the ANSI for infrared thermal effects criteria. This additional MPE was required primarily to obtain an individual pulse MPE criteria for the transmissometer pulses less than 10^{-2} seconds in duration, but consistency also required the use of this additional MPE in Average Power Limitation calculations (see Section B3.1.2 of ANSI Z136-1976) as it was the more conservative MPE for

total exposure times less than 10 seconds at wavelengths below .315 μm . This recommendation is equivalent to assuming that the MPE due to the photochemical interaction, if it existed for exposure durations less than 10^{-2} seconds, would be greater than the recommended MPE from thermal effects.

2. The use of the entry of Table 5, ANSI Z136.1-1976 at 1.06 0 to 1.4 μm , 10^{-9} to 10^{-5} second exposure durations as already including the factor of 5 of ANSI Section 8.5.2 for this wavelength region and the factor of 2 of ANSI Section 8.5.2.1, despite the statements of those two sections to the contrary.

3. The use of the total exposure time as the maximum total time one is exposed to the laser radiation in any 24-hour period, for both UV and IR radiation (see ANSI Section 8.5.4).

APPENDIX II

A QUANTUM MECHANICAL DERIVATION OF THE RAMAN SCATTERING DIFFERENTIAL TRANSITION PROBABILITY

Here is presented a quantum mechanical derivation of the general expression for the differential Raman transition probability based on Baym's treatment [20].

A quantum mechanical system is described by the wave equation

$$i\hbar \frac{\partial |\psi\rangle}{\partial t} = H|\psi\rangle \qquad \text{(A-1)}$$

where $|\psi\rangle$ is the eigenvector of the system and H is the total Hamiltonian. H may be written as the sum

$$H = H_o + H_{int} \qquad \text{(A-2)}$$

where H_o contains the Hamiltonian of the radiation field and the Hamiltonian of the molecule in the absence of radiation, and H_{int} is the interaction Hamiltonian.

We may denote the eigenvector of the system by $|n\rangle = |m_o ; N_{\vec{k}\vec{\lambda}}\rangle$ where m_o represents the state of the molecule and $N_{\vec{k}\vec{\lambda}}$ is the number of photons with wave vector $\vec{k}$ and polarization $\vec{\lambda}$.

The amplitude for a system in an initial state with energy E_o , denoted by 0 , to make the transition to a state with energy E_n , denoted by n , is given by Baym [20].

$$\langle n|H_{int}|0\rangle \qquad \text{(A-3)}$$

in the first order and by

$$\sum_m \frac{\langle n|H_{int}|m\rangle\langle m|H_{int}|0\rangle}{E_o - E_m + i\,\gamma_m\,\hbar} \tag{A-4}$$

in the second order, where m represents an intermediate state with energy E_m and γ_m is inversely proportional to the lifetime of the state m .

The total transition rate, $\Gamma_{o\to n}$, is obtained by summing the first and second order amplitudes and using the golden rule, Baym [20]:

$$\Gamma_{o\to n} = \frac{2\pi}{\hbar}\left|\langle n|H_{int}|0\rangle + \sum_m \langle n|H_{int}|m\rangle \cdot \frac{\langle m|H_{int}|0\rangle}{E_o - E_m + i\gamma_n\,\hbar}\right|^2 \delta(E_n - E_o) \tag{A-5}$$

In the quantum mechanical description of the scattering of light the system is initially in a state $|0\ ;\ N_{\vec{k}\vec{\lambda}}\ ,\ N_{\vec{k}'\vec{\lambda}'} = 0\rangle$ with $N_{\vec{k}\vec{\lambda}}$ photons in the state $\vec{k}$, $\vec{\lambda}$ and none in the state $\vec{k}'$, $\vec{\lambda}'$. After the interaction the system is in the state $|n\ ;\ N_{\vec{k}\vec{\lambda}} - 1\ ;\ N_{\vec{k}'\vec{\lambda}'} = 1\rangle$ where one photon in the state $\vec{k}$, $\vec{\lambda}$ has been scattered into the state $\vec{k}'$, $\vec{\lambda}'$. For such processes the interaction Hamiltonian is given by Baym [20]

$$H_{int} = \int d^3r \left[-\frac{e}{c}\,\vec{j}(\vec{r}) \cdot \vec{A}^{(OP)}(\vec{r}) + \frac{e^2}{2mc^2}\,\rho(\vec{r})\left[\vec{A}^{(OP)}(\vec{r})\right]^2\right] \tag{A-6}$$

where

$$\vec{A}^{(OP)}(\vec{r}) = \sum_{\vec{k}\vec{\lambda}} \left(A^{(OP)}_{\vec{k}\vec{\lambda}} \vec{\lambda} \frac{e^{i\vec{k}\cdot\vec{r}}}{\sqrt{V}} + A^{(OP)\dagger}_{\vec{k}\vec{\lambda}} \vec{\lambda}^* \frac{e^{-i\vec{k}\cdot\vec{r}}}{\sqrt{V}} \right) , \quad \text{(A-7)}$$

$$\rho(\vec{r}) = \sum_i \delta(\vec{r} - \vec{r}_i) , \quad \text{(A-8)}$$

and

$$\vec{j}(\vec{r}) = \frac{1}{2} \sum_i \left(\frac{p_i}{m} \delta(\vec{r} - \vec{r}_i) + \delta(\vec{r} - \vec{r}_i) \frac{p_i}{m} \right) . \quad \text{(A-9)}$$

r_i and p_i are the coordinate and momentum operators of the i^{th} particle. e and m are the charge and mass of the scattering particles assuming these particles all have the same charge and mass. $\vec{A}^{(OP)\dagger}_{\vec{k}\vec{\lambda}}$ and $\vec{A}^{(OP)}_{\vec{k}\vec{\lambda}}$ are creation and annihilation operators of the photons in the state $\vec{k}$, $\vec{\lambda}$, and V is a given volume. The creation and annihilation operators obey the following relations:

$$\vec{A}^{(OP)\dagger}_{\vec{k}\vec{\lambda}} \mid N_{\vec{k}_1\vec{\lambda}_1}, \ldots, N_{\vec{k}\vec{\lambda}}, \ldots >$$

$$= \sqrt{\frac{2\pi\hbar c^2}{\omega}} \sqrt{N_{\vec{k}\vec{\lambda}} + 1} \mid N_{k_1\lambda_1}, \ldots, N_{\vec{k}\vec{\lambda}} + 1, \ldots > \quad \text{(A-10)}$$

$$\vec{A}^{(OP)}_{\vec{k}\vec{\lambda}} \mid N_{\vec{k}_1\vec{\lambda}_1}, \ldots, N_{\vec{k}\vec{\lambda}}, \ldots > \sqrt{\frac{2\pi\hbar c^2}{\omega}} \sqrt{N_{\vec{k}\vec{\lambda}}}$$

$$\cdot \mid N_{\vec{k}_1\vec{\lambda}_1}, \ldots N_{\vec{k}\vec{\lambda}} - 1, \ldots > \quad \text{(A-11)}$$

The interaction Hamiltonian in Equation (A-6) may be considered as the sum of a first order term H^1_{int} and a second order term H^2_{int} , where

$$H^1_{int} = \frac{e^2}{mc^2} \int d^3r \; \rho(\vec{r}) \; A^{(QP)^2}_{(\vec{r})} \tag{A-12}$$

and

$$H^2_{int} = \frac{-e}{c} \int d^3r \; \vec{j}(\vec{r}) \cdot \vec{A}^{(QP)}_{(\vec{r})} \tag{A-13}$$

To calculate the transition rate for this process it is necessary to calculate the amplitudes for the system to make the transition by H^1_{int} using Equation (A-3) and by H^2_{int} using Equation (A-4).

The matrix element according to Equation (A-9) is

$$\begin{aligned} &\langle n \; ; \; N_{\vec{k}\vec{\lambda}} - 1, \; N_{\vec{k}',\vec{\lambda}'} = 1 \; | \; \frac{e^2}{2mc^2} \int d^3r \; \rho(\vec{r}) \; A^{(QP)^2}_{(\vec{r})} \\ &\qquad \cdot \; | \; 0; \; N_{\vec{k}\vec{\lambda}}, \; N_{k'\lambda'} = 0 \rangle \\ &= \frac{e^2}{2mc^2} \int d^3r \; \langle n | \rho(\vec{r}) | 0 \rangle \langle N_{\vec{k}\vec{\lambda}} - 1, \; N_{\vec{k}',\vec{\lambda}'} = 1 \; | \\ &\qquad \cdot \; \vec{A}^{(QP)}_{(\vec{r})} \cdot \vec{A}^{(QP)}_{(\vec{r})} \; | \; 0; \; N_{k\lambda}, \; N_{\vec{k}',\vec{\lambda}'} = 0 \rangle \end{aligned} \tag{A-14}$$

From Equations (A-10) and (A-11) it can be seen that the operator $A_{(\vec{r})}^{(QP)^2}$ creates and annihilates the photon in the state $\vec{k},\vec{\lambda}$. The only way for Equation (A-14) to be nonzero is if $\vec{A}_{(\vec{r})}^{(QP)}$ operating on one side annihilates a $\vec{k},\vec{\lambda}$ photon and $\vec{A}_{(\vec{r})}^{(QP)}$ operating on the other side creates a $\vec{k}',\vec{\lambda}'$ photon. Performing the operations and summing the terms, Equation (A-14) becomes

$$\frac{e^2}{mc^2}\frac{2\pi\hbar c^2}{\sqrt{\omega\omega'}}\frac{N_{\vec{k},\vec{\lambda}}}{V}\langle n|\int d^3r\ \rho(\vec{r})\ e^{i(\vec{k}-\vec{k}')\cdot\vec{r}}\cdot|0\rangle\vec{\lambda}\cdot\vec{\lambda}'^{*}\ . \tag{A-15}$$

There are two possible ways for light to be scattered in the second order process. In the first case a $\vec{k},\vec{\lambda}$ photon is absorbed leaving molecule in the state $|m\rangle$ with no photons present, then the molecule emits a photon $\vec{k}',\vec{\lambda}'$ leaving the molecule in the state $|n\rangle$. In the second case the molecule is considered to be in the state $|0\rangle$, it then emits a $\vec{k}',\vec{\lambda}'$ photon leaving the state $|m\rangle$ after which it absorbs a $\vec{k},\vec{\lambda}$ photon leaving the final state $|n\rangle$.

The intermediate state of the first process is $|m\ ;\ N_{\vec{k}\vec{\lambda}}-1\ ,\ N_{\vec{k}',\vec{\lambda}'}=0\rangle$ and it has energy $E_n+(N_{\vec{k}\vec{\lambda}}-1)\hbar ck$.

Using Equation (A-4) we obtain the transition amplitude

$$\sum_m \frac{\langle n;N_{\vec{k}\vec{\lambda}}-1,N_{\vec{k}',\vec{\lambda}'}=1 \mid \int d^3r\, \vec{j}(\vec{r}) \cdot \vec{A}^{(QP)}_{(\vec{r})} \mid m;N_{\vec{k}\vec{\lambda}}-1,N_{\vec{k}',\vec{\lambda}'}=0\rangle}{(E_o + N_{\vec{k}\vec{\lambda}}\hbar ck) - (E_m + (N_{\vec{k}\vec{\lambda}}-1)\hbar ck + i\gamma_m\hbar}$$

$$\cdot \langle m;N_{\vec{k}\vec{\lambda}}-1,N_{\vec{k}',\vec{\lambda}'}=0 \mid \int d^3r\, \vec{j}(\vec{r}) \cdot \vec{A}^{(QP)}_{(\vec{r})} \mid 0;N_{\vec{k}\vec{\lambda}},N_{\vec{k}',\vec{\lambda}'}=0\rangle$$

$$= \sum_m \langle n;N_{\vec{k}\vec{\lambda}}-1,N_{\vec{k}',\vec{\lambda}'}=1 \mid \int d^3r\, \vec{j}(\vec{r})$$

$$\cdot \left[\sum_{\vec{k}\vec{\lambda}} \left(A^{(QP)}_{\vec{k}\vec{\lambda}} \frac{\vec{\lambda} e^{i\vec{k}\cdot\vec{r}}}{\sqrt{V}} + A^{(QP)\dagger}_{\vec{k}\vec{\lambda}} \frac{\lambda^* e^{i\vec{k}\cdot\vec{r}}}{\sqrt{V}} \right)\right]$$

$$\cdot \frac{\mid m;N_{\vec{k}\vec{\lambda}}-1,N_{\vec{k}_1\vec{\lambda}_1}=0\rangle}{(E_o + N_{\vec{k}\vec{\lambda}}\hbar ck) - (E_m + (N_{\vec{k}\vec{\lambda}}-1)\hbar ck + i\gamma_m\hbar}$$

$$\cdot \langle m;N_{\vec{k}\vec{\lambda}}-1,N_{\vec{k}',\vec{\lambda}'}=0 \mid \int d^3r\, \vec{j}(\vec{r})$$

$$\cdot \left[\sum_m \left(A^{(QP)}_{\vec{k}\vec{\lambda}} \frac{\vec{\lambda} e^{i\vec{k}\cdot\vec{r}}}{\sqrt{V}} + A^{(QP)\dagger}_{\vec{k}\vec{\lambda}} \frac{\vec{\lambda}^* e^{-i\vec{k}\cdot\vec{r}}}{\sqrt{V}} \right)\right]$$

$$\cdot \mid 0;N_{\vec{k}\vec{\lambda}},N_{\vec{k}',\vec{\lambda}'}=0\rangle$$

From Equations (A-10) and (A-11) we then have

$$\frac{e^2}{c^2}\sqrt{\frac{2\pi\hbar c^2 N_{\vec{k}\vec{\lambda}}}{\omega V}}\sqrt{\frac{2\pi\hbar c^2}{\omega' V}}$$

$$\cdot \sum_m \frac{\langle n|\vec{j}_{k'}\cdot\vec{\lambda}'^*|m\rangle\langle m|\vec{j}_{-k}\cdot\vec{\lambda}|0\rangle}{\hbar\omega + (E_o - E_m) + i\gamma_m\hbar} \qquad \text{(A-16)}$$

where

$$\vec{j}_k = \int d^3r\, \vec{j}(\vec{r})\, e^{-i\vec{k}\cdot\vec{r}}\ . \qquad \text{(A-17)}$$

The transition amplitude for the second process with intermediate state $|m;N_{\vec{k}\vec{\lambda}},N_{\vec{k}',\vec{\lambda}'}, = 1\rangle$ and energy $E_m + N_{\vec{k}\vec{\lambda}}\hbar ck + \hbar ck'$ is similarly

$$\frac{e^2}{c^2}\sqrt{\frac{2\pi\hbar c^2 N_{\vec{k}\vec{\lambda}}}{\omega V}}\sqrt{\frac{2\pi\hbar c^2}{\omega' V}}$$

$$\cdot \sum_m \frac{\langle n|\vec{j}_{-k}\cdot\vec{\lambda}|m\rangle\langle m|\vec{j}_{k'}\cdot\lambda'^*|0\rangle}{(E_o - E_m) - \hbar\omega' + i\gamma_m\hbar} \qquad \text{(A-18)}$$

The total second-order transition amplitude is obtained by summing Equations (A-16) and (A-18):

$$\frac{2\pi\hbar e^2}{\sqrt{\omega\omega'}}\frac{\sqrt{N_{\vec{k}\vec{\lambda}}}}{V}\sum_m\left[\frac{\langle n|\vec{j}_{k'}\cdot\lambda'^*\, m\rangle\langle m|\vec{j}_{-k}\cdot\lambda|0\rangle}{\hbar\omega + (E_o - E_m) + i\,\gamma_m\hbar}\right.$$

$$\left. + \frac{\langle n|\vec{j}_{-k}\cdot\vec{\lambda}|m\rangle\langle m|\vec{j}_{k'}\cdot\vec{\lambda}'^*|0\rangle}{(E_o - E_m) - \hbar\omega' + i\,\gamma_m\hbar}\right] \qquad \text{(A-19)}$$

From Equation (A-9) we may write Equation (A-17) as

$$\vec{J}_k = \frac{1}{2} \sum_i \left[\frac{p_i}{m} e^{-i\vec{k}\cdot\vec{r}_i} + e^{-i\vec{k}\cdot\vec{r}_i} \frac{\vec{p}_i}{m} \right] \qquad \text{(A-20)}$$

Assuming the molecule is fixed about the position $\vec{r}_o = 0$ we may expand $\vec{J}_k$ as

$$\vec{J}_k = \int d^3r \left[1 - i\vec{k}\cdot\vec{r} + \ldots \right] \vec{j}(r)$$

$$= \vec{J}_o - i \int d^3r \, \vec{k}\cdot\vec{r} \, \vec{j}(\vec{r}) + \ldots \qquad \text{(A-21)}$$

Equation (A-20) gives

$$\vec{J}_o = \frac{\vec{P}}{m} = \frac{1}{ih} \left[R , H_o \right] \qquad \text{(A-22)}$$

where H_o is the Hamiltonian of the molecule in the absence of radiation, $\vec{R} = \sum_i \vec{r}_i$ and $\vec{P} = \sum_i \vec{p}_i$. $\vec{R}$ and $\vec{P}$ are the dipole moment operator and the total momentum operator of the system respectively.

If we consider only the first term in Equation (A-21) we may write the matrix element $\langle a|\vec{J}_k|b\rangle$, where a and b represent two states, as

$$\frac{1}{ih} \langle a|\vec{R}H_o - H_o\vec{R}|b\rangle = \frac{E_b - E_a}{ih} \langle a|\vec{R}|b\rangle \qquad \text{(A-23)}$$

This expression is the dipole approximation to $\langle a|\vec{J}_k|b\rangle$. Using this approximation Equation (A-19) becomes

$$\frac{1}{i\hbar m}\left[\frac{\langle n|\vec{P}\cdot\vec{\lambda}'^{*}|m\rangle\langle m|\vec{R}\cdot\vec{\lambda}|0\rangle\ (E_o - E_m)}{(E_o - E_m) + \hbar\omega + i\ \gamma_m \hbar}\right.$$

$$\left. + \frac{\langle n|\vec{R}\cdot\vec{\lambda}|m\rangle\langle m|\vec{P}\cdot\vec{\lambda}'^{*}|0\rangle\ (E_m - E_n)}{(E_o - E_m) - \hbar\omega' + \gamma_m \hbar}\right] \qquad \text{(A-24)}$$

Energy conservation requires that $E_o + \hbar\omega = E_n + \hbar\omega'$. Therefore, $E_o - E_m - \hbar\omega' + i\ \gamma_m \hbar = E_n - E_m - \hbar\omega + i\ \gamma_m \hbar$ and Equation (A-24) becomes

$$\frac{1}{i\hbar m}\left[\frac{\langle n|\vec{P}\cdot\vec{\lambda}'^{*}|m\rangle\langle m|\vec{R}\cdot\vec{\lambda}|0\rangle\ (E_o - E_m)}{E_o - E_m + \hbar\omega + i\ \gamma_m \hbar}\right.$$

$$\left. + \frac{\langle n|\vec{R}\cdot\vec{\lambda}|m\rangle\langle m|\vec{P}\cdot\vec{\lambda}'^{*}|0\rangle\ (E_m - E_n)}{E_n - E_m - \hbar\omega + i\ \gamma_m \hbar}\right] \qquad \text{(A-25)}$$

Since

$$\frac{E_o - E_m}{E_o - E_m + \hbar\omega + i\ \gamma_m \hbar}$$

$$= \frac{E_o - E_m + \hbar\omega - \hbar\omega}{E_o - E_m + \hbar\omega + i\ \gamma_m \hbar}$$

$$= 1 - \frac{\hbar\omega}{E_o - E_m + \hbar\omega + i\ \gamma_m \hbar}$$

and

$$\frac{E_m - E_n}{E_n - E_m - \hbar\omega + i\ \gamma_m \hbar} = -1 + \frac{\hbar\omega}{E_n - E_m - \hbar\omega + i\ \gamma_m \hbar}\ ,$$

Equation (A-25) may be written as

$$\frac{1}{i\hbar m}\left(\langle n|\vec{P}\cdot\vec{\lambda}'^{*}|m\rangle\langle m|\vec{R}\cdot\vec{\lambda}|0\rangle - \langle n|\vec{R}\cdot\vec{\lambda}|m\rangle\langle m|\vec{P}\cdot\vec{\lambda}'^{*}|0\rangle\right)$$

$$+\frac{i\omega}{m}\left[\frac{\langle n|\vec{P}\cdot\vec{\lambda}'^{*}|m\rangle\langle m|\vec{R}\cdot\vec{\lambda}|0\rangle}{E_n - E_m + \hbar\omega' + i\,\gamma_m\hbar}\right.$$

$$\left.+\frac{\langle n|\vec{R}\cdot\vec{\lambda}|m\rangle\langle m|\vec{P}\cdot\vec{\lambda}'^{*}|0\rangle}{E_o - E_m - \hbar\omega' + i\,\gamma_m\hbar}\right]. \qquad \text{(A-26)}$$

Letting $\frac{\vec{P}}{m} = [R\ ,\ H_o]/i\hbar$ and knowing

$$\langle n|\frac{\vec{P}}{m}\cdot\vec{\lambda}'^{*}|m\rangle = \frac{1}{i\hbar}\langle n|\vec{R}\cdot\vec{\lambda}'^{*}|m\rangle\,(E_m - E_n)$$

$$= \frac{1}{i\hbar}\langle n|R\cdot\lambda'^{*}|m\rangle\,(E_m - E_n - \hbar\omega' + \hbar\omega') \qquad \text{(A-27)}$$

Equation (A-26) may be written in the form

$$\frac{1}{i\hbar m}\left(\langle n|\vec{P}\cdot\vec{\lambda}'^{*}|m\rangle\langle m|\vec{R}\cdot\vec{\lambda}|0\rangle - \langle n|\vec{R}\cdot\vec{\lambda}|m\rangle\cdot\langle m|P\cdot\lambda'^{*}|0\rangle\right)$$

$$-\frac{\omega}{\hbar}\left(\langle n|\vec{R}\cdot\vec{\lambda}'^{*}|m\rangle\langle m|\vec{R}\cdot\vec{\lambda}|0\rangle - \langle n|\vec{R}\cdot\vec{\lambda}|m\rangle\cdot\langle m|\vec{R}\cdot\vec{\lambda}'^{*}|0\rangle\right)$$

$$+\omega\omega'\left[\frac{\langle n|\vec{R}\cdot\vec{\lambda}'^{*}|m\rangle\langle m|\vec{R}\cdot\vec{\lambda}|0\rangle}{E_n - E_m + \hbar\omega' + i\,\gamma_m\hbar}\right.$$

$$\left.+\frac{\langle n|\vec{R}\cdot\vec{\lambda}|m\rangle\langle m|\vec{R}\cdot\vec{\lambda}'^{*}|0\rangle}{E_o - E_m - \hbar\omega' + i\,\gamma_m\hbar}\right] \qquad \text{(A-28)}$$

Summing over all intermediate states the first term in Equation (A-28) becomes

$$\frac{1}{i\hbar m} \langle n|[(\vec{P} \cdot \vec{\lambda}'^*)(\vec{R} \cdot \vec{\lambda}) - (\vec{R} \cdot \vec{\lambda})(\vec{P} \cdot \vec{\lambda}'^*)]|0\rangle$$

$$= \frac{1}{i\hbar m} \langle n|[\vec{P} \cdot \vec{\lambda}^*, \vec{R} \cdot \vec{\lambda}]|0\rangle = - \frac{\vec{\lambda} \cdot \vec{\lambda}'^*}{i\hbar m} \langle n| \sum_{ij} i\hbar \delta_{ij}|0\rangle$$

$$= - \frac{\vec{\lambda} \cdot \vec{\lambda}'^*}{m} \langle m|N|0\rangle \qquad \text{(A-29)}$$

where i and j represent the i^{th} and j^{th} molecules and N is the number of scattering centers available. Similarly, the second term in Equation (A-28) becomes

$$- \frac{\omega}{\hbar} \langle n|[(\vec{R} \cdot \vec{\lambda}'^*)(\vec{R} \cdot \vec{\lambda}) - (\vec{R} \cdot \vec{\lambda})(\vec{R} \cdot \vec{\lambda}'^*)]|0\rangle = 0 \ . \qquad \text{(A-30)}$$

Therefore, the entire second-order matrix element is

$$\frac{2\pi\hbar e^2}{\sqrt{\omega\omega'}} \frac{\sqrt{N_{\vec{k}\vec{\lambda}}}}{V} \left(- \frac{\vec{\lambda} \cdot \vec{\lambda}'^*}{m} \langle n|N|0\rangle \right.$$

$$+ \omega\omega' \sum_m \left[\frac{\langle n|\vec{R} \cdot \vec{\lambda}'^*|m\rangle\langle m|\vec{R} \cdot \vec{\lambda}|0\rangle}{E_o - E_m + \hbar\omega + i\,\gamma_m\,\hbar} \right.$$

$$\left. \left. + \frac{\langle n|R \cdot \lambda|m\rangle\langle m|R \cdot \lambda'^*|0\rangle}{E_o - E_m - \hbar\omega' + i\,\gamma_m\,\hbar} \right] \right) \qquad \text{(A-31)}$$

In the dipole approximation we may write

$$\int d^3r\ \rho(\vec{r})\ e^{i(\vec{k}-\vec{k}')\cdot\vec{r}}$$

as

$$\rho_{\vec{k}-\vec{k}'} = \int d^3r\ \rho(\vec{r})\ e^{i(\vec{k}-\vec{k}')\cdot\vec{r}}$$

$$= \int d^3r\ \rho(\vec{r})\left[1 - i(\vec{k}-\vec{k}')\cdot\vec{r} + \ldots\right]$$

$$\cong \int d^3r\ \rho(\vec{r})$$

$$\cong \sum_i \delta(\vec{r}-\vec{r}_i)$$

$$= N \qquad \text{(A-32)}$$

Adding Equation (A-15) and Equation (A-31) we obtain the total transition amplitude due to the ρA^2 and $\vec{j}\cdot\vec{A}$ processes:

$$\frac{2\pi\hbar e^2}{V}\ \sqrt{N_{\vec{k}\lambda}}\ \sqrt{\omega\omega'}$$

$$\cdot \sum_m \left[\frac{\langle n|\vec{R}\cdot\vec{\lambda}'^*\ m\rangle\langle m|\vec{R}\cdot\vec{\lambda}|0\rangle}{E_o - E_m + \hbar\omega + i\,\gamma_m\hbar}\right.$$

$$\left. + \frac{\langle n|\vec{R}\cdot\vec{\lambda}|m\rangle\langle m|\vec{R}\cdot\vec{\lambda}'^*|0\rangle}{E_o - E_m - \hbar\omega' + i\,\gamma_m\hbar}\right] \qquad \text{(A-33)}$$

To obtain the total differential scattering transition probability we use Equation (A-33) in Equation (A-5) and divide by the photon flux $N_{\vec{k}\vec{\lambda}}\, c/V$. This results in

$$\frac{d\omega}{d\Omega} = \frac{e^4 \omega \omega'^3}{c^4} \left| \sum_m \frac{\langle n|\vec{R}\cdot\vec{\lambda}'^*|m\rangle\langle m|\vec{R}\cdot\vec{\lambda}|0\rangle}{E_o - E_m + \hbar\omega + i\,\gamma_m \hbar} \right.$$

$$\left. + \frac{\langle n|\vec{R}\cdot\vec{\lambda}|m\rangle\langle m|\vec{R}\cdot\vec{\lambda}'^*|0\rangle}{E_o - E_m - \hbar\omega' + i\,\gamma_m \hbar} \right|^2$$

$$= \frac{e^4 \omega \omega'^3}{c^4 \hbar^2} \left| \sum_m \frac{\langle n|\vec{R}\cdot\vec{\lambda}'^*|m\rangle\langle m|\vec{R}\cdot\vec{\lambda}|0\rangle}{\omega_{mo} - \omega_o + i\,\gamma_m} \right.$$

$$\left. + \frac{\langle n|\vec{R}\cdot\vec{\lambda}|m\rangle\langle m|\vec{R}\cdot\vec{\lambda}'^*|0\rangle}{\omega_{mn} + \omega_o + i\,\gamma_m} \right|^2 , \qquad \text{(A-34)}$$

where $\omega_o = E_n - E_m + \hbar\omega'/\hbar$, $\omega_{mo} = E_m - E_o/\hbar$, and $\omega_{mn} = E_m - E_n/\hbar$.

If the energy of the molecule is raised from the energy of the initial state, the frequency of the scattered light will be less than that of the incident light and the process is called Stokes scattering. If the molecule loses energy in the process, the frequency of the scattered light will be greater than that of the incident light and the process is called anti-Stokes scattering. The other possibility is that the energy of the molecule is unchanged in the process, in which case we have Rayleigh scattering.

VITA

Michael James Guthrie was born in Wilmington, Delaware, on November 2, 1955. He graduated from Salesianum School in June 1973. The following August he entered the Virginia Military Institute, and in May 1977 he received a Bachelor of Science degree in Physics and a commission in the United States Army. After graduation from VMI he was elected into the Beta Commission of the Kappa Alpha Order. In September 1977 he entered The University of Tennessee Space Institute and began study towards a Master's degree in Physics. In May 1978 he received Federal recognition as an officer in the Tennessee Army National Guard. While on active duty, from June 1979 to November 1979, he completed the Field Artillery Officer Basic, Cannon Battery Officer, and the Nuclear, Biological and Chemical courses at the U. S. Army Field Artillery School at Ft. Sill, Oklahoma. He returned to The University of Tennessee Space Institute in January 1980 to resume working toward his Master's degree. This degree was awarded in June 1980.